湿式析出法によるリチウムイオン二次電池用新規合金負極

（研究課題番号　15205024）

平成15年度～平成17年度科学研究費補助金

（基盤研究（A））

研 究 成 果 報 告 書

平成 18 年 3 月

研究代表者　　逢坂　哲彌

（早稲田大学・理工学術院・教授）

《はしがき》

この報告書は、平成15～17年度の3年間、文部科学省科学研究費補助金　基盤研究(A)(研究課題番号 15205024)により、「湿式析出法によるリチウムイオン二次電池用新規合金負極」と題して行った研究結果をまとめたものである。

《研究組織》

研究代表者　：　逢坂　哲彌　（早稲田大学・理工学術院）

研究分担者　：　門間　聰之　（早稲田大学・理工学術院）

《研究経費》

交付決定額(配分額)　　(金額単位:千円)

	直接経費	間接経費	合　計
平成15年度	14,000	4,200	18,200
平成16年度	10,400	3,120	13,520
平成17年度	9,000	2,700	11,700
総　計	33,400	10,020	43,420

《研究成果概要》

二次電池は，化学反応から得られる電気エネルギーを繰り返し蓄積，放出でき，かつそのエネルギーを容易に輸送できることから，種々のデバイスに用いられている．近年では，携帯電子機器の著しい発展やエネルギーの有効利用の必要性等から，二次電池には更なる大容量，長寿命，低環境負荷が求められている．

大変低い反応電位でリチウム（Li）イオンと可逆的に反応し、しかも単位重量あたりに多くの電子を蓄えることができる炭素を負極に用いることで広く実用に供されているのがLiイオン二次電池である．このLiイオン二次電池において，スズ(Sn)は現行の炭素負極に対してより高いエネルギー密度を有する材料として注目されているが，充放電時の体積変化が大きいため，電極の崩壊欠落が生じ易く，寿命が短いという致命的な問題がある．

本研究はこのような現状に対し、新しい発想を元に材料開発から二次電池システムの構築までを検討することを目的とし、湿式金属析出（めっき）プロセスを利用したLiイオン二次電池用負極材料の創製を目指した。特にLiと合金化するSnに着目し、様々な組成を有するSnと第三元素の合金について、Liとの電気化学的合金化・脱合金化反応の際の構造変化、合金・脱合金化反応の解析を行い、最適設計を行った。

本研究ではまず、次世代Liイオン二次電池の負極材料として期待されるSnに着目した。その欠点である充放電時の大きな体積膨張・収縮による電極破壊に対し、Liと合金化しない金属であるニッケル(Ni)との複合化の効果を検討した。まず二次電池を形成する上で有利である集電体上への直接成膜を行うため電解析出法にてSn-Ni合金薄膜の形成を行った。またLiイオンの電気化学的挿入脱離を検討したところ、$Sn_{62}Ni_{38}$組成のもの以外は従来のLiイオン二次電池負極材料である炭素材料の理論容量値372 mAh/gよりも低い値となったが、$Sn_{62}Ni_{38}$組成のものは100サイクル以上500 mAh/gを超える可逆容量を示すことを明らかとした。このことから、本$Sn_{62}Ni_{38}$膜はLiイオン二次電池負極として期待できるものであることが示された。

各種組成のNiSn合金を銅箔上に析出させ初期充放電時における構造評価を行った結果、$Sn_{62}Ni_{38}$組成のもののみにおいてNi_3Sn_4相に帰属されるXRDピークが観測された。また

この $Sn_{62}Ni_{38}$ 合金負極について、電気化学的な Li との合金化・脱合金化反応時に伴う構造変化について詳細に検討した結果、Li の挿入にともない Ni_3Sn_4 合金相の結晶規則性が失われ、LiSn 合金相が現われることが示唆された。続く Li の脱離の過程では LiSn 合金相の低減、および Ni_3Sn_4 合金相の結晶性が復元されることが確認された。これより Li と Ni_3Sn_4 合金が可逆的に反応しそれがこの薄膜の高容量につながっていることが示唆された。この知見は今後の負極材料設計の一つの指針を示すものとして非常に有用であると考えられる。さらに充放電状態が異なる負極のマイクロ ED(微小部電子線回折)の観察を行った。得られた電子線回折パターンより、充放電前には合金薄膜の高い結晶性が確認され、膜中の原子の並びが高い規則性を有することが確認された。しかしながら、薄膜への Li の挿入脱離を繰り返すことにより、原子配列の規則性が少しずつ損なわれ、二サイクル目ではすでに薄膜中の微結晶は *ex-situ* XRD 解析では確認できなかったナノオーダーでアモルファス化が進行し始めていることが示唆された。相分離状態を視覚的に明らかにすることはできなかったが、上記の検討より Ni-Sn 合金と Li との合金化により生成すると考えられる Ni リッチ相と LiSn リッチ相が明確に分離している状態ではない可能性が示唆された。

また Ni-Sn 合金薄膜の熱処理により負極の劣化が抑制されることが示唆された。これは熱処理により合金薄膜と Cu 基板(集電体)の間で原子の相互拡散が起こり、密着性を向上させたためだと考えられる。

本 $Sn_{62}Ni_{38}$ 電極の長期充放電サイクル特性の評価、およびそれに伴う電極物性の変化を追跡した結果、電析 $Sn_{62}Ni_{38}$ 合金薄膜は 500 mAh/g の高容量を保持しつつ 150 以上のサイクルを達成する良好な負極特性を示すことを明らかとした。長期充放電による電極の結晶構造の変化については、Li と合金薄膜との反応が繰り返されるに伴い、その結晶の周期性が乱れていくことが示唆された。特に、充放電を重ねることにより、未反応の低結晶性 LiSn 合金相が放電後に確認されるようになることを明らかとした。

またそのサイクルに伴う電極形状の変化挙動を追跡したところ、大きな変化を示すことが明らかとなった。銅箔上にめっき法により析出させた SnNi 薄膜は平滑な表面形状であったが、1 回目の充電プロセスすなわち Li との合金化により、大きく体積膨張して塊

状の集合体となることが確認された。続く放電（Li との脱合金化）プロセス後は、クラックの多く入った形状となった。これは一旦膨張した SnNi 薄膜が収縮したためであると考えられる。充電・放電を繰り返した際の表面形態変化の観察から、初期の多孔質状態が 50 サイクル以上充放電を重ねることによりふさがる様子が確認された。このことより $Sn_{62}Ni_{38}$ 合金においても、Sn と同様、充放電時の体積変化が大きいという特徴を有していることが明らかとなった。

上記のような構造・形状の変化にも関わらず良好な長期充放電特性が保たれた要因の一つとして、電極内の Li 拡散係数に注目した。初期 3 サイクル目までは大きな拡散係数の変化はなく、約 $6.43 \times 10^{-10}\ cm^2\ s^{-1}$ であることが示唆された。10 サイクルを経た後もその値の増加は $8.04 \times 10^{-10}\ cm^2\ s^{-1}$ にとどまり、固体内の Li の良好な拡散性が保持されることを明らかとした。また、電極の焼成効果の検討より、Li の拡散経路としてその粒界が関与している可能性も明らかとした。

Sn 系の合金負極材料の長期使用を視野に入れて行った上記研究は体積変化を伴う Sn 系負極材料の設計指針を示唆するものとして非常に有用であると考えられる。

また、負極の検討とあわせて Li 系二次電池電解質について、新たな電解質として高分子ゲル電解質に関する検討をすすめており、相互連続性を有するミクロ相分離構造からなるゲルホストマトリックスを開発している。導入的検討としてポリオキシエチレン（PEO）とポリスチレンのポリマーコンポジットを形成し、その PEO 相を可塑剤にてゲル化することで Li 電池電解質として利用可能であることを示した。作製されたゲル電解質と Li 金属で半電池を形成し、その Li 金属負極特性を検討したところ、Li 金属との反応性が低いことが確認された。一方、本電解質は貴な電位では酸化されやすいことも明らかとなり、今後の更なる検討が必要であることがわかった。

《研 究 発 表》

【 学会誌等 】

(1) 角友秀, 向坊仁美, 横島時彦, Mohamedi Mohamed, 門間聰之, 逢坂哲彌, "化学的還元法により作製したNi-Sn合金粉末のLiイオン二次電池負極特性", 2003年電気化学秋季大会講演要旨集, pp. 46 (2003).

(平成15年9月)

(2) T. Osaka, H. Mukaibo, and T. Momma, "New Anodes for Advanced Li Batteries", *Abstract of The 5th Korea-Japan Joint Seminar on Advanced Batteries* (2003).

(平成15年9月)

(3) H. Mukaibo, T. Sumi, T. Yokoshima, T. Momma, T. Osaka, "Electrodeposited Sn-Ni alloy film as a high capacity anode material for lithium-ion secondary batteries", *Electrochemical and Solid State Letters*, vol. **6**, pp. A218-A2201 (2003).

(平成15年10月)

(4) T. Momma, H. Mukaibo, T. Sumi, T. Yokoshima, and T. Osaka, "Characteristics of Electro-Deposited Sn-Ni Alloys as Lithium Ion Secondary Battery Anode", *Abstract of the 204th Meeting of The Electrochemical Society*, vol. **2003-02**, Abstract No. 324 (2003).

(平成15年10月)

(5) 向坊仁美, 和田安正, 横島時彦, Mohamedi Mohamed, 門間聰之, 逢坂哲彌, "リチウムイオン二次電池用Sn-Ni合金負極の充放電特性", 第44回電池討論会講演要旨集, pp. 432-433 (2003).

(平成15年11月)

(6) T. Momma, H. Ito, H. Nara, H. Mukaibo, S. Passerini, T. Osaka, "PEO-$LiBF_4$錯体 およびポリスチレンからなる相互連続複合体電解質のリチウム二次電池電解質としての評価", *Electrochemistry*, vol. **71**, pp. 1182-1186 (2003).

(平成 15 年 12 月)

(7) H. Mukaibo, T. Sumi, T. Yokoshima, T. Momma, T. Osaka, " Structural and Morphological Differences in the Cycled Electro-Deposited Sn-Ni Alloy Lithium Ion Battery Anodes with Different Composition", *12th International Meeting on Lithium Batteries Meeting Abstracts*, Abs. 252 (2004).

(平成 16 年 6 月)

(8) 門間聰之, 向坊仁美, 逢坂哲彌, "リチウムイオン二次電池用 Sn 系負極材料の開発", セラミックス協会第 17 回秋季シンポジウム講演予稿集, pp. 20 (2004).

(平成 16 年 9 月)

(9) 角友秀, 向坊仁美, 門間聰之, 逢坂哲彌, "リチウムイオン二次電池用 Sn-Ni 合金負極の微粒子作製の検討", 第 45 回電池討論会講演要旨集, pp. 304-305 (2004).

(平成 16 年 11 月)

(10) H. Mukaibo, T. Momma, M. Mohamedi, and T. Osaka, "Structural and Morphological Modifications of a Nanosized 62 Atom Percent Sn-Ni Thin Film Anode during Reaction with Lithium", *Journal of The Electrochemical Society*, vol. **152**, pp.A560-A565 (2005).

(平成 17 年 3 月)

(11) H. Mukaibo, T. Momma, and T. Osaka, " Changes of electro-deposited Sn-Ni alloy thin film for lithium ion battery anodes during charge discharge cycling", *Journal of Power Sources*, vol.**146**, pp.457-463 (2005).

(平成 17 年 8 月)

(12) 向坊仁美, 福原佳樹, 門間聰之, 逢坂哲彌, 小平宗男、"高分子ゲル電解質被覆による $Sn_{62}Ni_{38}$ 合金負極の負極特性向上の検討", 第 46 回電池討論会講演要旨集, pp. 484-485 (2005).

(平成 17 年 11 月)

【 口頭発表 】

(1) 角友秀, 向坊仁美, 横島時彦, Mohamedi Mohamed, 門間聰之, 逢坂哲彌, "化学的還元法により作製した Ni-Sn 合金粉末の Li イオン二次電池負極特性", 電気化学会第 71 回秋季大会, 北海道 (日本).

(平成 15 年 9 月)

(2) T. Osaka, H. Mukaibo, and T. Momma, "New Anodes for Advanced Li Batteries", The 5th Korea-Japan Joint Seminar on Advanced Batteries, Seoul (Korea).

(平成 15 年 9 月)

(3) T. Momma, H. Mukaibo, T. Sumi, T. Yokoshima, and T. Osaka, "Characteristics of Electro-Deposited Sn-Ni Alloys as Lithium Ion Secondary Battery Anode", 204th Meeting of The Electrochemical Society, Florida (USA).

(平成 15 年 10 月)

(4) 向坊仁美, 和田安正, 横島時彦, Mohamedi Mohamed, 門間聰之, 逢坂哲彌, "リチウムイオン二次電池用 Sn-Ni 合金負極の充放電特性", 第 44 回電池討論会, 大阪 (日本).

(平成 15 年 11 月)

(5) H. Mukaibo, Y. Wada, T. Yokoshima, M. Mohamed, T. Momma, and T. Osaka, "Thin Film Sn-Ni Alloy as a Novel Anode Material for Li-ion Batteries", 21COE International Symposium on 'Practical Nano-Chemistry', Tokyo (Japan).

(平成 15 年 12 月)

(6) H. Mukaibo, Y. Wada, T. Yokoshima, M. Mohamed, T. Momma, and T. Osaka, "Structural and Morphological Changes of the Sn-Ni Alloy during Cycling as the Novel Li Ion Battery Anode Material", International Symposium on Molecular Nano-Engineering and Its Development into Microsystems Molecular Nano-engineering for Bio-Science and Technology Applications, Tokyo (Japan).

(平成 15 年 12 月)

(7) H. Mukaibo, T. Sumi, T. Yokoshima, T. Momma, T. Osaka, " Structural and Morphological Differences in the Cycled Electro-Deposited Sn-Ni Alloy Lithium Ion Battery Anodes with Different Composition", 12th International Meeting on Lithium Batteries, Nara (Japan).

(平成 16 年 6-7 月)

(8) 向坊仁美, 門間聰之, 逢坂哲彌, "リチウムイオン二次電池用 Sn 系負極材料の開発" セラミックス協会第 17 回秋季シンポジウム, 石川 (日本).

(平成 16 年 9 月)

(9) 角友秀, 向坊仁美, 門間聰之, 逢坂哲彌, "リチウムイオン二次電池用 Sn-Ni 合金負極の微粒子作製の検討", 第 45 回電池討論会, 京都 (日本).

(平成 16 年 11 月)

(10) 向坊仁美, 福原佳樹, 門間聰之, 逢坂哲彌, 小平宗男, "高分子ゲル電解質被覆による $Sn_{62}Ni_{38}$ 合金負極の負極特性向上の検討", 第 46 回電池討論会, 名古屋 (日本).

(平成 17 年 11 月)

学会発表論文など

2B18 化学的還元法により作製したNi-Sn合金粉末のLiイオン二次電池負極特性

(1早大院理工・理工総研セ・理工, 2CREST, JST)○角 友秀1, 向坊仁美1, 横島時彦1, Mohamedi Mohamed1, 門間聰之1,2, 逢坂哲彌1

Ni-Sn Alloy Powder Prepared by Chemical Reduction for Lithium Ion Battery Anode

Tomohide Sumi[1], Hitomi Mukaibo[1], Tokihiko Yokoshima[1], Mohamedi Mohamed[1], Toshiyuki Momma[1,2], Tetsuya Osaka[1] ([1]Waseda Univ., [2]CREST, JST)

1.目的

高エネルギー密度化への要求を満たすLiイオン二次電池用の新規負極材料の一つとしてSnが期待されている．Snは，高い理論エネルギー密度を有するものの，充放電反応に伴う著しい体積変化のため電極内部が損傷し，容量劣化してしまうことが大きな問題となっている．我々は，Liと合金化しない金属中に，Sn微粒子を分散させた系で容量劣化の緩和が期待されることから，良好な負極材料として着目し研究を行っている．特に，マトリクスにNiを選択し，電析法により作製したNi-Sn合金薄膜負極の提案をしている．Ni_3Sn_4相を含む電析薄膜負極は，60サイクル以上放電容量約650 mAh/gの良好な負極特性を示した．これは現在実用化されている炭素材料の理論容量よりも高く，Ni_3Sn_4相が新規負極材料になりうる可能性を有していることを示唆する[1]．本研究では，良好な負極特性を示した電析薄膜を作製する際に用いた浴と同じものを用い，薄膜よりも扱いやすく汎用性が高いNi-Sn合金粉末を化学的還元法により作製し，その負極特性について評価を行った．

2.方法

Ni-Sn合金粉末は，表1に示す組成の浴に水素化ホウ素ナトリウムを添加することにより作製した．試料の電気化学的特性は，作用極に試料：AB：PVdF-HFP=8：1：1 (wt.%)，対極および参照極に金属Liを用い，電解液を1M-$LiClO_4$/EC+PC (1：1vol.%)とする三極式セルにて，充放電試験により評価した．測定条件として，電位範囲を0.01 ～ 2 V vs. Li/Li+，電流密度を50 mA/gとするCC－CVモードを用いた．また，得られた試料の構造解析にはXRD(CuK$_\alpha$線)，形態観察にはFE-SEMを用いた．

表1 浴組成

塩化ニッケル六水和物	0.075 mol l^{-1}
塩化スズ二水和物	0.175 mol l^{-1}
ピロりん酸カリウム	0.500 mol l^{-1}
グリシン	0.125 mol l^{-1}
アンモニア水	5 ml l^{-1}

3.結果

作製した試料は，約150 nmの大きな粒子の存在がいくつか確認されたものの，全体としては約40～60 nmの微粒子が凝集している状態であることが確認された．また試料の構造は，Ni_3Sn_4相およびNi_3Sn相からなることが確認された．この試料のサイクル特性を図1に示す．また，比較のため，同様の浴を用いて電析法により作製したNi-Sn合金薄膜負極のサイクル特性も示す．図より，作製したNi-Sn合金粉末の放電容量は最大約250 mAh/gであることが確認され，電析薄膜負極と比較して低いことが分かった．この原因として，Ni-Sn合金粉末にはNi_3Sn_4相に加え，良好な特性を示す電析薄膜電極では確認されなかったNi_3Sn相が存在しており，充放電能力を低下させたことが考えられる．

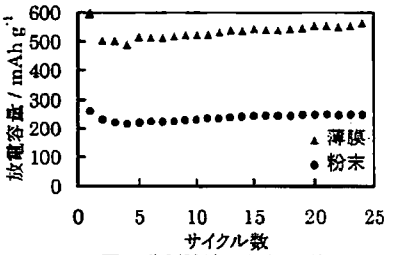

図1 作製試料のサイクル特性

本研究は一部，文部科学省特別推進研究(COE)「分子 ナノ工学」の助成を受け，21世紀COEプログラム「実践的ナノ化学教育研究拠点」にて行なわれた．

1) H. Mukaibo, T. Sumi, T. Yokoshima, T. Momma, T. Osaka, Electrochemical and Solid-State Letters 6, 2003 (in-press).

2B19 CH_4分解による半導体化Siの炭素被覆とリチウムイオン2次電池特性

(大分大工、九大工*)○中洲正史・西口宏泰・石原達己*・滝田祐作

Carbon-coated and Cr doped silicon as a new anode for Li ion rechargeable battery

○M.Nakasu・H.Nishiguchi・T.Ishihara*・Y.Takita (Oita University,Kyushu University*)

1.目的

リチウムイオン２次電池は携帯機器の電源として広く普及しており、その高容量化は重要な課題となっている。Siは、理論容量が4000mAh/gと極めて大きく高容量負極として期待されているが繰り返し特性の向上が課題である。Si系負極として、スパッタして得たSi膜が良好な繰り返し特性を有すると報告されているが、量産性等に依然課題がある。本研究では、Si系負極の繰り返し特性の低い理由は伝導度が低いためと考えた。そこで、伝導度の向上を目的にCrドープにより半導体化したSiの負極特性を検討するとともに、炭素チューブで被覆することで、繰り返し特性の向上を検討した。

2.実験

SiとしてはWako純薬製の高純度Si及びCrを添加した半導体Siウェハー（東芝セラミック）をボールミルして得た半導体Siを用いた。炭素の被覆は、半導体SiにNiを担持した炭素を混合後、700℃でCH_4分解することで行った。リチウムイオン2次電池の負極特性は正極に金属Liを用い電解液として、1mM$LiPF_6$を溶解したEC:DMC(UBE製)を用いた。測定は半開放型セルを用い、定電流（0.4mA/cm^2）を印加して、1.5～0Vで測定した。

3.結果及び考察

Fig.1には、本研究で検討した種々のSiにおける負極容量の繰り返し特性を示した。高純度Siでは0.5V付近に放電電位を示すSiに特徴的な充放電曲線を示した。Fig.1に示すように高純度Siでは2000mAh/gに近い挿入容量を示すものの、容量は繰り返し回数とともに大きく低下した。一方、少量のCrを添加し半導体化したSiでは、容量が向上するとともに繰り返し特性も向上し、5回の繰り返し後の容量は295mAh/gとなった。Siは抵抗が大きく、印加した電位の不均一により表面での電解液の分解等を生じ、Si表面にSiO_2が生じるので、繰り返す毎に容量は低下すると考えた。そこで、伝導度の向上が、負極特性の向上に有効であると考えた。既に芳尾らが報告しているように表面への炭素被覆を検討した。その結果、Fig.1に示すように炭素で被覆すると、初回の充電容量が大きく向上するとともに、繰り返し特性も向上したが、Liの挿入容量は繰り返し回数とともに低下した。次に、Fig.1中では1000mAh/gで容量カットオフした結果も示した。明らかなように5回の繰り返しでは1000mAh/gの容量を安定に示した。以上より炭素被覆したn型半導体Siは新しい高容量負極として期待できる材料であることがわかった。また、伝導度を向上させることで、Si表面の酸化をある程度抑制できるものと考えられる。

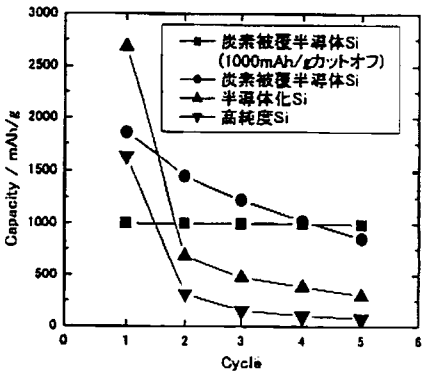

Fig.1 炭素被覆した半導性Siの負極容量の繰り返し特性

New Anodes for Advanced Li Battery

Tetsuya Osaka[a], Hitomi Mukaibo[a, b], Toshiyuki Momma[a, b]

a) *Waseda University, Shinjuku, Tokyo 169-8555, Japan*
b) CREST, Japan Science and Technology Corporation

Secondary batteries have been applied to various devices in all sorts of shape and size for its ability to charge and discharge electric energy. But as the power source of portable electronic devices which is a very progressive market, it is essential that they show higher performance, *i.e.*, higher capacity, longer life, and smaller size.

Compared with other secondary batteries in practical application, Li-ion batteries possess the highest energy density, higher operating voltage, no memory effect, higher stability and longer life. Therefore, it is highly expected that the needs of the market could be satisfied from the improvement of this battery, and many research and development on this theme have been in progress throughout the world.

As one of such researches, Fuji Film Co., Ltd. have filed a patent in 1994 for Sn oxides as a novel anode material for lithium ion batteries with higher theoretical capacity than conventional carbon anodes.[1] However, this material showed two fatal defects; high initial retention and short life. Courtney and Dahn have developed a theory of the reaction mechanism of this material[2] which explained the reason of these two defects.

During the initial cycling, Sn oxide anodes go through a reaction that is shown in figure 1. First, with the charge of the electrode, the irreversible reaction of

$$SnO_2 + 4Li^+ + 4e^- \rightarrow Sn + 2Li_2O \qquad (1)$$

proceeds where the Sn phase and the surrounding inactive Li_2O phase are formed. The Sn phase contributes to the successive charge and discharge. With further charging, the Sn phase alloys with Li^+ (reaction (2)). Only the counter reaction of the reaction (2) proceeds during the following discharge (reaction (2')).

$$Sn + 4.4Li \rightleftarrows Li_{4.4}Sn \qquad (2), (2')$$

The reaction (2) and (2') is repeated during the following charge and discharge.

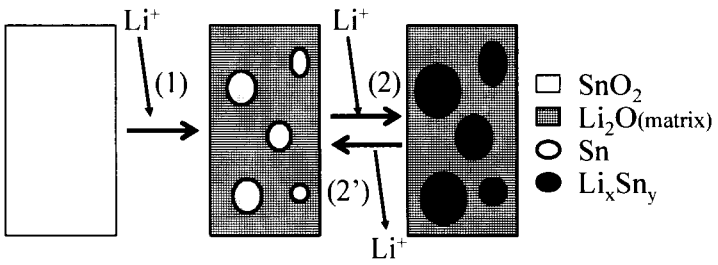

Figure 1. Model of the reaction of Sn oxide with Li^+ during charge and discharge.

The Li^+ consumed during the irreversible reaction (1) stays within the anode for the rest of the cycling, which is the reason why this material shows high initial retention. The short life is due to the volumetric changes in the electrode during

charge and discharge. The alloying and dealloying of Sn and Li (reaction (2) and (2')) is known to show a very large volumetric change. Therefore, when pure Sn is applied as an anode material, the electrode goes through rapid degradation and shows a very short cycle life. The Li_2O formed during the reaction (1) is believed to work as a matrix that eases this degradation of Sn and lengthen the cycle life of the electrode. Nevertheless, it is still short compared to that of the carbon anodes.

Attempts to gain Sn compounds with low initial retention and matrices that are more effective in preventing the degradation of the electrode are one of the major target of the recent studies in this field.[3-19]

We have also been investigating such candidates, and our previous work on SnS_x (x = 1 or 2) has proved this compound to possess a high potential as a novel anode material.[20] Using this compound, we made further investigation to see how the particle size could affect its anode property.[21]

The surface area per unit weight of nano-sized particles is much larger than the bulk of the same material and the former is expected to show higher reactivity (lower reaction resistance) than the latter. Therefore, higher capacity can also be expected from smaller SnS_x particles with its lower reaction resistance of Li^+ and SnS_x resulting in a decreased over voltage of the Sn–Li alloying reaction. Furthermore, the small void between the nano sized particles could work as the matrix to ease the volumetric change of the overall electrode and contribute to the lengthening of the electrode life. It is also presumed that smaller Sn phase would form from smaller SnS_2 particles, and this would also contribute to the longer electrode life for its stress caused by the volume change would be lighter then that of large Sn phases.

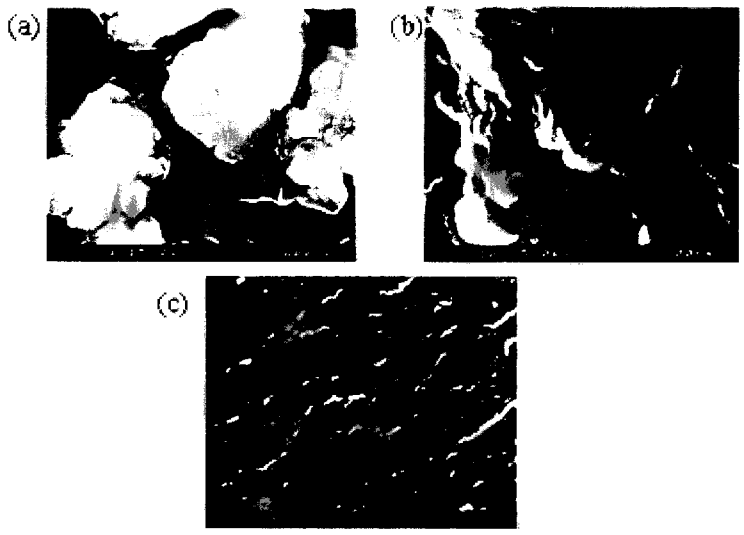

Figure 2. FE-SEM images of SnS_2 synthesized from (a) solution 1/1, (b) solution 1/2, (c) solution 1/3.

We have applied supersonic radiation synthesis, which is known for its simple controllability on the synthesized particle size, as the method to prepare this sample. The samples were synthesized by applying supersonic radiation to the starting solution with different concentration. The starting solution with the highest concentration is defined as the standard of this study, and is named "1/1". The solution with half its

concentration is "1/2", and with third is "1/3". Figure 2 shows the image of each samples obtained from the Field Emission SEM (FE-SEM). From this figure, it can be confirmed that the particle size decreases with lower concentration of the starting solution. By controlling the concentration of the starting solution, we were able to control the size in nano scale. Figure 3 shows the cycle performance of these samples. They are a result of a galvanostatic experiment performed to evaluate the difference caused from particle size. Higher discharge capacity and smaller degradation were seen from smaller SnS_2 particles, indicating that better performance could be gained from smaller particles. Nevertheless, SnSx is still not good enough to meet the high demands of the market and assuming that the selection of adequate matrix is the key to a successful Sn compound anode, we decided to do some research on other Sn compounds.

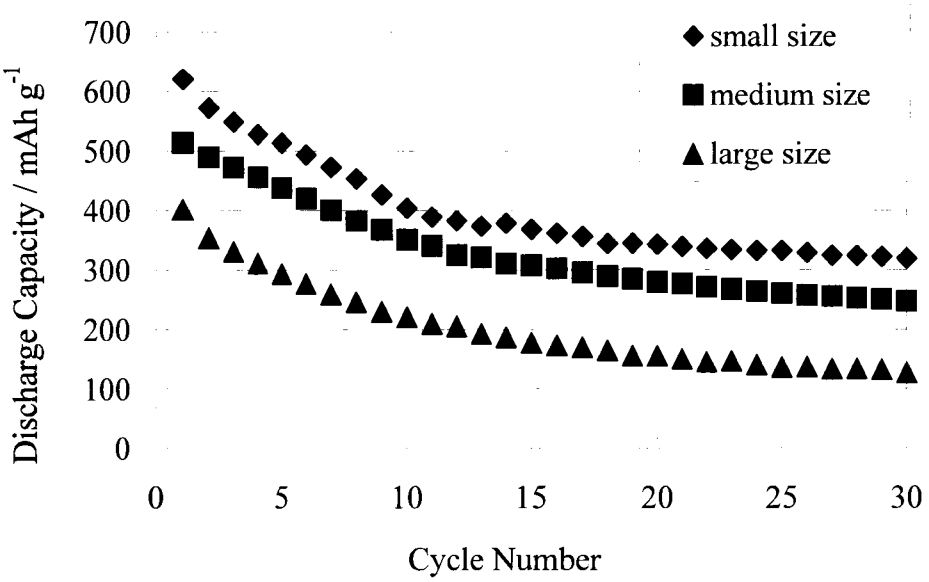

Figure 3. Size dependence of the cycle performance of SnS_2.

Elements that are inactive against Li are assumed to suppress the volume change effectively without much irreversible capacity.[7] Alloying Sn with elements such as Fe,[10-14] Cu,[15-18] Mn,[13,19] and Co[13] has been investigated based on this assumption. Ni is a typical element which does not react with Li and can be expected to serve as an appropriate matrix to improve the cyclability of the electrode without a high initial irreversible capacity. There have been studies on Sn-Ni compounds prepared by ball-milling[7,8] and electroplating,[9] but a capacity exceeding that of the current carbon material has not yet been reported.

We have prepared Sn-Ni alloy thin films with various Ni/Sn ratios by varying the ratio of Ni and Sn ions in the plating bath to obtain a high anode capacity Sn-Ni material.[22] From the results of the ICP, the compositions of our samples were defined as $Sn_{54}Ni_{45}$, $Sn_{62}Ni_{38}$, $Sn_{84}Ni_{16}$, and $Sn_{92}Ni_8$.

FE-SEM images of $Sn_{62}Ni_{38}$ as deposited, after 1st charge until 0V vs. Li/Li^+, and after 1st discharge until 3V vs. Li/Li^+ are shown in Figure 4. It is seen that the

film as deposited consists of aggregates of small grains with the average size of 95nm. After the 1st charge at the constant current, the grain size of the film increased to a size 8 times as large (average size approx. 760nm) as that of the as deposited sample. With further cycling of the sample to the discharge potential of 3V vs. Li/Li^+, the grains of the film decreased in size to an average of 150nm, and they were aggregated forming a complicated three dimensional porous structure. These changes in the electrode structure at different states of the initial cycle may be due to the insertion and desorption of Li.

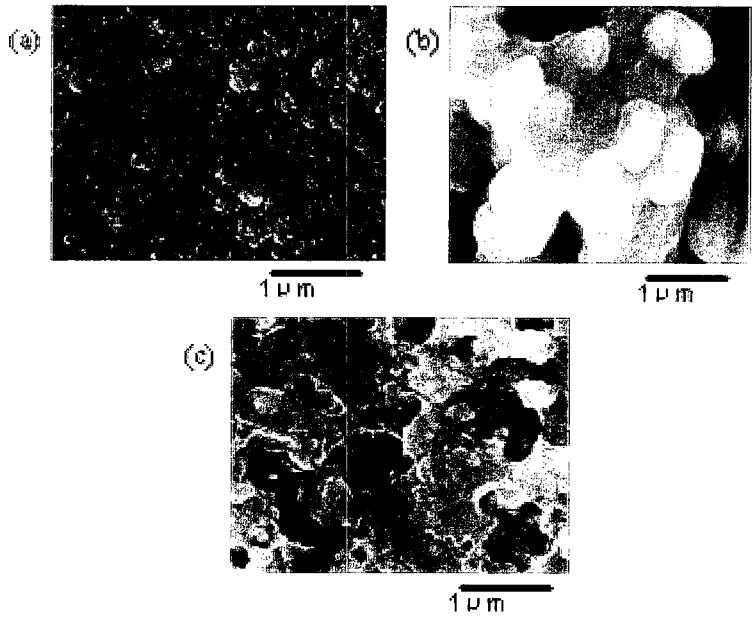

Figure 4. FE-SEM images of 62 atom% Sn (a) as deposited, (b) after 1st charge, and (c) after 1st discharge.

Figure 5 shows cycle performance of the four samples. The cycle performance of $Sn_{62}Ni_{38}$ was outstanding among them, showing the highest discharge capacity of *ca.* 650mAh/g at the 70th cycle. The $Sn_{54}Ni_{46}$, $Sn_{84}Ni_{16}$ and $Sn_{92}Ni_8$ samples showed similar cycle characteristics after the second cycle with a discharge capacity of about 300mAh/g. The samples showed a stable coulombic efficiency after 2 to 3 cycles. The magnitude of the sharp drop in discharge capacity after the first cycle was greater for the higher Sn content samples which may indicate the deterioration of the pure Sn phase which was confirmed from the XRD analysis only in $Sn_{84}Ni_{16}$ and $Sn_{92}Ni_8$. A unique characteristic observed in Figure 5 is the increase in capacity with the number of cycles for all samples. The $Sn_{62}Ni_{38}$ showed the highest capacity increase of all, which was approximately 140 mAh/g. This may be due to the changes in surface condition accompanying a volume change during cycling (as seen in Figure 4), which should lower the resistance to Li diffusion within the sample. Overall, the cyclability of each sample was adequate after the first several cycles, indicating the effectiveness of the Ni matrix.

We would like to conclude that the $Sn_{62}Ni_{38}$ has the most appropriate

composition and structure that lead to the small initial degradation, good cycleability and the highest capacity.

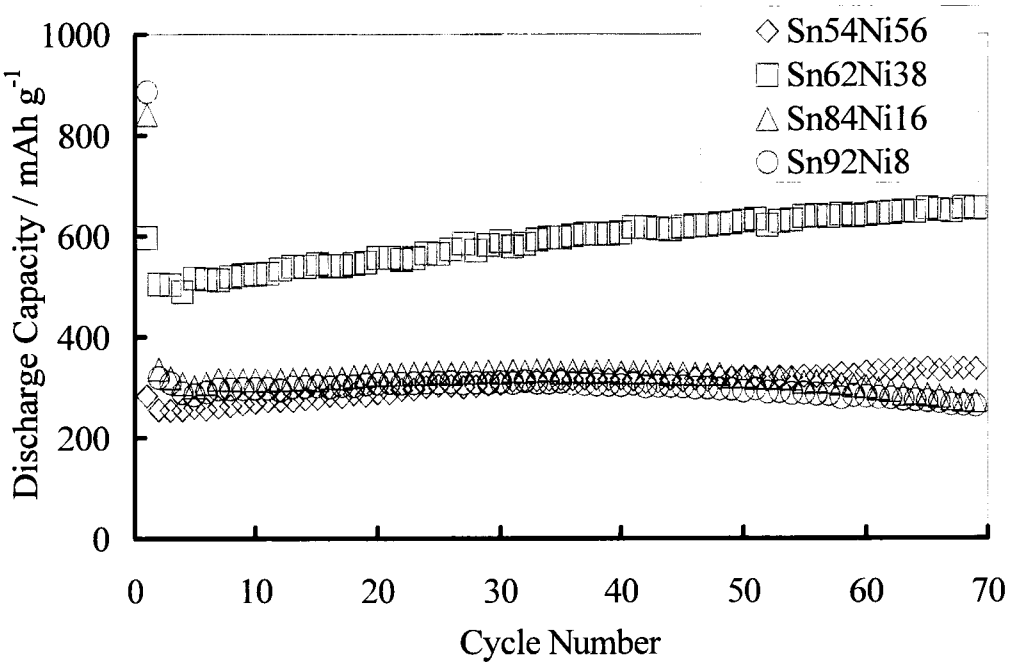

Figure 5. Cycle performance of electrodes with various Ni/Sn ratios.

Acknowledgements

This work is supported in part by a Grant-in-Aid for Center of Excellence (COE) Research "Molecular Nano Engineering", and the 21st Century COE Program "Practical Nano-Chemistry" from the Ministry of Education, Culture, Sports, Science and Technology.

References

1. Fuji Photo Film Co., *Ltd., Euro. Pat.* 0,651,450, A1 (1995).
2. I.A. Courtney and J.R. Dahn, *J. Electrochem. Soc.*, **144**, 2045 (1997).
3. I.A. Courtney and J.R. Dahn, *J. Electrochem. Soc.*, **144**, 2943 (1997).
4. J. Morales and L. Sanchez, *J. Electrochem. Soc.*, **146**, 1640 (1999).
5. J. Santos-Pena, T. Brousse and D.M. Schleich, *Solid State Ionics*, **135**, 87 (2000).
6. X. Zhang, C. Wang, A.J. Appleby and F.E. Little, *J. Power Sources*, **109**, 136 (2002).
7. J. Ahn, Y. Kim, G. Wang, M. Lindsay, H.K. Liu and S. Dou, *Mater. Trans.*, **43**, 63 (2002).
8. G.M. Ehrlich, C. Durand, X. Chen, T.A. Hugener, F. Spiess and S.L. Suib, *J. Electrochem. Soc.*, **147**, 886 (2000).
9. O. Crosnier, T. Brousse, X. Devaux, P. Fragnaud and D.M. Schleich, *J. Power Sources*, **94**, 169 (2001).
10. O. Mao, R.L. Turner, I.A. Courtney, B.D. Fredericksen, M.I. Buckett, L.J. Krause, and J.R. Dahn, *Electrochem. Solid-State Lett.*, **2**, 3 (1999).

11. O. Mao, R.A. Dunlap and J.R. Dahn, *J. Electrochem. Soc.*, **146**, 405 (1999).
12. O. Mao, R.A. Dunlap and J.R. Dahn, *J. Electrochem. Soc.*, **146**, 414 (1999).
13. O. Mao, R.A. Dunlap and J.R. Dahn, *J. Electrochem. Soc.*, **146**, 423 (1999).
14. D. Larcher, L.Y. Beaulieu, O. Mao, A.E. George and J.R. Dahn, *J. Electrochem. Soc.*, **147**, 1703 (2000).
15. K.D. Kepler, J.T. Vaughey and M.M. Thackeray, *Electrochem. Solid-State Lett.*, **2**, 307 (1999).
16. D. Larcher, L.Y. Beaulieu, D.D. MacNeil and J.R. Dahn, *J. Electrochem. Soc.*, **147**, 1658 (2000).
17. G.X. Wang, L. Sun, D.H. Bradhurst, S.X. Dou and H.K. Liu, *J. Alloy Compd.*, **299**, L12 (2000).
18. N. Tamura, R. Ohshita, M. Fujimoto, S. Fujitani, M. Kamino and I. Yonezu, *J. Power Sources*, **107**, 48 (2002).
19. L. Beaulieu, D. Larcher, R.A. Dunlap and J.R. Dahn, *J. Alloys Compd.*, **297**, 122 (2000).
20. T. Momma, N. Shiraishi, A. Yoshizawa, T. Osaka, A. Gedanken, J. Zhu and L. Sominski, *J. Power Sources*, **97-98**, 198 (2001).
21. H. Mukaibo, A. Yoshizawa, T. Momma and T. Osaka, *J. Power Sources*, **119-121**, 60 (2003).
22. H. Mukaibo, T. Sumi, T. Yokoshima, T. Momma, and T.Osaka, *Electrochem. Solid-State Lett.*, **6 -10**, 1 (2003)

Electrochemical and Solid-State Letters, **6** (10) A218-A220 (2003)
0013-4651/2003/6(10)/A218/3/$7.00 © The Electrochemical Society, Inc.

Electrodeposited Sn-Ni Alloy Film as a High Capacity Anode Material for Lithium-Ion Secondary Batteries

Hitomi Mukaibo,[a,b] Tomohide Sumi,[a] Tokihiko Yokoshima,[a] Toshiyuki Momma,[a,b,*] and Tetsuya Osaka[a,,z]**

[a]*Waseda University, Shinjuku, Tokyo 169-8555, Japan*
[b]*CREST, Japan Science and Technology Corporation, Tokyo 102-8666, Japan*

Thin Sn-Ni alloy films containing various Sn/Ni ratios were prepared by electrodeposition and characterized as lithium-ion secondary battery anodes. The initial drop in discharge capacity varied with the Sn content of the sample; *i.e.*, for samples with 54 atom % Sn and 62 atom % Sn, the drop was less than 100 mAh/g, whereas for those with 84 atom % Sn and 92 atom % Sn, the drop exceeded 500 mAh/g. Among these thin films, the 62 atom % Sn film showed the highest reversible capacity of *ca.* 650 mAh/g at about the 70th cycle, whereas the other samples (54 atom % Sn, 84 atom % Sn, 92 atom % Sn) showed a capacity of 300 mAh/g.
© 2003 The Electrochemical Society. [DOI: 10.1149/1.1602331] All rights reserved.

Manuscript received December 30, 2002. Available electronically August 4, 2003.

With the advancement of portable electronic devices, further improvement of their power sources is required. Li-ion batteries possess the highest energy density among batteries in practical use, and the development of an improved anode material is considered as a breakthrough to meet such demand.

Presently, carbon is used as the anode material for Li-ion batteries, and it shows a capacity close to its theoretical value of 372 mAh/g. In 1994, Fuji Film Co., Ltd. filed a patent for Sn oxides as a novel anode material for lithium-ion batteries with a higher theoretical capacity than carbon.[1] However, this material showed high retention, which was a fatal defect. Courtney and Dahn have developed a theory for the reaction mechanism of such materials.[2] Many attempts have been made to develop other Sn compounds in search of a suitable matrix that leads to high cyclability.[3-19] We are also investigating such candidates, and our previous work on SnS_2 has proved this compound to have high potential as a novel anode material.[20] The effect of particle size has also been studied with this material. A matrix consisting of nanoparticles should have spaces between the particles, which may absorb the problematic volume change resulting from the reaction of Sn with Li during cycling. The large surface area of nanoparticles should also ease the stress accompanying such a volume change. Our results have shown that by controlling the size of nanoparticles, improved cyclability can be achieved.[21]

The selection of an adequate matrix is the key to a successful Sn compound anode. Elements that are inactive against Li are assumed to suppress the volume change effectively without much irreversible capacity.[7] The use of Sn compounds with elements such as Fe,[10-14] Cu,[15-18] Mn,[13,19] and Co[13] has been investigated based on this assumption. Ni is a typical element which does not react with Li. Therefore, this element can be expected to serve as an appropriate matrix to improve the cyclability of the electrode without a high initial irreversible capacity. There have been studies on Sn-Ni compounds prepared by ballmilling[7,8] and electroplating,[9] but a capacity exceeding that of the current carbon material has not yet been reported. In this study, Sn-Ni alloy thin films with various Ni/Sn ratios were prepared by varying the ratio of Ni and Sn ions in the plating bath to obtain a high anode capacity Sn-Ni material.

Experimental

The Sn-Ni thin-film alloy used here was prepared by electrodeposition.[22] Thin films containing different Ni/Sn ratios were prepared on Cu sheets from the baths listed in Table I. The samples were designated in terms of the atomic percentage of Sn in the deposited film, which was determined by inductively coupled plasma atomic emission spectroscopy (ICP). The samples obtained were as follows: 54 atom % Sn, 62 atom % Sn, 84 atom % Sn, and 92 atom % Sn. The deposition time was 5 min for most samples except for those prepared for X-ray diffraction (XRD) analysis, which were deposited for 1 h to obtain higher peak intensities and to suppress signals from the Cu sheet. The XRD apparatus using Cu Kα radiation was equipped with the capability for evaluating structural differences between the thin films with different Ni/Sn compositions. Electrochemical measurements were performed in conventional glass cells with two pieces of lithium foil as counter and reference electrodes, and 1 M $LiClO_4$/ethylene carbonate (EC) + propylene carbonate (PC) (1:1 vol %) as the organic electrolyte. Cyclic voltammetry (CV) was carried out in the potential range of open-circuit potential (OCP) to 0 V *vs.* Li/Li^+, at a scan rate of 0.02 mV/s. The cyclability of the cells was evaluated by galvanostatic charge-discharge tests in the potential range of 0 to 3 V *vs.* Li/Li^+. Both charge and discharge were carried out at a current density of 50 mA/g of Sn-Ni alloy. A field emission scanning electron microscope (FESEM) was used to observe the morphology of the samples.

Results and Discussion

XRD was used to evaluate the structural differences between the samples with various compositional ratios of Ni to Sn. XRD patterns of samples obtained after 1 h electrodeposition were compared with those obtained after 5 min deposition, and it was confirmed that there was no significant difference between the two samples except for signal intensities. Electrodeposited Sn-Ni film forms metastable phases that do not appear in the equilibrium phase diagram. Watanabe *et al.* carried out a detailed study of the structure of Sn-Ni films.[23] The peak assignments made for our samples shown in Fig. 1 are based on the result of their work. The metastable phase M1 is a NiSn phase with a composition ratio of almost 50:50, and the metastable phase M2 is a phase where Ni is melted into Sn crystals. Samples with higher Sn contents were confirmed to have a structure similar to that of 100 atom % Sn. It is assumed that these electrodes with a high Sn content may show electrode properties similar to those of pure Sn electrodes, which means a high initial capacity, but a poor cyclability resulting from electrode degradation.

The first CV cycles recorded with four different samples are shown in Fig. 2. It has been reported that in 100 atom % Sn, three anodic peaks appear at 0.69, 0.61, and 0.45 V *vs.* Li/Li^+ in the anodic scan, and four peaks at 0.43, 0.57, 0.71, and 0.78 V *vs.* Li/Li^+ in the cathodic scan.[2] The high Sn content films with pure Sn phase showed CV characteristics close to those of pure Sn. This result is consistent with the XRD result.

FESEM images of 62 atom % Sn as deposited, after first charge until 0 V *vs.* Li/Li^+, and after first discharge until 3 V *vs.* Li/Li^+ are

* Electrochemical Society Active Member.
** Electrochemical Society Fellow.
z E-mail: osakatet@waseda.jp

Table I. Bath compositions and operating conditions for preparing Sn-Ni Alloy films.

Sn content of samples (atom % Sn)	54	62	84	92
$NiCl_2 \cdot 6H_2O$ (mol L^{-1})	0.125	0.075	0.063	0.050
$SnCl_2 \cdot 2H_2O$ (mol L^{-1})	0.125	0.175	0.187	0.200
Potassium pyrophosphate ($K_4P_2O_7$) (mol L^{-1})	0.500	0.500	0.500	0.500
Glycine (H_2NCH_2COOH) (mol L^{-1})	0.250	0.125	0.100	0.075
Ammonium hydroxide (NH_4OH) (mL L^{-1})	5	5	5	5

Current density: 5 mA/cm^2.
Bath temperature: 50°C.
Agitation by magnetic stirrer.

shown in Fig. 3. It is seen that the film as deposited consists of aggregates of small grains with an average size of 95 nm. After the first charge at a constant current, the grain size of the film increased to eight times as large (average size approx. 760 nm) as that of the as-deposited sample. With further cycling of the sample to the discharge potential of 3 V *vs.* Li/Li^+, the grains of the film decreased to an average of 150 nm, and they were aggregated to form a complicated three-dimensional porous structure. These changes in the electrode structure at different states of the initial cycle may be due to the insertion and desorption of Li.

Figure 4 shows cycle performance of the electrodes with various Ni/Sn ratios. The cycle performance of 62 atom % Sn was outstanding among the four samples, showing the highest discharge capacity of *ca.* 650 mAh/g at about the 70th cycle. The 54 atom % Sn, 84 atom % Sn, and 92 atom % Sn samples showed similar cycle characteristics after the second cycle with a discharge capacity of about 300 mAh/g. The initial coulombic efficiencies of the samples were as follows: 54 atom % Sn = 84.8%, 62 atom % Sn = 105.0%, 84 atom % Sn = 121.8%, and 92 atom % Sn = 121.7%. The coulombic efficiency exceeding 100% may be due to a side reaction (*e.g.*, the elution of impurities within samples). The samples showed a stable coulombic efficiency after two to three cycles, and the efficiencies after the 69th cycle were as follows: 54 atom % Sn = 92.2%, 62 atom % Sn = 99.3%, 84 atom % Sn = 97.4%, and 92 atom % Sn = 96.0%. The magnitude of the sharp drop in discharge capacity after the first cycle was greater for the higher Sn content samples. The fall of capacity of the 84 atom % Sn (after 40 cycles) and 92 atom % Sn (after 35 cycles) samples may indicate the deterioration of the pure Sn phase in those electrodes. This result is consistent with our assumption that the samples with a high Sn content are easier to degradate. A unique characteristic observed in Fig. 4 is the increase in capacity with the number of cycles for all samples. The 62 atom % Sn showed the highest capacity increase of all, which was approximately 140 mAh/g. This may be due to the changes in surface condition accompanying a volume change during cycling (as seen in Fig. 3), which should lower the resistance to Li diffusion within the sample. Overall, the cyclability of each sample

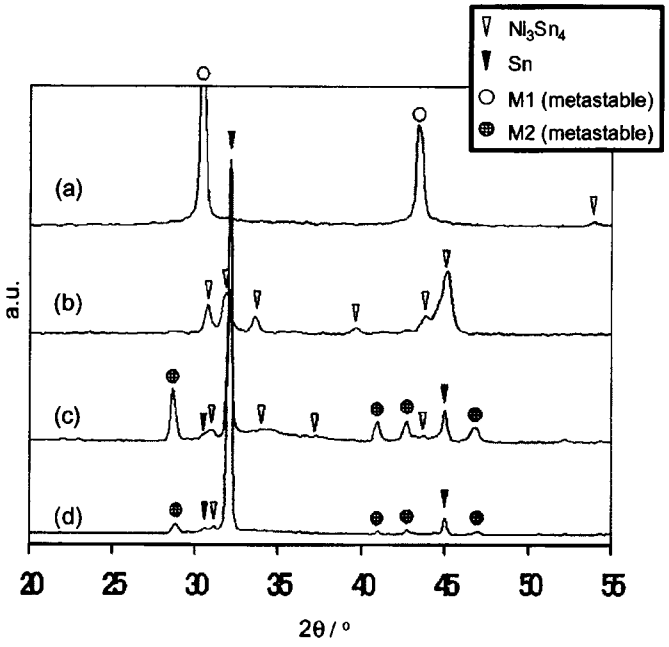

Figure 1. XRD patterns of samples obtained by 1 h deposition (a) 54 atom % Sn, (b) 62 atom % Sn, (c) 84 atom % Sn, and (d) 92 atom % Sn.

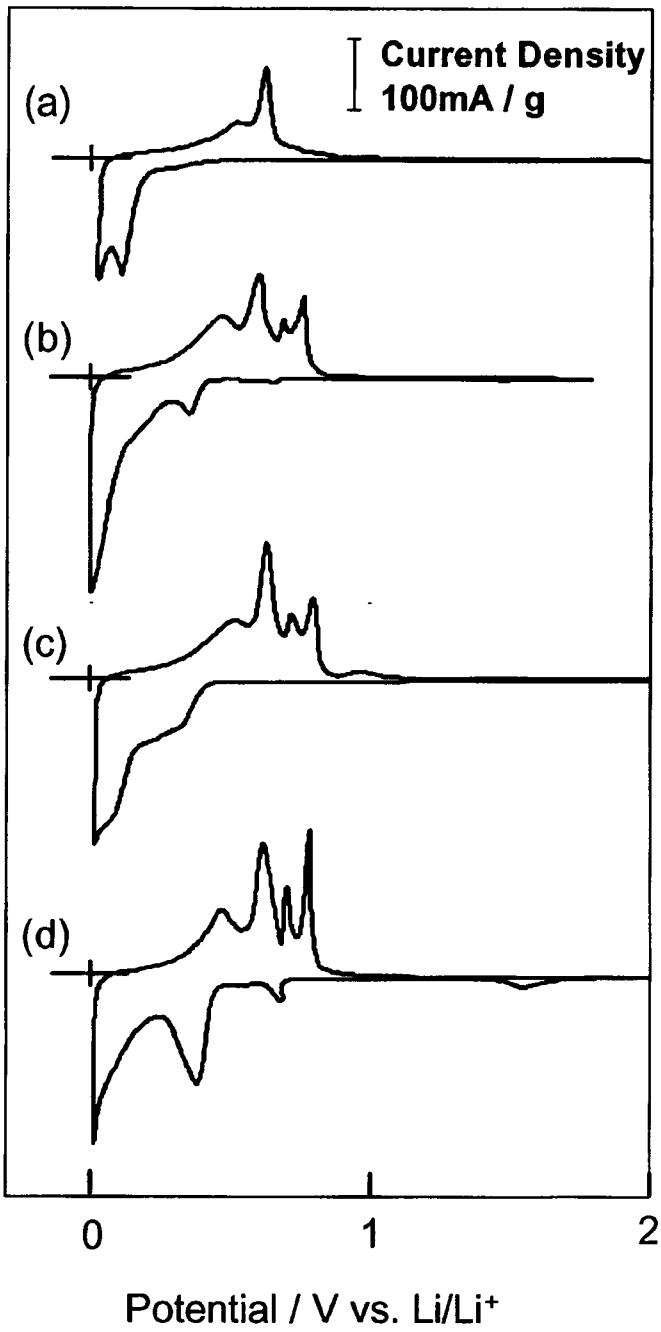

Figure 2. CVs of (a) 54 atom % Sn, (b) 62 atom % Sn, (c) 84 atom % Sn, and (d) 92 atom % Sn in the potential range of OCP to 0 V *vs.* Li/Li^+ at the scan rate of 0.02 mV/s in 1 M $LiClO_4$ /EC + PC (1:1 vol %) organic electrolyte.

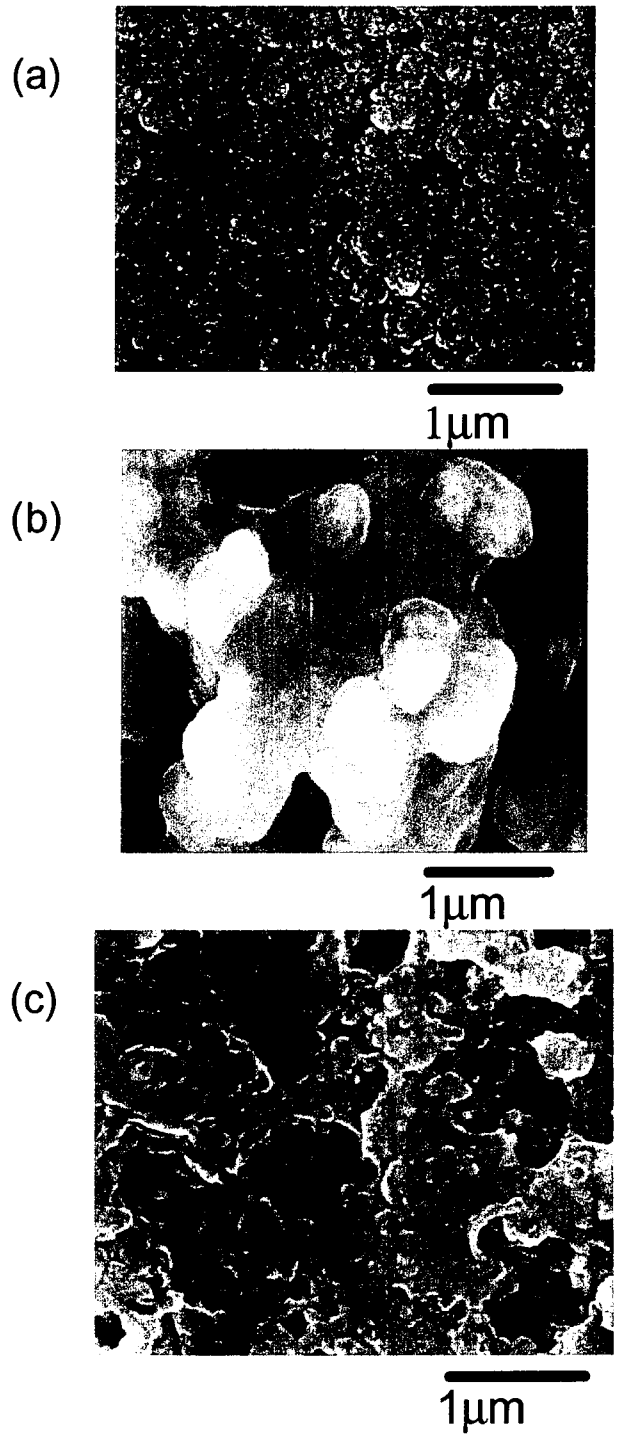

Figure 3. FESEM images of 62 atom % Sn electrode (a) as deposited, (b) after first charge until 0 V *vs.* Li/Li^+, and (c) after first discharge until 3 V *vs.* Li/Li^+. Charge and discharge were performed at a constant current density of 50 mA/g.

was adequate after the first several cycles, indicating the effectiveness of the Ni matrix. It is concluded that the 62 atom % Sn is the most appropriate composition with a structure leading to a small initial degradation, good cyclability, and the highest capacity.

Conclusions

Electrodeposited Sn-Ni films with various Sn-Ni composition ratios were prepared to evaluate their characteristics as lithium-ion battery anodes. The cycle performance of 62 atom % Sn was most

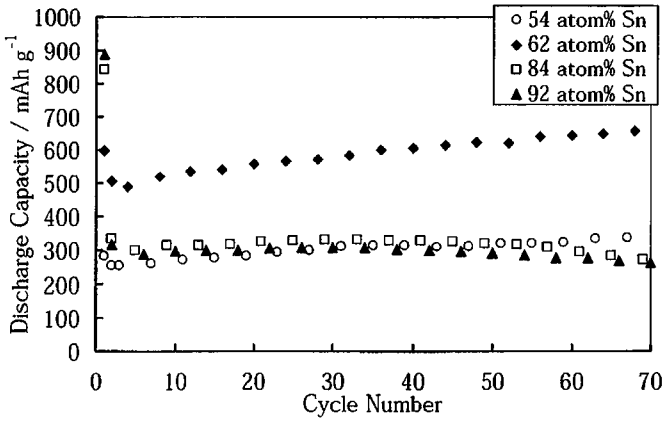

Figure 4. Cycle performance of electrodes with various Ni/Sn ratios at a constant current density of 50 mA/g in the potential range of 0 to 3 V *vs.* Li/Li^+ in 1 M $LiClO_4$/EC + PC (1:1 vol %) organic electrolyte.

outstanding, showing the highest discharge capacity of *ca.* 650 mAh/g. The other samples showed similar cycle characteristics after the second cycle with a discharge capacity of about 300 mAh/g. Although they showed an initial drop in discharge capacity, the overall cyclability of all samples was adequate after the first several cycles, indicating the effectiveness of the Ni matrix. It is concluded that the 62 atom % Sn is the most appropriate composition and possesses a micromatrix structure that leads to a small initial degradation, good cyclability, and the highest discharge capacity.

Acknowledgment

This work is supported in part by a Grant-in-Aid for Center of Excellence (COE) Research "Molecular Nano Engineering" and the 21st century COE Program "Practical Nano Chemistry" from the Ministry of Education, Culture, Sports, Science and Technology.

Waseda University assisted in meeting the publication costs of this article.

References

1. Fuji Photo Film Co., Ltd., Eu. Pat. 0,651,450, A1 (1995).
2. I. A. Courtney and J. R. Dahn, *J. Electrochem. Soc.*, **144**, 2045 (1997).
3. I. A. Courtney and J. R. Dahn, *J. Electrochem. Soc.*, **144**, 2943 (1997).
4. J. Morales and L. Sanchez, *J. Electrochem. Soc.*, **146**, 1640 (1999).
5. J. Santos-Pena, T. Brousse, and D. M. Schleich, *Solid State Ionics*, **135**, 87 (2000).
6. X. Zhang, C. Wang, A. J. Appleby, and F. E. Little, *J. Power Sources*, **109**, 136 (2002).
7. J. Ahn, Y. Kim, G. Wang, M. Lindsay, H. K. Liu, and S. Dou, *Mater. Trans., JIM*, **43**, 63 (2002).
8. G. M. Ehrlich, C. Durand, X. Chen, T. A. Hugener, F. Spiess, and S. L. Suib, *J. Electrochem. Soc.*, **147**, 886 (2000).
9. O. Crosnier, T. Brousse, X. Devaux, P. Fragnaud, and D. M. Schleich, *J. Power Sources*, **94**, 169 (2001).
10. O. Mao, R. L. Turner, I. A. Courtney, B. D. Fredericksen, M. I. Buckett, L. J. Krause, and J. R. Dahn, *Electrochem. Solid-State Lett.*, **2**, 3 (1999).
11. O. Mao, R. A. Dunlap, and J. R. Dahn, *J. Electrochem. Soc.*, **146**, 405 (1999).
12. O. Mao, R. A. Dunlap, and J. R. Dahn, *J. Electrochem. Soc.*, **146**, 414 (1999).
13. O. Mao, R. A. Dunlap, and J. R. Dahn, *J. Electrochem. Soc.*, **146**, 423 (1999).
14. D. Larcher, L. Y. Beaulieu, O. Mao, A. E. George, and J. R. Dahn, *J. Electrochem. Soc.*, **147**, 1703 (2000).
15. K. D. Kepler, J. T. Vaughey, and M. M. Thackeray, *Electrochem. Solid-State Lett.*, **2**, 307 (1999).
16. D. Larcher, L. Y. Beaulieu, D. D. MacNeil, and J. R. Dahn, *J. Electrochem. Soc.*, **147**, 1658 (2000).
17. G. X. Wang, L. Sun, D. H. Bradhurst, S. X. Dou, and H. K. Liu, *J. Alloys Compd.*, **299**, L12 (2000).
18. N. Tamura, R. Ohshita, M. Fujimoto, S. Fujitani, M. Kamino, and I. Yonezu, *J. Power Sources*, **107**, 48 (2002).
19. L. Beaulieu, D. Larcher, R. A. Dunlap, and J. R. Dahn, *J. Alloys Compd.*, **297**, 122 (2000).
20. T. Momma, N. Shiraishi, A. Yoshizawa, T. Osaka, A. Gedanken, J. Zhu, and L. Sominski, *J. Power Sources*, **97-98**, 198 (2001).
21. H. Mukaibo, A. Yoshizawa, T. Momma, and T. Osaka, *J. Power Sources*, **119-121**, 60 (2003).
22. A. Ito and H. Enomoto, *J. Met. Finish. Soc. Jpn.*, **36**, 466 (1985).
23. T. Watanabe, T. Hirose, K. Arai, and M. Chikazawa, *J. Jpn. Inst. Met.*, **63**, 496 (1999).

Lithium Ion Secondary Battery Anode

T. Momma[a,c)], H. Mukaibo[a)], T. Sumi[a)], T. Yokoshima[b)], T. Osaka[a)]

[a]Graduate School of Sci. and Eng., Waseda University,
[b]Advanced Research Institute for Sci. & Eng.,
Waseda Universtity,
3-4-1, Okubo, Shinjuku-Ku, Tokyo, 169-8555, Japan
[c]CREST, Japan Science and Technology Corporation

Li-ion batteries possess the highest energy density among the practical batteries, and the development of its anode material is considered as a breakthrough to meet the demands for power sources with higher performance for portable electronic devices.

Sn anode shows a theoretical capacity of 994 mAh/g, which exceeds that of the conventional carbon anode. However, it suffers a large volume change during cycling, which results in rapid electrode degradation. A selection of adequate matrix to ease such stress and lengthen its electrode life is one of the key to gain a successful novel anode material. Elements that are inactive against Li (such as Ni) are assumed to suppress the volume change effectively without much irreversible capacity [1]. There have been studies on Sn-Ni compounds [1, 2, 3], but a capacity exceeding that of the current carbon material has not yet been reported. In the present study, Sn-Ni alloy thin films with various Ni:Sn ratios were prepared to obtain a high-capacity long-life anode material.

The Sn-Ni thin films used in this study were prepared by electrodeposition [4] on Cu sheet from potassium pyrophosphate baths at 50 °C. Each film was deposited for 5 min with the current density of 5mA cm^{-2}.

The compositions of the samples were determined by Inductively Coupled Plasma Atomic Emission Spectroscopy (ICP-AES). The anode properties were evaluated from electrochemical measurements performed in conventional glass cells with two pieces of Li foils as counter and reference electrodes, and 1M $LiClO_4$ / ethylene carbonate (EC) + propylene carbonate (PC) (1:1 vol%) as the organic electrolyte. The cycleability of the cells was evaluated by galvanostatic charge-discharge tests, in the potential range of 0 to 3 V vs. Li/Li^+. Both charge and discharge were carried out at the current density of 50 mA g^{-1} of Sn-Ni alloy. A Field Emission-Scanning Electron Microscope (FE-SEM) was used to observe the morphology of the samples.

From the FE-SEM (Fig. 1) images, the change in the electrode surface as it is charged and discharged as the anode of Li ion battery can be observed. Increase in the grain size of the film can be confirmed after the initial charge, whereas the following discharge results in the shrinkage of the grains and their aggregation, forming a complicated three dimensional porous structure. Figure 2 shows the cycle performances of various NiSn films with different composition. This result confirms that the NiSn alloy has the potential ability to perform as the anode of Li ion battery. Among them, $Ni_{38}Sn_{62}$ showed the highest discharge capacity of ca. 650mAh/g at about the 70th cycle.

This work is supported in part by a Grant-in-Aid for Center of Excellence (COE) Research "Molecular Nano-Engineering", and the 21st Century COE Program "Practical Nano-Chemistry" from the

REFERENCES

1. J. Ahn, Y. Kim, G. Wang, M. Lindsay, H.K. Liu and S. Dou, Mater. Trans., **43**, 63 (2002).
2. G.M. Ehrlich, C. Durand, X. Chen, T.A. Hugener, F. Spiess and S.L. Suib, J. Electrochem. Soc., **147**, 886 (2000).
3. O. Crosnier, T. Brousse, X. Devaux, P. Fragnaud and D.M. Schleich, J. Power Sources, **94**, 169 (2001).
4. A. Ito and H. Enomoto, J. Met. Fin. Soc. Jpn., **36**, 466 (1985).

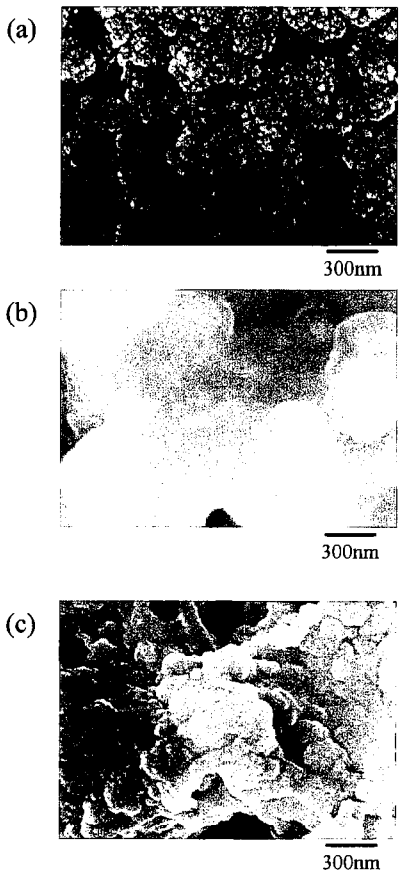

Figure 1 FE-SEM images of $Ni_{38}Sn_{62}$ electrode (a) as deposited, (b) after 1st charge until 0 V vs. Li/Li^+, and (c) after 1st discharge until 3 V vs. Li/Li^+. Charge and discharge were performed at the constant current density of 50 mA g^{-1}.

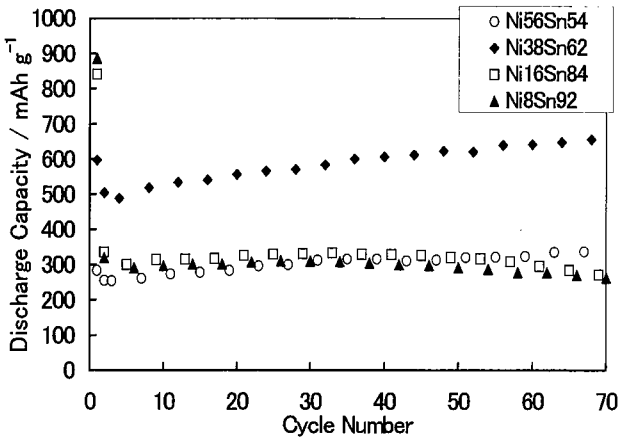

Figure 2 Cycle performance of electrodes with various Ni:Sn ratios at the constant current density of 50mA g^{-1} in the potential range of 0 to 3 V vs. Li/Li^+ in 1M $LiClO_4$ / EC + PC (1:1 vol%) organic electrolyte.

第44回電池討論会講演要旨集, pp. 432-433 (2003).

リチウムイオン二次電池用 Sn-Ni 合金負極の充放電特性

(早大理工[*]・早大院理工[**]・理工総研[***]・CREST, JST[****])
○向坊仁美[*,****], 和田安正[**], 横島時彦[***], Mohamedi Mohamed[*],
門間聰之[*,****], 逢坂哲彌[*,**,***]

Charge-Discharge Characteristics of Sn-Ni Alloy Anodes for Lithium Ion Secondary Battery

Hitomi Mukaibo[*,****], Yasumasa Wada[**], Tokihiko Yokoshima[***], Mohamedi Mohamed[*],
Toshiyuki Momma[*,****], Tetsuya Osaka[*,**,***]
*~***Waseda University, 3-4-1 Okubo Shinjuku, Tokyo 169-8555, Japan
****CREST, JST

We have shown in our previous study that Sn-Ni alloy, prepared by electrodeposition, shows good anode property with the discharge capacity above 600mAh/g after 70 cycles. In this study, the Sn-Ni alloy anode was cycled to different charged / discharged states, and the changes caused to the structure, morphology and electrochemical properties by the Li insertion and desorption were examined. Influence of Sn composition on the cycling performance will also be discussed.

1．緒言

Li と可逆的に合金化，脱合金化する Sn は新規高容量負極材料として期待されているが，充放電の際の大きな体積変化により電極内に大きな負荷がかかるため寿命が短い．今までに Sn 元素の周りに他元素を共存させることにより，サイクル特性が向上したという報告がされている[1]．この他元素として Li と反応しない金属元素を用いた Sn 系合金は初期の不可逆容量が低く高容量で長寿命な負極材料が得られると考えられる[2]．Ni は Sn と合金化させる手法が既に確立されており扱い易く、過去に Sn-Ni 合金を作製した例がいくつか報告されている[2-4]．しかし、初期不可逆容量の低減は実現されたものの、短命・低容量などの問題点を抱えていたためまだ新規負極材料へのブレイクスルーとはなっていない．過去の検討で我々は電析の作製時の条件を変えることにより Sn の含有量を制御した Sn-Ni 合金が 70 サイクル後でも 600mAh/g を超える高容量を保持している，良好な負極特性を有することを示した[5]．本報告ではこの材料の充放電時に起きている変化についてより詳細な知見を得るため，電極を充放電させたときの形態・構造・電気化学的特性の変化について検討を行い解析した結果，および考察を報告する．

2．実験方法

Sn-Ni 薄膜は工業化されているピロリン酸浴[6]を用いて Cu 基板上に電析させることにより作製し，作用極とした．この際，浴中の $NiCl_2 \cdot 6H_2O$ と $SnCl_2 \cdot 2H_2O$ の比や電析時間を変化させることにより膜中の Sn/Ni 比を制御した[5]．セルは，Sn-Ni 作用極，補助電極(= Li)，及び基準電極(= Li)を用い，電解液を 1M - $LiClO_4$ / EC+PC (1:1 vol.) とした三極式セルになっている．電気化学的特性の評価は Ar 雰囲気中でセルを組み密閉後，Ar 雰囲気中，あるいは露点-60℃以下のドライルーム中にて定電流充放電試

験機を用いて行った．この際の実験条件は電位範囲：0.01～2V vs. Li/Li^+，電流密度：50mA/g である．適当な電位まで充放電をした試料は XRD (Cu Kα線)による構造解析に加え，形態，電気化学的特性についての解析も行った．

3．結果及び考察

Figure 1にSn : Ni比を変えて作製したサンプルの中で最も良好なサイクル特性を示した$Sn_{62}Ni_{38}$の初期サイクル時の構造変化をXRDにより測定した結果を示す．ここで，◇ で表されているピークはブロードであり x, y 値が同定できなかった為 Li_xSn_y と表記した．

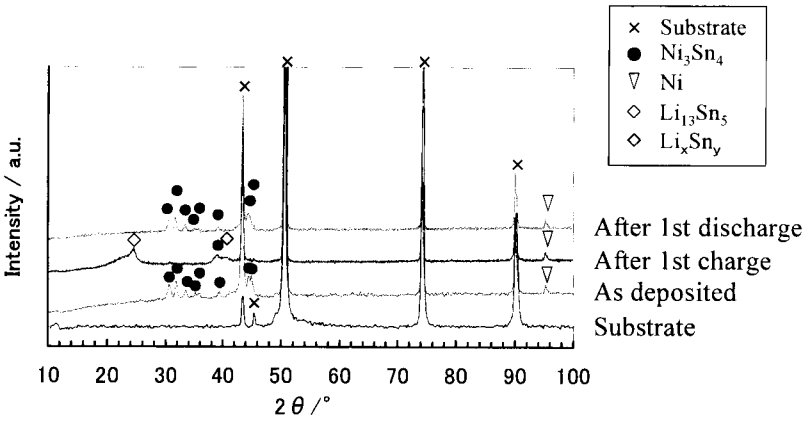

Fig. 1 Changes in the XRD (Cu K_α radiation) patterns during the initial cycling of electrodeposited $Sn_{62}Ni_{38}$ as Li ion battery anode.

Figure 1より，Cuの基板上に析出させただけの段階ではNi_3Sn_4とNiに帰属されるピークしか見られない．充電をすることにより38° 付近以外のNi_3Sn_4のピークはすべて消え，その代わりにLi-Sn合金相のピークが新たに確認された．続く放電後のパターンでは合金相のピークは全て消え，再び充放電前と同様なNi_3Sn_4とNiに帰属されるピークのみの状態に戻ることが確認された．充放電のサイクルを通してNi相のピークに変化は確認されなかったことから，この相は充放電時に変化はしないものであると考えられる．

以上より，$Sn_{62}Ni_{38}$はNi_3Sn_4相とNi相を含み，充放電にはNi_3Sn_4相のみが寄与していることが示唆された．反応としてはNi_3Sn_4相のSnがLiと合金化・脱合金化反応を繰り返しているものと考えられる．

本報告では更に他の組成の電極の構造変化，および表面形態の変化，電気化学的特性の変化について検討した結果について報告する．

謝辞

本研究は一部、文部科学省特別推進研究 (COE)「分子ナノ工学」の助成を受け，21COEプログラム「実践的ナノ化学教育研究拠点」にて行われた．

参考文献

1) M. Winter, and J. O. Besenhard, *Electrochimica Acta*, **45**, 31 (1999).
2) J. Ahn, Y. Kim, G. Wang, M. Lindsay, H. K. Liu, and S. Dou, *Mater. Trans., JIM,* **43**, 63 (2002).
3) G. M. Ehrlich, C. Durand, X. Chen, T. A. Hugener, F. Spiess, and S. L. Suib, *J.Electrochem. Soc.*, **147**, 886 (2000).
4) O. Crosnier, T. Brousse, X. Devaux, P. Fragnaud, and D. M. Schleich, *J. Power Sources*, **94**, 169 (2001).
5) H. Mukaibo, T. Sumi, T. Yokoshima, T. Momma, and T. Osaka, *Electrochem. Solid-State Lett.*, **6,** A218 (2003).
6) 伊崎　昌伸，榎本　英彦，*金属表面技術*, **36,** 466 (1985).

—Article—

Characteristics of Interpenetrated Polymer Network System made of Polyethylene Oxide-$LiBF_4$ Complex and Polystyrene as the Electrolyte for Lithium Secondary Battery

Toshiyuki MOMMA,[a,c] Hiroaki ITO,[a] Hiroki NARA,[a] Hitomi MUKAIBO,[a,c] Stefano PASSERINI,[b] and Tetsuya OSAKA[a]

[a]Graduate School of Science and Engineering, Waseda University (3-4-1, Okubo, Shinjuku-Ku, Tokyo 169-8555, Japan)
[b]ENEA, C.R. Casaccia (Via Anguillarese 301, 00060 Rome, Italy)
[c]CREST, Japan Science and Technology Agency

Received May 30, 2003 ; Accepted September 2, 2003

We propose a polymer blending method for preparing the PEO (polyethylene oxide)-$LiBF_4$ complex electrolyte for lithium secondary battery applying to the IPN (interpenetrated polymer network) gel electrolyte. The polymer blend mixture of PEO-PS (polystyrene)-$LiBF_4$ was prepared as a film by the hot-pressing method. The resulting IPN film was plasticized with the electrolyte solution of 0.5 M $LiBF_4$/EC(ethylene carbonate)-PC(propylene carbonate) (1 : 1 vol.), in which the formation of PEO-$LiBF_4$ complex was confirmed by the Raman spectroscopy. The basic properties as an electrolyte of Li metal batteries, *i.e.*, ionic conductivity, chemical stability at the polymer gel electrolyte/lithium metal interface, and charge-discharge performance of the Li/(PEO-$LiBF_4$/PS) gel electrolyte/$LiCoO_2$ cell were studied and discussed.

Key Words : PEO-$LiBF_4$, Interpenetrated Polymer Network, Co-continuous, Polymer Blend, Gel Polymer Electrolyte, Lithium Battery

1 Introduction

Polymer electrolytes for lithium secondary battery have been studied for several years for safety issues in future Li batteries, and gel polymer electrolytes are one of the most promising candidates to be considered in the coming first stage. However, gel polymer electrolytes have two major problems to be realized in practical use that relates to the nature of the polymer-solvent interaction. For example, polymers with weak solvent interaction such as PVdF (polyvinylidene fluoride) and PAN (polyacrylonitrile) form unstable gels, and are likely to lose the plasticizer from the gel matrix, even though they exhibit good mechanical strength. On the other hand, the polymers with strong solvent interaction such as PEO (polyethylene oxide) and PMMA (polymethylmethacrylate) form stable gels with plasticizer and show higher ionic conductivity than that of solid polymer electrolytes, while the gels in the system have poor mechanical strength. It is indeed difficult to achieve both properties of high ionic conductivity and mechanical strength.

However, recently, many excellent studies were undertaken to tackle these problems, *i.e.*, the copolymerization of the host polymer, a three-dimensional cross-link of the host polymer, or polymerization of room temperature molten salt (ionic liquid).[1-5] When using these technologies, the problem has been solved and the electrolyte having both merits is obtained. However, these techniques are complicated processes and require high-cost materials. Electrolytes with low-cost and easy processes, with both merits, are thus still strongly desired.

For this purpose, we have proposed a polymer blending method to get the novel polymer matrix of gel electrolyte for lithium secondary batteries.[6,7] Our proposal is to use the simple hot blending method for combining common polymers. Two immiscible polymers, PEO and PS (polystyrene), were blended to obtain the electrolyte demonstrating both merits of ionic conduction and mechanical strength. The PEO was plasticized to provide the ionic conductivity whereas the PS as the framed network to yield the membrane mechanical strength. This blended polymer system showed co-continuous morphology. This morphology was formed with the IPN (interpenetrated polymer network) of the two polymers. Figure 1 illustrates a schematic model for co-continuous polymer blend system, where lithium ion transfers through the ion conductive phase. The phase of frame of the film keeps the mechanical strength when the ion

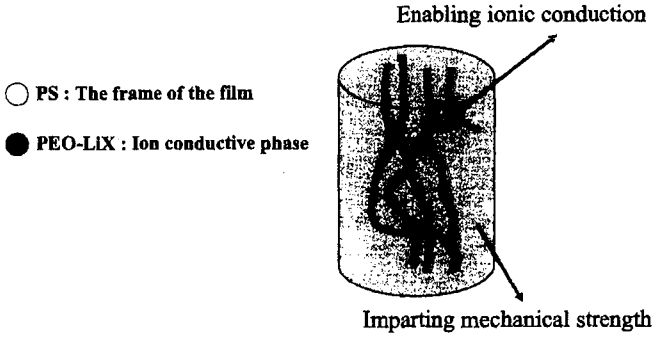

Fig. 1 Schematic model for co-continuous polymer blend interpenetrated polymer network system.

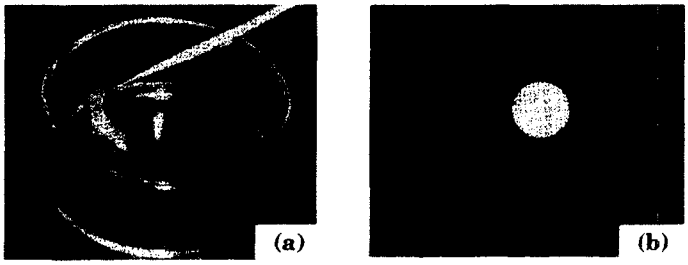

Fig. 2 Photographs of the films of PEO (a) and PEO-PS IPN (b) films which are plasticized with $LiBF_4$/EC-PC.

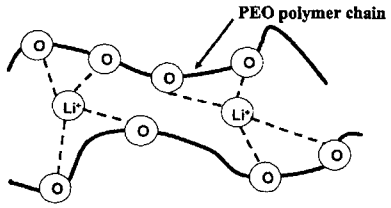

Fig. 3 Schematic illustration of the formation of PEO-LiX complex.

conductive phase is plasticized. Figure 2 shows the photographs comparing the PEO film with and without PS, *i.e.*, PEO film (a) and IPN film (b) after the plasticizing process. As seen in Fig. 2, the IPN film keeps free-standing state, however the PEO films with plasticizing process could not keep the free-standing state due to its soft and viscous texture. This plasticized IPN electrolyte is expected to possess a high ionic conductivity and a good mechanical strength, while there are some possibilities to lose the ion conductive phase by flowing out of the soft plasticized PEO phase from PS frame with the large amount of plasticizer. In the practical use, a higher conductivity is requested, and one of the solutions would be to increase the amount of plasticizer for the gel electrolytes.

There are some reports that a complex is formed when PEO and LiX are mixed.[8,9] The lithium ion serves as the bridging of PEO chains as shown in Fig. 3. The PEO-LiX complex keeps high viscosity in spite of impregnation with the plasticizer. Therefore, the formation of PEO-LiX complex is to give the potential to prevent the conductive phase from running out of the frame phase in the IPN.

In this work, we applied PEO-$LiBF_4$ complex to the polymer blend gel electrolyte. Characteristics of the gel polymer electrolyte made with IPN film of PEO-$LiBF_4$ complex and PS, and the possibility of the electrolyte formed with this IPN matrix were examined for the future Li metal secondary batteries.

2 Experimental

PEO (POLYOX WSR N-300, Union Carbide; $M_w = 400,000$), PS (STYRON 656D, Dow Chemical; $M_w = 30,000$) and $LiBF_4$ (Stella Chemifa, Japan) were dried under dry airflow (dew point below -60℃). PS was porphyrized before hot-blending. The mixture of weighted PEO, PS and $LiBF_4$ powders was hot-blended by Imoto (Japan) blend equipment (Small Amount Blend Machine). The conditions of blending were as follows, PEO : PS = 48 : 52 by wt., O : Li = 6 : 1 by mol, 180℃, 30 min., 107 rpm. The blended samples were quenched in liquid N_2. Adequate amounts of the blends were hot-pressed at 120℃ under 30 MPa by sandwiching between aluminum foils to form thin films. The thickness of the IPN films was controlled to be 100 μm by using appropriate spacers during the hot-press step. The pressing time was reduced to a minimum by setting the hold-under-pressure time to zero.

To perform morphological investigation, the PEO-$LiBF_4$ phase in the IPN films was removed by dissolution of PEO-$LiBF_4$ in water. After dissolution, the samples were rinsed with water and dried under vacuum. Scanning Electron Microscope (SEM) images were taken with a Hitachi, S-2500CX to investigate the structure of the prepared blends.

The formation of PEO-$LiBF_4$ complex was confirmed by means of Raman spectroscopy. Raman spectra were recorded using JASCO spectrometer equipment (RFT-800, FT/IR-800), with the condition as follows, excitation laser: He-Ne, 1064 nm, 10 mW, resolution : 4 cm^{-1}, scanning velocity : 0.5 mm s^{-1}.

To prepare the gel electrolyte, a 0.5 M $LiBF_4$/EC (ethylene carbonate)-PC (propylene carbonate) (1 : 1 vol.) was used as a plasticizer.

The PEO-$LiBF_4$ phase was plasticized with the solution containing the desired concentration of Li^+, which was quickly absorbed into the PEO-$LiBF_4$ phase, by wetting the surfaces of the IPN film. SUS/IPN-Gel/SUS cell was assembled and the ionic conductivity of IPN gel electrolyte was evaluated by a.c. impedance measurements (FRA 5080, NF, Japan, GPIB Potentiostat/Galvanostat HA-501 G, Hokuto Denko, Japan). The impedance spectrum was measured in the constant potential mode by sweeping the frequencies from 20 kHz to 1 Hz range at an a.c. amplitude of 10 mV.

Li/IPN-Gel/Li cell was assembled, and the chemical stability at the interface between the IPN gel electrolyte and lithium metal was evaluated by a.c. impedance measurements with the conditions of a.c. amplitude voltage of 10 mV and of the frequency range of 20 kHz~100 mHz.

Li/IPN-Gel/Au cell was assembled to evaluate the oxidation stability of the IPN gel electrolyte by LSV (linear sweep voltammetry) (Function Generator HB-104, Hokuto Denko, Japan, Potentiostat/Galvanostat HA-501 G, Hokuto Denko, Japan) at the scan rate of 20 mV s^{-1} in the potential ranging from the OCP (open circuit potential) to 6.0 V vs. Li/Li^+.

The charge-discharge test was conducted to evaluate the performance of the IPN gel electrolyte as an electrolyte for lithium secondary battery. Li/IPN-Gel/$LiCoO_2$ cell was assembled with the $LiCoO_2$ supplied from Japan Chemical Industry. The charge-discharge test was performed (HJ1010mSM8, Hokuto Denko, Japan) under CC-CV (constant current-constant voltage) mode at C/5 rate of loading current and the voltage upper limit of 4.2 V for charging and CC mode for discharging with C/5 rate of current with cut-off voltage of 3.0 V.

3 Results and Discussion

Since PEO and $LiBF_4$ can be dissolved in H_2O, the IPN film was dipped in the water to confirm the matrix formations, where the PS phase remains after PEO and $LiBF_4$ are dissolved into H_2O. The remained PS phase of the IPN film was observed with SEM and is shown in Fig. 4. The pore in the image is the part occupied by PEO-$LiBF_4$ phase. From the morphology of the PS phase in the resulting film, co-continuous polymer blend film was confirmed to have the IPN structure by the hot blending of PEO, PS and $LiBF_4$.

In order to confirm the formation of PEO-$LiBF_4$ complex expected during hot-blending, Raman spectra were measured and are shown in Fig. 5. In Fig. 5 the spectra of four samples are reported, *i.e.*, hot-blended PEO-$LiBF_4$,

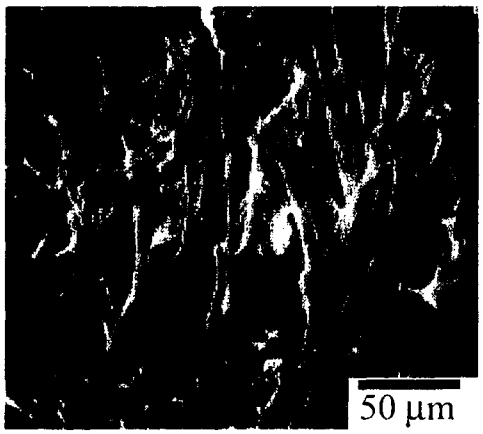

Fig. 4 SEM image of PS phase of polymer blend film. The PEO-$LiBF_4$ phase was removed by rinsing the polymer blend with H_2O.

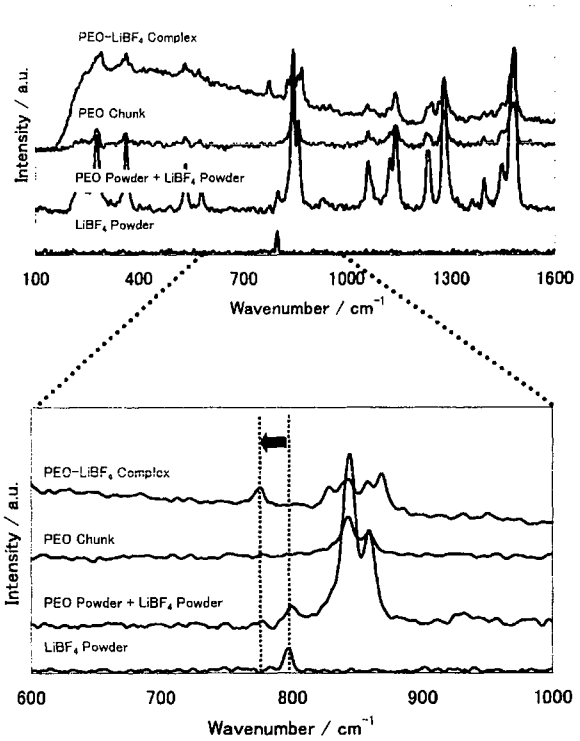

Fig. 5 Raman spectra of four samples of hot-blended PEO-$LiBF_4$, PEO melted once and cooled from PEO powder, $LiBF_4$ powder, and mixture of PEO powder + $LiBF_4$ powder.

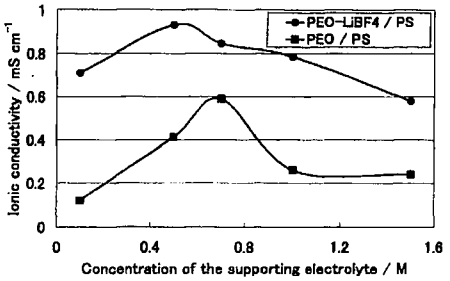

Fig. 6 Room temperature ionic conductivity of IPN gel electrolyte as a function of the concentration of the supporting electrolyte in plasticizer. Uptake of the plasticizer was 50 wt %.

cooled down PEO melted with the heat treatment of PEO powder, $LiBF_4$ powder, and mixture of PEO powder with $LiBF_4$ powder. The spectra of the heated and cooled PEO without $LiBF_4$ and the mixture of PEO powder and $LiBF_4$ powder show similar peaks except the peak at 800 cm^{-1} that appeared in the spectrum of the mixture of PEO powder and $LiBF_4$ powder. In contrast, both of the spectra of $LiBF_4$ powder and the mixture of PEO powder and $LiBF_4$ powder have the peak at 800 cm^{-1}. From these results, it is concluded that the peak at 800 cm^{-1} is due to $LiBF_4$, and the operation of melting PEO powder without $LiBF_4$ does not alter the solid-state properties of PEO. On the other hand, the peak around 800 cm^{-1} in the spectrum of the hot-blended PEO-$LiBF_4$ shifted to lower wave number, 777 cm^{-1}. Generally, the peak of BF_4^- anion is observed at 777 cm^{-1}, whereas the peak of $LiBF_4$ powder was observed at 800 cm^{-1}. This may be the effect of Li^+ cation. It may be considered that the peak of BF_4^- anion changed back into the original peak by the formation the complex of PEO and Li^+. This result suggests that the complex of PEO and $LiBF_4$ may be formed as reported in the literatures.[10,11] The formation of PEO-$LiBF_4$ complex in the matrix is thus confirmed. Furthermore, it is expected that the ion conducting phase would keep high viscosity by the interaction between PEO and $LiBF_4$, when large amount of plasticizer is added.

Figure 6 shows the variation of the ionic conductivity of IPN gel electrolytes as function of the concentration of the supporting electrolyte in the plasticizer. For the sake of comparison, the ionic conductivity of gelled PEO-$LiBF_4$ /PS polymer blend film and PEO/PS polymer blend film were also measured at room temperature. Uptake of the plasticizer is calculated according to the following formula (1).

$$\textit{Uptake of the plasticizer}[\%] = \frac{\textit{Plasticizer}[g]}{\textit{PEO}[g] + \textit{LiBF}_4[g] + \textit{Plasticizer}[g]} \times 100 \quad (1)$$

The ionic conductivity of PEO-$LiBF_4$/PS is higher than that of PEO/PS in the range of the investigated concentration. This is presumably due to the anion of $LiBF_4$ added during the hot-blend step. The cation Li^+ is used to form the complex, while the anion BF_4^- is comparatively free in the conductive phase in the IPN. Besides,

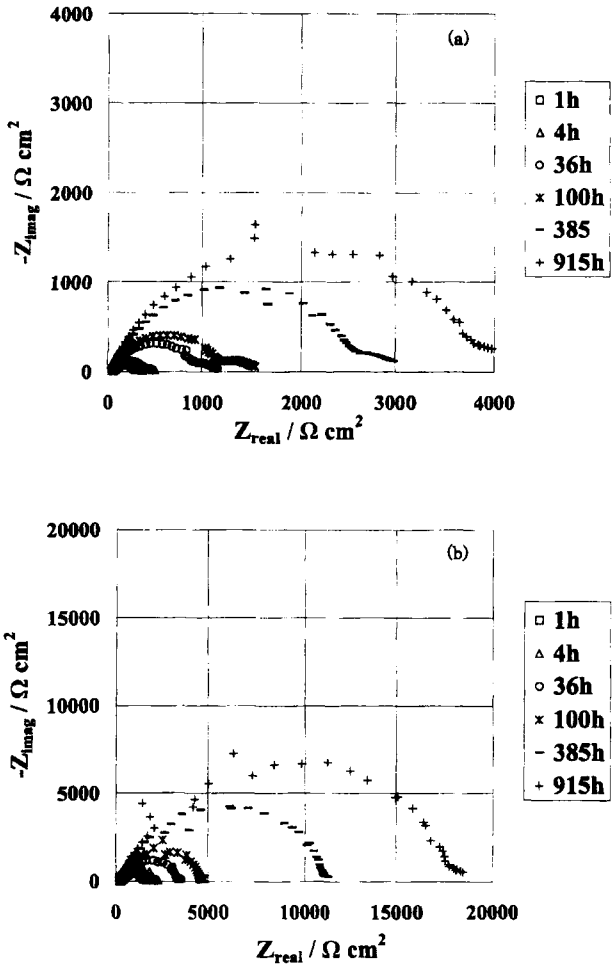

Fig. 7 Cole-Cole plot of Li/IPN-Gel/Li cell. The IPN film was plasticized with plasticizer containing electrolyte. (a) PEO-$LiBF_4$/PS gel electrolyte, (b) PEO/PS gel electrolyte.

the ionic conductivity of PEO-$LiBF_4$/PS has a peak at 0.5 M, and that of PEO/PS has a peak at 0.7 M. This is presumably due to the high concentration of the supporting electrolyte in the PEO-$LiBF_4$/PS. $LiBF_4$ added during the hot-blend step would increase the concentration of $LiBF_4$ in the PEO-$LiBF_4$/PS gel electrolyte. However, accurate concentrations of Li^+ and BF_4^- ion were unidentified, because the percent of $LiBF_4$ that was used for the formation of PEO-$LiBF_4$ complex and the degree of $LiBF_4$ dissociation in the matrix are unknown. Therefore, the increase of concentration of $LiBF_4$ causes solvated ions, ternary ions and other ion complexes to start forming at lower concentration of the supporting electrolyte in the plasticizer. Owing to these multiple factors, the ionic conductivity as a function of the supporting electrolyte in the plasticizer showed the phenomena in Fig. 6. In the following investigation, 0.5 M $LiBF_4$/EC-PC would be used to plasticize PEO-$LiBF_4$/PS, and 0.7 M $LiBF_4$/EC-PC would be used to plasticize PEO/PS.

Figure 7 shows the Cole-Cole plots of the Li/IPN-Gel/Li cell investigated by a.c. impedance measurements. For the sake of comparison, PEO-$LiBF_4$/PS polymer blend film and PEO/PS polymer blend film were applied. From the fitting data of the Cole-Cole plots, the diameter of the first semi-circle is assigned to be the sum of interfacial

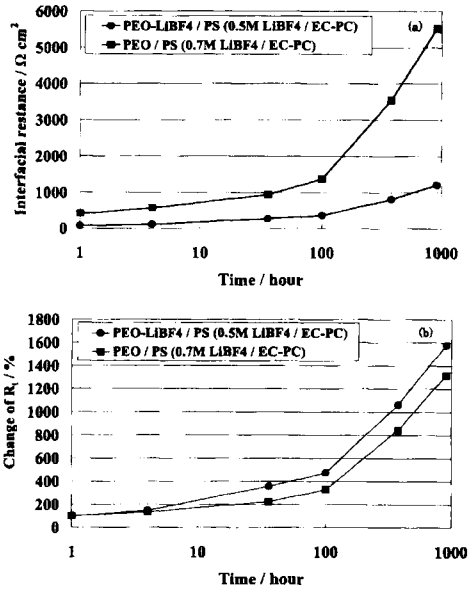

Fig. 8 Chemical stability of IPN gel electrolyte and lithium metal. (a) variation per hour, (b) change per hour. Uptake of the plasticizer is 80 wt%.

resistances of the two interfaces of gel polymer electrolyte and lithium metal in the sandwiched type cell. Figure 8(a) shows the change in the interfacial resistance of the gel polymer electrolyte and lithium metal as a function of the time, and the normalized change by the interfacial values of both resistance are shown in Fig. 8(b). The interfacial resistance was calculated by the radius of fitting curve for Fig. 7 divided by 2 with the assumption of the interfaces of both side of gel electrolyte is almost the same. The resistance of PEO-$LiBF_4$/PS gel electrolyte is lower than that of PEO/PS gel electrolyte, while both of the normalized change of PEO-$LiBF_4$/PS and PEO/PS gel electrolyte are the same. This is presumably due to that a small amount of plasticizer covered the Li surface in contact with the PEO-$LiBF_4$/PS gel electrolyte. Because PEO-$LiBF_4$/PS gel electrolyte contains large amount of plasticizer compared to the PEO/PS. The Li surface covered with plasticizer has less chance to contact with PEO or PS polymer molecules and the SEI (solid electrolyte interface) formed with the reaction between the plasticizer and Li might have smaller interfacial resistance than that formed by the reaction between Li and PEO or PS used in this study. This suggests that application of PEO-$LiBF_4$ complex to IPN system improved the interfacial properties of the gel polymer electrolyte and lithium metal.

Figure 9 shows LSV curves of Li/IPN-Gel/Au cell. For the sake of comparison, PEO-$LiBF_4$/PS polymer blend film (Fig. 9(a)) and PE (polyethylene) separator with electrolytic solution (Fig. 9(b)) were also investigated. The same solution was used as plasticizer of the polymer blend film and electrolytic solution. From this result, both of the curves in PEO-$LiBF_4$/PS gel electrolyte and 0.7 M $LiBF_4$/EC-PC stand about 4.5 V vs. Li/Li^+. The oxidation current starting at 4.5 V vs. Li/Li^+ is ascribed to the oxidation of 0.7 M $LiBF_4$/EC-PC. This result suggests that PEO-$LiBF_4$/PS can be applied to $Li/LiCoO_2$

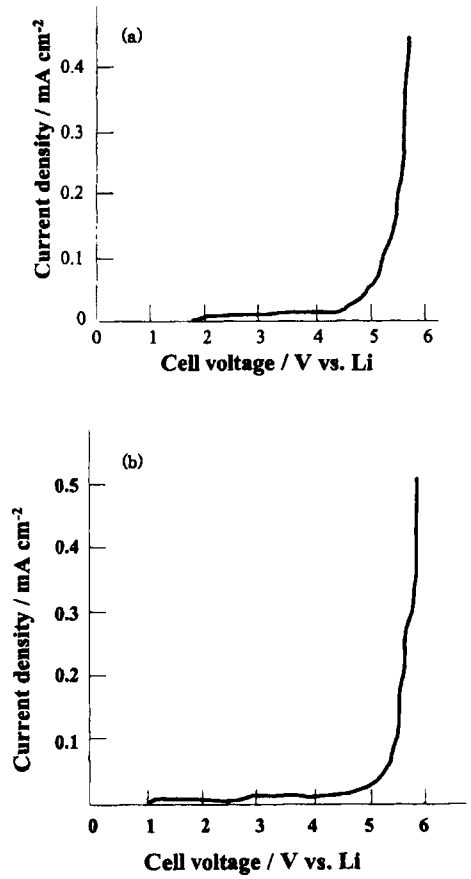

Fig. 9 Linear sweep voltammetry of Li/electrolyte/Au cell with (a) PEO-$LiBF_4$/PS gel electrolyte, (b) polyethylene separator with electrolyte solution at the scan rate of 20 mV s^{-1}.

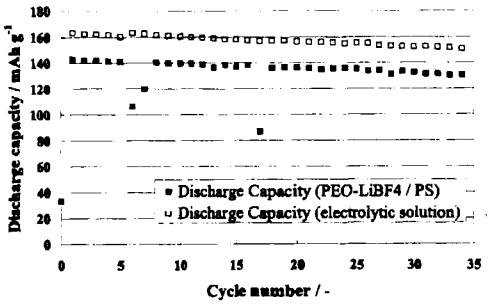

Fig. 10 Charge-discharge test of Li/(PEO-$LiBF_4$/PS) IPN-Gel/$LiCoO_2$ cell and Li/(0.7 M $LiBF_4$/EC-PC)/$LiCoO_2$ cell. Charge-discharge rate was C/5 in CC-CV charge mode and CC discharge mode.

cell as the electrolyte in the range between 0 and 4.2 V.

Figure 10 shows the discharge capacity per gram of cathode. For the sake of comparison, PEO-$LiBF_4$/PS polymer blend film and PE separator with electrolytic solution were used. The capacity of the cell using PEO-$LiBF_4$/PS is a little lower than that of the cell using PE separator with electrolytic solution. Besides, there are some cycles with deathly low capacity. However, the degradation rate is small. The capacity per gram of cathode keeps 130 mAh g^{-1} over 30 cycles.

4. Conclusions

By hot-blending powders of PEO, $LiBF_4$, and PS, a PEO-$LiBF_4$/PS polymer blend with three-dimensional IPN structure was obtained. PEO and $LiBF_4$ were confirmed to form PEO-$LiBF_4$ complex in IPN made in these conditions. The ionic conductivity of PEO-$LiBF_4$/PS gel electrolyte was about 0.9×10^{-3} S cm^{-1}. The chemical stability of the interface between the IPN gel electrolyte and lithium metal was improved by applying PEO-$LiBF_4$ complex to IPN. PEO-$LiBF_4$/PS gel electrolyte showed oxidation stability below 4.5 V vs. Li/Li^+. The IPN gel electrolyte was applied to $Li/LiCoO_2$ cell as the electrolyte. With the charge-discharge rate of C/5, the capacity per gram of cathode was found over 130 mAh g^{-1} over 30 cycles. This suggests that PEO-$liBF_4$/PS polymer blend can be applied to lithium secondary battery as the electrolyte.

Acknowledgements

This work was supported in part by a Grant-in-Aid for COE Research "Molecular Nano-Engineering" and for 21st century COE program "Practical NanoChemistry" from the Ministry of Education, Culture, Sports, Science and Technology, Japan.

References

1) M. Watanabe, Y. Suzuki, and A. Nishimoto, *Electrochim. Acta*, **45**, 1187 (2000).
2) M. Watanabe, H. Tokuda, and S. Muto, *Electrochim. Acta*, **46**, 1487 (2001).
3) A. Noda, J. Nishimoto, and M. Watanabe, *Polymer Preprints, Japan*, **46**, 511 (1997).
4) H. Ohno, *Electrochim. Acta*, **46**, 1407 (2001).
5) A. Noda, T. Kaneko, and M. Watanabe, *Polymer Preprints, Japan*, **49**, 754 (2000).
6) S. Passerini, F. Alessandrini, T. Momma, H. Ohta, H Ito, and T. Osaka, *Electrochem. Solid State Lett.*, **4**, A 124 (2001).
7) S. Passerini, M. Lisi, T. Momma, H. Ito, T. Shimizu, and T. Osaka, submitted to *J. Electrochem. Soc.*
8) P. P. Prosini and S. Passerini, *Solid State Ionics*, **146**, 65 (2002).
9) F. Croce, L. Persi, F. Ronci, and B. Scrosati, *Solid State Ionics*, **135**, 47 (2000).
10) J. Adebahr, P. Gavelin, P. Jannasch, D. Ostrovskii, B. Wesslen, and P. Jacobsson, *Solid State Ionics*, **135**, 149 (2000).
11) C. Capiglia, N. Imanishi, Y. Takeda, W. A. Henderson, and S. Passerini, *J. Electrochem. Soc.*, **150**, A 525 (2003).

Structural and morphological differences in the cycled Electro-Deposited Sn-Ni Alloy Lithium Ion Battery Anodes with different composition

H. Mukaibo [a,c], T. Sumi [a], T. Yokoshima[a], T. Momma[a,b], and T. Osaka [a]
[a] Waseda University.
3-4-1, Okubo, Shinjuku-Ku, Tokyo, 169-8555, Japan.
[b]CREST, Japan Science and Technology Corporation.
[C]JSPS Research Fellow

Li-ion batteries possess the highest energy density among the practical batteries, and the development of its anode material is considered as a breakthrough to meet the demands for power sources with higher performance for portable electronic devices.

Sn anode shows a theoretical capacity of 994 mAh/g, which exceeds that of the conventional carbon anode. However, it suffers a large volume change during cycling, which results in rapid electrode degradation. A selection of adequate matrix to ease such stress and lengthen its electrode life is one of the keys to gain a successful novel anode material. Elements that are inactive against Li (such as Ni) are assumed to suppress the volume change effectively without much irreversible capacity [1]. We have confirmed in our past work that the Sn-Ni alloy with different Ni/Sn composition has the potential ability to perform as the anode of Li ion battery, and among them, $Ni_{38}Sn_{62}$ showed the highest discharge capacity of ca. 650mAh/g at about the 70th cycle [2]. The present study focuses on the differences in morphology and structure of these samples to evaluate the cause of the difference seen between their anode performances.

The Sn-Ni thin films with different composition were prepared by electrodeposition [3] on Cu sheet from potassium pyrophosphate baths at 50 °C. Each film was deposited for 5 min with the current density of 5mA cm^{-2}. The compositions of the samples were determined by Inductively Coupled Plasma Atomic Emission Spectroscopy (ICP-AES). The anodes were cycled in conventional glass cells with two pieces of Li foils as counter and reference electrodes, and 1M $LiClO_4$ / ethylene carbonate (EC) + propylene carbonate (PC) (1:1 vol%) as the organic electrolyte. The cycling was performed using galvanostatic charge-discharge equipments in the potential range of 0.01 to 2.00 V vs. Li/Li^+. Both charge and discharge were carried out at the current density of 250 mA g^{-1} of Sn-Ni alloy. A X-ray diffraction (XRD) apparatus using Cu Ka radiation was equipped with the capability to evaluate structural difference between the cycled thin films with different Ni/Sn compositions. Also, a Scanning Electron Microscope (SEM) was used to observe the morphology of the cycled samples

Figure 1 shows the XRD patterns of $Ni_{38}Sn_{62}$ in a different charged/discharged state. Ni_3Sn_4 was the main phase confirmed from the as deposited state. When Li^+ was inserted to the electrode with the initial charge, most of the peaks due to Ni_3Sn_4 phase disappeared and instead, new peaks indicating the presence of Sn-Li alloys were confirmed. After the following discharge process, peaks of Ni_3Sn_4 were confirmed again, and the peaks attributing to Li-Sn alloy phases disappeared. Ni_3Sn_4 phase was confirmed in all the XRD patterns of the following cycling indicating the reversibility of the reaction between Ni_3Sn_4 and Li^+. This result suggests that this reversible reaction is the key to the high reversible capacity seen from this electrode.

On the contrary, the XRD patterns of $Ni_{46}Sn_{54}$ indicated the reversible reaction of metastable phase with Li^+, where part of the metastable phase reacted with Li^+, that resulted in a state of microcrystal or amorphous phase that could not be detected by the XRD. In the case of $Ni_{16}Sn_{84}$, the XRD pattern suggested a reversible reaction between Ni_3Sn_4, metastable phase, and Sn phase. Here, a small peak that is attributed to Li-Sn alloy phase was confirmed in the discharged (delithiated) state after repeated cycling, indicating Li^+ trapping within the Li-Sn alloy.

Such differences in the reaction mechanism between the electrode and Li^+ were indicated as direct cause for the difference in its anode performance.

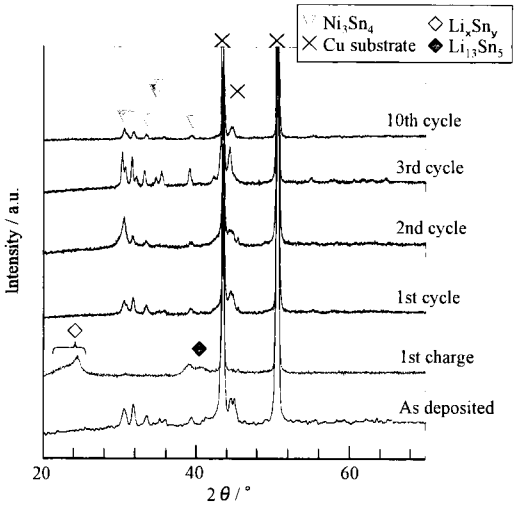

Fig. 1 XRD patterns of $Ni_{38}Sn_{62}$, in a different charged / discharged state.

ACKNOWLEDGEMENT

This work is supported in part by a Grant-in-Aid for Center of Excellence (COE) Research "Molecular Nano-Engineering", and the 21st Century COE Program "Practical Nano-Chemistry" from the Ministry of Education, Culture, Sports, Science and Technology.

REFERENCES

1. J. Ahn, Y. Kim, G. Wang, M. Lindsay, H.K. Liu and S. Dou, *Mater. Trans.*, **43**, 63 (2002).
2. H. Mukaibo, T. Sumi, T. Yokoshima, T. Momma and T. Osaka, *Electrochem. Solid-State Lett.*, **6**, A218 (2003)
3. A. Ito and H. Enomoto, *J. Met. Fin. Soc. Jpn.*, **36**, 466 (1985).

セラミックス協会第17回秋季シンポジウム講演予稿集, pp. 20 (2004).

リチウムイオン二次電池用 Sn 系負極材料の開発

(早稲田大学、CREST, JST)○ 門間聰之・(早稲田大学、学振特別研究員) 向坊 仁美・(早稲田大学) 逢坂哲彌

Sn Based Anode Materials for Li ion Battery

/ ○T. Momma (Waseda U., CREST JST), H. Mukaibo (Waseda U., JSPS Research Fellow), T. Osaka(Waseda U.) /

New anode materials based on electrochemical Sn-Li alloying reaction for rechargeable Li ion batteries were proposed. SnSx material prepared by sono-chemical reaction exhibit higher performance compared with the conventional C materials. Ni Sn alloy was revealed to have potentials to apply for the anode material with higher capacity of 500 mAh/g.

問合先：E-mail momma@waseda.jp

リチウムイオン二次電池は現在、もっとも大きな容量を有する市販デバイス用二次電池として更なる高容量化に向けた研究が盛んになされている．その高容量化のためには、現在用いられている炭素系負極材料（理論容量 372mAh/g）に代わる新たな高容量負極材料の実現が望まれている．Li と可逆的に合金化，脱合金化する Sn は新規高容量負極材料として期待されているが，充放電の際の大きな体積変化により電極内に大きな負荷がかかるため寿命が短い．今までに、Sn 酸化物を出発物質とし、初期充電の際に酸化物を Sn 金属と Li_2O に電気化学的に変換させてリチウムイオン二次電池負極材料として利用する提案がなされている．また、Sn 元素の周りに他元素を共存させることにより，サイクル特性が向上したという報告がされている [1]．この他元素として Li と反応しない金属元素を用いた Sn 系合金は初期の不可逆容量が低く高容量で長寿命な負極材料が得られると考えられる [2]．Ni は Sn と合金化させる手法が既に確立されており扱い易く、過去に Sn-Ni 合金を作製した例がいくつか報告されている [2-4]．しかし、初期不可逆容量の低減は実現されたものの、短命・低容量などの問題点を抱えていたためまだ新規負極材料へのブレイクスルーとはなっていない．

我々は、まず Sn 酸化物の代わりに Sn 硫化物の適用を検討した。SnS_x は初期充電の際に Li_2S に包括された Sn 微粒子となり、その Sn 微粒子がリチウムと電気化学的に合金化脱合金化反応することによりリチウムイオン二次電池負極としての作動が期待される。Sonochemistry により作製された SnS_x につき検討を加えたところ、450mAh/g 以上の大きな可逆的充放電容量を示すことを見いだした（Fig. 1）。このことから Sn のリチウムとの合金化反応を利用する負極材料の可能性が示された。これら Sn 酸化物や Sn 硫化物は Sn 化合物を還元して Sn 微粒子を生成させることから、可逆的充放電容量に寄与しない還元電流が必要となる欠点を持っている。そこで次に、Sn 微粒子を担持するマトリックスとして、電子伝導性を有し、かつ Sn が金属状態である負極として、SnNi 合金系の適用を試みた。この新規 $Sn_{62}Ni_{38}$ 合金負極材料は Fig. 1 に示すように、500mAh/g 以上の可逆的充放電容量を長いサイクルにわたって示し、次世代リチウムイオン二次電池負極として有望であることが示された。

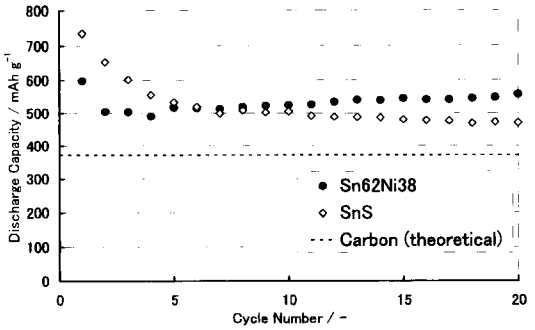

Fig. 1 Discharge capacity of Sn based anode materials for rechargeable Li ion batteries.

References
1) M. Winter, *et al.*, *Electrochimica Acta*, 45, 31 (1999).
2) J. Ahn, *et al.*, *Mater. Trans., JIM*, 43, 63 (2002).
3) G. M. Ehrlich, *et al.*, *J.Electrochem. Soc.*, 147, 886 (2000).
4) O. Crosnier, *et al.*, *J. Power Sources*, 94, 169 (2001).

第45回電池討論会講演要旨集, pp. 304-305 (2004).

リチウムイオン二次電池用 Sn-Ni 合金負極の微粒子作製の検討

([1] 早大院理工・[2] 学術振興会特別研究員・[3]CREST, JST)
○角　友秀[1]，向坊仁美[1,2]，門間聰之[1,3]，逢坂哲彌[1]

Preparation of Sn-Ni Alloy Powder Anode for Lithium Ion Secondary Battery

Tomohide Sumi[1], Hitomi Mukaibo[1,2], Toshiyuki Momma[1,3], Tetsuya Osaka[1]
[1]Graduate School of Science and Engineering, Waseda University, 3-4-1 Okubo Shinjuku, Tokyo 169-8555, Japan
[2]JSPS Research Fellow・[3]CREST, JST

We have reported that electrodeposited Sn-Ni alloy thin film shows good property as anode for Li ion battery with the discharge capacity above 600mAh/g beyond 70 cycles. However, thicker film is required for higher electrode capacity. But, this would lead to larger Li^+ diffusion resistance and degradation performance. In the case of powders, such effect is expected to be lower, due to its shorter diffusion length of ions and higher surface area. In this work, we prepared different structured Sn-Ni alloy powders by chemical reduction. We report the anode characteristics of these powders.

１．緒言

市場の電池高エネルギー密度化への要求を満たすLiイオン二次電池用の新規負極材料の一つとしてSnが期待されている．しかし，Snは高い理論エネルギー密度を有するものの，充放電反応に伴う著しい体積変化により電極内部が損傷し，容量が劣化してしまうことが大きな問題となっている．過去の検討において，我々は電析法により構造の異なるSn-Ni合金薄膜負極を作製した．その結果，Ni_3Sn_4合金相を含む薄膜負極は70サイクル以降も放電容量600mAh/gを超える値を示した．この値は現在実用化されている炭素材料の理論容量よりも高く，Ni_3Sn_4合金が炭素材料に代わる負極材料になりうる可能性を示唆した．以上より，Liと合金化しない金属であるNiにSnを取り囲むマトリクスの働きをさせることで容量劣化の緩和が期待される[1]．しかしながら，薄膜では電極全体の容量を増加させるためには活物質である膜を厚くする必要がある．それにより，Li^+の拡散抵抗が大きくなり，負極特性が低下することが予想される．一方，粉末状の電極ではLi^+の拡散抵抗が小さく，かつ反応表面積が大きくなるため，負極特性の低下を抑制しつつ電極全体の容量を増加させることができることが期待される．そこで，本検討では簡便な手法である化学的還元法により，Sn-Ni合金微粒子の作製を行っている．今回は，薄膜負極において良好な負極特性を示すことが示唆されたNi_3Sn_4合金微粒子の作製を試みた．

２．実験方法

Sn-Ni合金微粒子は，過去の検討である薄膜負極作製に用いた浴と同様のものを用い[2]，水素化ホウ素ナトリウムを添加することにより作製した．試料の電気化学的特性は，作用極に複合電極（試料：AB : PVdF - HFP = 8 : 1 : 1 (wt.%)），補助電極および基準電極に金属Liを用い，電解液を1M - $LiClO_4$ / EC + PC (1 : 1vol.%)とした三極式セルを用いて，充放電試験により評価した．測定条件は，電位範囲を0.01 ～ 2 V vs. Li / Li^+，電極あたりの電流密度を50 mA / g（活物質あたり：40 mA / g）とした．また，得られた試料の構

造解析にはXRD(CuK$_\alpha$線)，形態観察にはFE-SEMを用いた．

3．結果及び考察

粉末作製時にTable 1のように浴中のSn/Ni比を変化させて試料の作製を行った．各試料のXRDパターンをFig. 1に示す．Fig. 1より，浴中のSn/Ni比を変化させることで異なる構造を有するSn-Ni合金粉末の作製が可能であることが確認された．特に試料Aでは，過去の検討である薄膜負極において良好な負極特性を示すことが示唆されたNi_3Sn_4合金相のみが確認された．

Table 1 Sample name of each powder.

Sample name	A	B	C	D
Sn/Ni ratio in bath	8/2	7/3	6/4	5/5

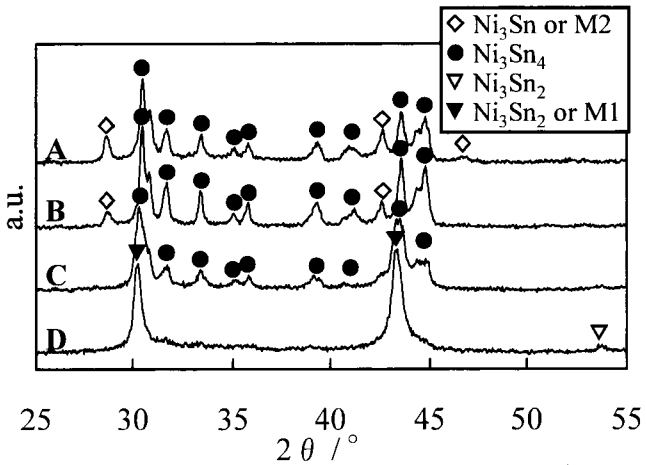

Fig. 1 XRD patterns of Sn-Ni alloy powder.

構造の異なる各試料のサイクル特性をFig. 2に示す．また，構造に伴うサイクル特性の違いをまとめたものをTable 2に示す．この結果より，浴中のSnイオン量が多くなるにつれて，初期放電容量は増加していることが確認された．また，Ni_3Sn_4合金相を有する試料Aは，初期から30サイクル目までの容量保持率が他のサンプルと比較して高いことが示された．このことから，粉末負極においても薄膜負極の場合と同様にNi_3Sn_4合金が良好なサイクル特性を示すことが示唆された．しかし，放電容量は薄膜負極に比べ，低い値を示す結果となった．そこで，本報告では更に薄膜との違いについて，更なる詳細な比較検討を行った結果について報告する．

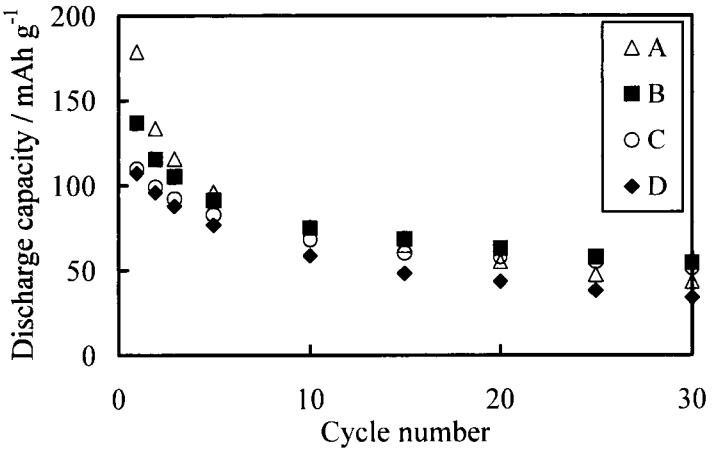

Fig. 2 Cycle performances of Sn-Ni alloy powder.

Table 2 Cycle performances of Sn-Ni alloy powder.

Sample name	Identified phase	Discharge capacity at 1st cycle / mAh g^{-1}	Retention rate* / %
A	Ni_3Sn_4, M2	179	24.2
B	Ni_3Sn_4, M2	137	39.8
C	Ni_3Sn_4	110	46.8
D	Ni_3Sn_2 or M1	107	31.5

＊ = { Discharge capacity (30th) / Discharge capacity (1st) } × 100

本研究は一部，文部科学省科学研究費(基盤研究(A), No. 15205024)および文部科学省特別推進研究(COE)「分子 ナノ工学」の助成を受け，21世紀COEプログラム「実践的ナノ化学教育研究拠点」にて行なわれた．

参考文献

1) H. Mukaibo, T. Sumi, T. Yokoshima, T. Momma, and T. Osaka, *Electrochem. Solid-State Lett.*, **6**, A218 (2003).

2) 伊崎　昌伸，榎本　英彦，*金属表面技術*, 36, 466 (1985).

Journal of The Electrochemical Society, **152** (3) A560-A565 (2005)
0013-4651/2005/152(3)/A560/6/$7.00 © The Electrochemical Society, Inc.

Structural and Morphological Modifications of a Nanosized 62 Atom Percent Sn-Ni Thin Film Anode during Reaction with Lithium

Hitomi Mukaibo,[a] Toshiyuki Momma,[a,b,*] Mohamed Mohamedi,[a,c,*,z] and Tetsuya Osaka[a,]**

[a]*Graduate School of Science and Engineering, Waseda University, Tokyo 169-8555, Japan*
[b]*CREST, Japan Science and Technology Agency, Tokyo 105-6218, Japan*

Nanosized electrodeposited 62 atom % Sn-Ni alloy was tested to highlight the effects of volume changes on the cycling life of the electrode during lithiation and delithiation. X-ray diffraction showed that the Ni_3Sn_4 was the main phase of the as-deposited alloy. A unique feature of the 62 atom % Sn-Ni is that it exhibited a capacity recovery upon cycling. When cycled galvanostatically, the $Sn_{62}Ni_{38}$ offers low capacity fade while reversibly incorporating lithium up to 600 mAh/g. At the first charge LiSn alloy phases are formed. This led to volume expansion of the electrode causing the formation of cracks. At the following cycles the Ni_3Sn_4 phase was restored and preserved over extensive cycling revealing the reversibility of the reaction between Ni_3Sn_4 and Li^+. As to the reasons of the capacity recovery noticed with this alloy, scanning electron microscopy images provided evidence of modifications of the surface condition accompanying a volume change during cycling. The chemical diffusion coefficient (D_{Li}) value determined from electrochemical impedence spectroscopy measurements during lithium insertion was within 10^{-9} to 10^{-10} cm^2 s^{-1}.
© 2005 The Electrochemical Society. [DOI: 10.1149/1.1856913] All rights reserved.

Manuscript submitted May 13, 2004; revised manuscript received August 5, 2004. Available electronically January 26, 2005.

There is a strong incentive to develop and characterize noncarbonaceous materials for use as negative electrodes that deliver capacities higher than carbon. In 1994, Fuji Film Co., Ltd., filed a patent for Sn oxides as a novel anode material for lithium ion batteries with a theoretical capacity exceeding that of carbon.[1] However, the tin oxide material showed high irreversible capacity during the first cycle, which has precluded its commercial success as an anode in lithium ion secondary batteries. The large irreversible capacity is caused by the reduction of the tin oxides and the formation of lithium oxide during the first cycle.[2] Nonetheless, the studies on tin oxide material demonstrated the possible performance given a tin-based negative electrode material. To mitigate the irreversible capacity associated with tin oxides, several attempts have been made to develop nonoxide tin materials with both high capacity and long cycle life.[3-26] From these studies, it may be seen that the selection of an adequate matrix that can accommodate the volume change of tin during cycling is crucial to a successful tin anode compound that can deliver both high capacity and long cycle life. Elements that are inactive against lithium are assumed to suppress the volume change effectively without appreciable irreversible capacity. Alloying Sn with elements such as Fe,[15-19] Cu,[20-23] Mn,[19,24] and Co,[19] has been investigated based on this assumption. Nickel is a typical element, which does not react with lithium and can be expected to serve as an adequate matrix for improving the cycleability of the electrode without high initial irreversible capacity. Studies on Sn-Ni alloys prepared by ballmilling,[7,9,11] sintering,[10,12] E-beam evaporating,[14] and electroplating[8,10,13] have been reported.

In our recent Letter,[27] by means of the electrodeposition route, we have synthesized Sn-Ni thin-film alloys of various compositions and demonstrated their lithium storage capacities. Among the alloys fabricated, we have shown that the 62 atom % Sn-Ni alloy can store lithium with capacities well in excess of a typical carbon electrode. An intriguing feature of the 62 atom % Sn-Ni is that it exhibited a capacity recovery upon cycling.[27] The capacity *vs.* cycle number profile demonstrated two stages: (*i*) a rapid decline in the capacity followed by (*ii*) a significant recovery in the capacity that sustained up to 70 cycles tested.

In this work, by means of cyclic voltammetry, electrochemical impedance spectroscopy (EIS), and charge-discharge methods, we focus onto gaining further insight into the behavior of the 62 atom % Sn-Ni alloy. The cycling was extended up to 150 cycles of charge-discharge. At some stages of the capacity *vs.* cycle number profile, *ex situ* X-ray and scanning electron microscopy (SEM) were employed to evaluate the changes in the structure and for imaging the evolution of the surface morphology, respectively.

Experimental

A thin film of pure tin was synthesized on a copper foil from an electrolytic bath containing $SnSO_4$ (40 g L^{-1}), H_2SO_4 (60 g L^{-1}), *o*-Cresolsulfonic acid (40 g L^{-1}), and polyethylene glycol (100 ppm).[28] The electrodeposition was carried out at room temperature with a current density of 10 mA cm^{-2} for 5 min.

The $Sn_{62}Ni_{38}$ was prepared by electrodeposition on a copper foil using an electrolytic bath of $NiCl_2 \cdot 6H_2O$ (0.075 mol L^{-1}), $SnCl_2 \cdot 2H_2O$ (0.175 mol L^{-1}), $K_4P_2O_7$ (0.5 mol L^{-1}), glycine (0.125 mol L^{-1}), and NH_4OH (5 ml L^{-1}); the mixture was stirred at 50°C.[29] The electrodeposition time was 5 min with a current density of 5 mA cm^{-2}. The pH values of solutions were $\ll 1$ for pure Sn solution (a very acidic bath containing 0.61 M of H_2SO_4) and 8 for Sn-Ni alloys. No alkali or acidic solution were used to adjust the pH. The sample dimension of the electrochemical measurements was 4 cm^2. The thickness of the film was 14 μm for Sn and 1.2 μm for $Sn_{62}Ni_{38}$.

X-ray diffraction (XRD) was performed on Rigaku RAD-1C using Cu Kα radiation. XRD conditions of voltage and current measurements were 40 kV and 20 mA, respectively. Morphology of the film was imaged using a scanning electron microscope (SEM, HITACHI S2500CX). For SEM observations, a Pt-Pd layer was sputtered on the sample surface. The samples are designated in terms of the atomic percentage of Sn in the deposited film, which was determined by inductively coupled plasma atomic emission spectroscopy instrument (ICP-AES: Thermo Electron K.K., IRIS-AP). Electrochemical measurements were performed in a conventional glass cell using two lithium foils as reference and counter electrode. The electrolyte was 1 M $LiClO_4$ (Tomiyama Pure Chemical Industries, battery grade)/ethylene carbonate (EC)/propylene carbonate (PC) 1:1 volume (Mitsubishi Chemicals, battery grade).

Cyclic voltammetry (CV) was carried out with a function generator (Hokuto Denko, HB104) and a potentiostat (Hokuto Denko, HA501G) at the scan rate of 0.02 mV/s. The cycleability of the cells was evaluated by galvanostatic charge-discharge tests (Hokuto Denko, HJR-110mSM6). Both charge and discharge were carried

* Electrochemical Society Active Member.
** Electrochemical Society Fellow.
[c] Present address: INRS-Énergie, Matériaux et Télécommunications, University of Quebec, Varennes, Québec, Canada J3X 1S2.
[z] E-mail: mohamedi@emt.inrs.ca

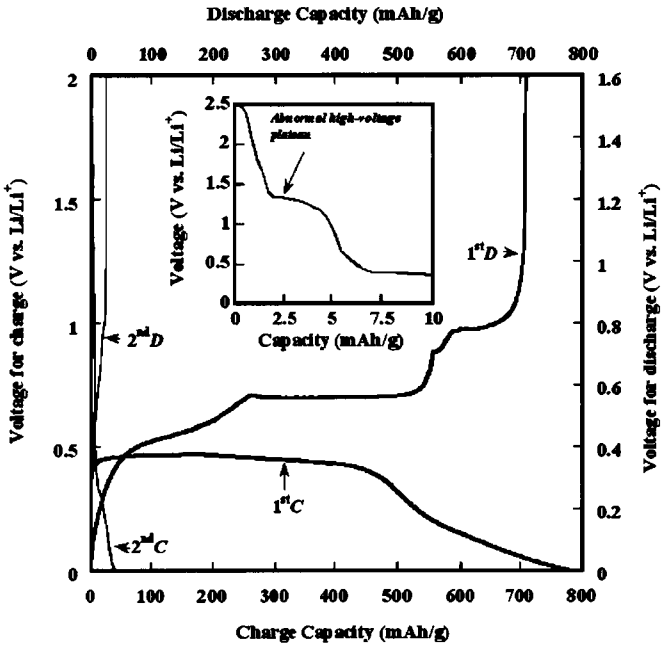

Figure 1. Voltage *vs.* capacity profiles in 1 M $LiClO_4$ /EC-PC for the electrodeposited Sn electrode on Cu substrate. The electrode was charged and discharged with currents of 50 mA/g. The insert shows the second voltage charge (lithiation) curve illustrating the presence of the abnormal high-voltage plateau. The letters *C* and *D* in the figure stand for charge and for discharge, respectively.

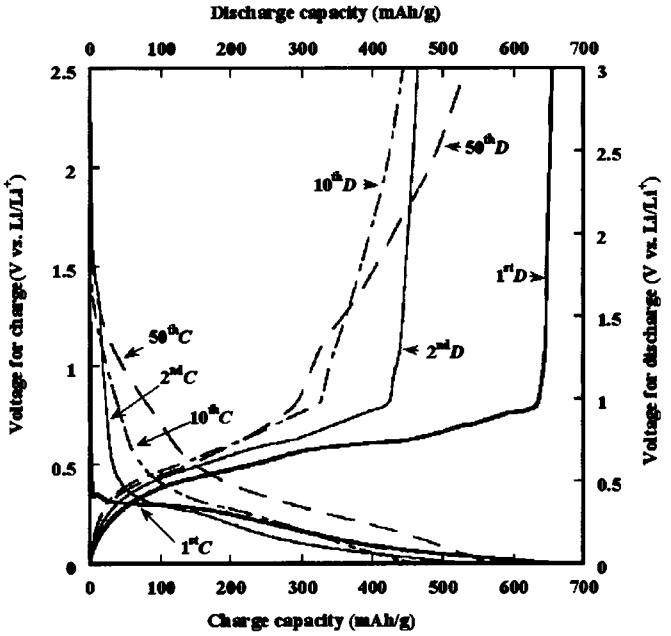

Figure 2. Voltage *vs.* capacity profiles in 1 M $LiClO_4$ /EC-PC for the electrodeposited 62 atom % Sn-Ni on Cu substrate. The electrode was charged and discharged with currents of 50 mA/g. The letters *C* and *D* in the figure stand for charge and for discharge, respectively.

out at the current density of 50 mA/g for both pure Sn and Sn-Ni alloy. Electrochemical impedance spectroscopy (EIS) measurements were carried out using a frequency response analyzer (NF Electronic Instruments, S-5720C) combined with a potentiostat (Hokuto Denko, HA501G). The alternating voltage signal was ±10 mV rms, and the frequency range was from 20 kHz to 10 mHz. EIS was performed according to the following sequences: galvanostatic charge (lithium insertion) to 0.01 V *vs.* $Li^+/Li \rightarrow$ impedance $\rightarrow$ galvanostatic discharge (lithium extraction) to 2.00 V $\rightarrow$ impedance. This cycle was repeated ten times. Impedance spectra were modeled using complex nonlinear least-squares (CNLS) fitting program EQUIVCRT developed by B. A. Boukamp. Then, to get an indication on how well the modeling function reproduces the actual data set, we first observed the parameter values and their relative error estimate (in %). The Chi-square (χ^2) function also gives a good indication of the quality of the fit; a value of 10^{-4}-10^{-5} or less for χ^2 indicates a reasonably good fit.

Results and Discussion

Electrochemical characterization of a pure tin electrode.—The charge (lithiation) and discharge (delithiation) profiles of the electrodeposited tin anode in the first two cycles are shown in Fig. 1. During the first charge, the potential of the tin anode dropped rapidly to about 0.4 V *vs.* Li/Li^+, stabilized, and then gradually changed toward cathodic values again. The plateau at 0.4 V is considered to result from the reaction of LiSn with metallic lithium.[30] The gradual decrease of the voltage results from the coexistence with several LiSn alloy phases in the active material. During discharging, multiple plateaus were clearly observed. By the second charge, the capacity dramatically dropped to values less than 40 mAh g^{-1} and was worse in the subsequent cycles. The profiles are similar to these reported by Tamura *et al.* for an electrodeposited tin on copper foil using different bath compositions.[23] The significant drop in the capacity was considered by Tamura *et al.* to result from a lack of interface strength between the entire part of the active material and the copper current collector.[23] It is well known that the electrochemical reduction of a tin electrode in a Li^+-containing electrolyte leads to the subsequent formation of a number of intermetallic phases Li_xSn.[2] On the other hand, the tin pulverizes rapidly when it experiences full lithiation due to the large volume increase leading to the electrode failure in the subsequent cycles. Indeed, only a visual observation of our electrode showed that the electrodeposited tin has detached from the copper substrate.

A point we would like to briefly discuss here is the appearance of the abnormal high-voltage plateau during the charge of pure tin electrode. This phenomenon has not been often investigated and was reported only by Tamura *et al.*[23] and by Beaulieu *et al.*[31] In our experiments, when the tin electrode was charged from 2.5 to 0 V, a voltage plateau close to 1.5 V could be seen as shown in the insert of Fig. 1. The occurrence of this plateau is believed to be due to the formation of a thin film resulting from a catalytic decomposition of electrolyte by the pure tin electrode.[23,31] We thus confirm here, that the occurrence of the high-voltage plateau is not an experimental artifact in agreement with Tamura *et al.*[23] and Beaulieu *et al.*[31] In conclusion, the abnormal high-voltage behavior of Sn certainly deserves further investigations onto the nature of the catalytic Sn surface.

Electrochemical characterization of $Sn_{62}Ni_{38}$ electrode.—Figure 2 shows the charge-discharge curves of electrodeposited $Sn_{62}Ni_{38}$ alloy in the first, second, tenth, and fiftieth cycles against Li metal. The first charge and discharge capacities are both the same, *ca.* 660 mAh g^{-1}, which shows that the initial cycling efficiency is 100%. A very interesting feature of Fig. 2 is that the discharge capacity decreased as cycling extended to ten cycles and started to increase for higher cycles. The 50th cycle is illustrated in the figure for clarity, indeed the recovery of the capacity was observed by the 10th cycle as shown later in this paper.

As to the anomalous high-voltage, one expects that alloying other metal with Sn would likely avoid the occurrence of the abnormal high-voltage irreversible capacity.[37] Figure 3, illustrates the second and third charge curves related to the $Sn_{62}Ni_{38}$ alloy electrode. It clearly shows the high-voltage plateau at the second-charge process, whereas the plateau disappeared at the third charge process. Although we do not show the data here, we have tested three other

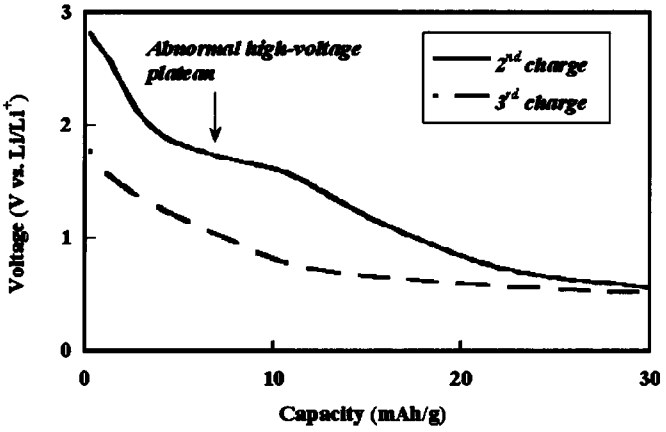

Figure 3. The second and third charge *vs.* capacity profiles in 1 M $LiClO_4$ /EC-PC for the electrodeposited 62 atom % Sn-Ni on Cu substrate. The figure illustrates the presence of the abnormal high-voltage plateau at the second charge only.

SnNi alloys by changing the Sn content (in atom %), namely, $Sn_{54}Ni_{46}$, $Sn_{84}Ni_{16}$, and $Sn_{92}Ni_8$. The high-voltage plateau was observed with $Sn_{84}Ni_{16}$ and $Sn_{92}Ni_8$ but not with the $Sn_{54}Ni_{46}$ alloy. It is quite clear from Fig. 3 that Sn alloyed with another metal (for instance, nickel) does exhibit a high-voltage plateau for an Sn content higher than 62 atom %. As for the pure tin electrode, these phenomena require further investigations.

The cyclic voltammograms (CVs) for the $Sn_{62}Ni_{38}$ film for the first three cycles at 0.02 mV s^{-1} are shown in Fig. 4. The samples were cycled between the open circuit potential (OCP) and 0.0 V *vs.* Li/Li^+. During the first reduction process, the voltammograms are characterized by two reduction peaks at 0.65 and 0.34 V. The peak at

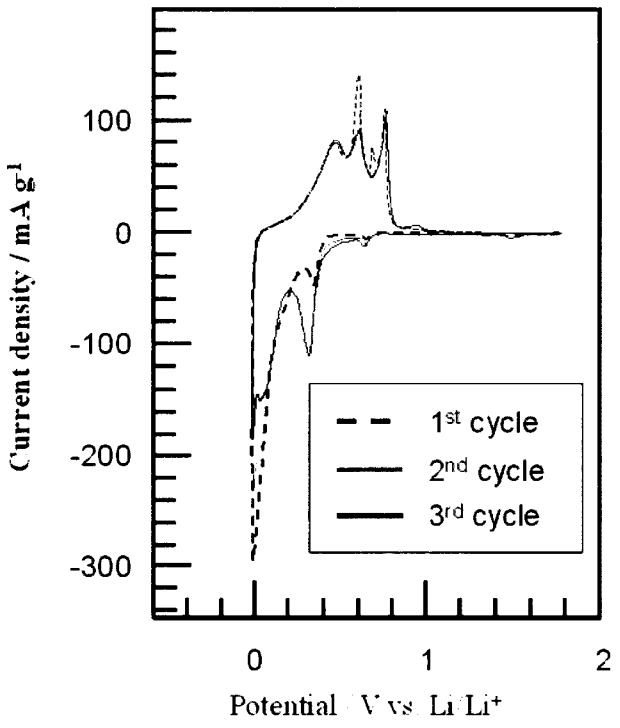

Figure 4. The first three cyclic voltammograms in 1 M $LiClO_4$ /EC-PC for electrodeposited 62 atom % Sn-Ni on Cu substrate. The voltammograms were recorded at the scan rate of 0.02 mV s^{-1}. The thin line represents the first cycle, the bold lines represent the second and third cycles.

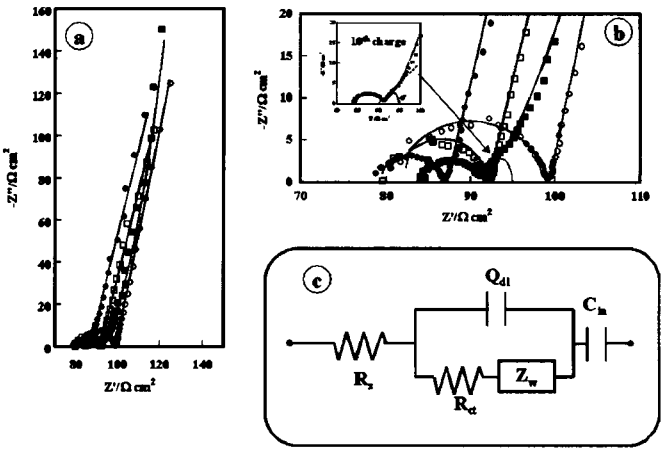

Figure 5. Nyquist plots at 62 atom % Sn-Ni on Cu substrate in 1 M $LiClO_4$ /EC-PC solution. (a) Full scale, (b) enlarged view of the high frequency domain of the impedance spectra. (○) 1st, (□) 2nd, (•) 3rd, and (■) 10th charge. (c) Modified Randles-Ershler model used to simulate the impedance spectra. Solid lines in Fig. 5a and 5b represent the simulation results.

0.65 V was found to depend on the Sn content, *i.e.*, its maximum current increased when the Sn content in the alloy increased.[27] The peak at 0.65 V has been observed during the second and subsequent cycles with SnO materials,[32] however, it has not been observed during the first reduction of SnO_2,[33] nor with tin-iron based alloys,[16-18] thus it may be associated with the Li-Sn alloying process.

Figure 5a shows a family of four Nyquist plots of $Sn_{62}Ni_{38}$ thin film electrode subjected to up to ten cycles of lithium insertion. Figure 5b displays an enlarged view of their high frequency domain. The impedance spectra of Fig. 5 are basically the typical Nyquist plot of an ion insertion thin-film electrode. There is one semicircle in the high-frequency region, and a steep sloping line at the lower frequencies due to the onset of the finite length effect. The high frequency semicircle was found to be dependent upon cycling, *i.e.*, it decreased in size from the first to the tenth cycle. It is interesting to note that no diffusion impedance is clearly seen at the first three charging processes. However, Warburg diffusion impedance appeared at the tenth cycle in the middle frequency region (see insert in Fig. 5b). This is naturally ascribed to solid-state diffusion of lithium-ion into the bulk anode material. We explain the appearance of the Warburg impedance by an increase in the electrode thickness. Indeed, the theoretical analysis of the complex impedance for insertion electrodes predicts that the diffusion control expands with increasing film thickness.[34] For very thin films, the kinetic control region may overlap with the charge saturation region and the diffusion region may appear in a very narrow range of frequencies. As the film thickness gets bigger, charge saturation dominates only at the very low frequencies, and diffusional control is observed over a large frequency range. The steep sloping line reflects a capacitive behavior, which is due to accumulation of the intercalant (Li) into the bulk anode.

According to the solid electrolyte interphase (SEI) model, one would expect to observe two semicircles in the impedance spectrum, one semicircle reflecting the charge-transfer process at the $Sn_{62}Ni_{38}$/electrolyte interface, and one related to the formation of SEI. However, if their time constants are similar, the semicircles could overlap one another and become irresolvable. Moreover, it has been demonstrated with mesocarbon microbeads single-particle anode (no binder and no conductive agent) that the SEI has to be aged or forcibly grown for long hours at its formation potential to be able to see two separate semicircles in the impedance spectra.[35,36]

Table I. Parameters of interest determined from fitting the experimental impedance spectra of Fig. 5a to the equivalent circuit of Fig. 5c.

	$R_s(\Omega\ cm^2)$	$R_{ct}(\Omega\ cm^2)$	$C_{dl}(\mu F\ cm^{-2})$	$D_{Li}(cm^2\ s^{-1})$
1st charge	80.7	18.6	22.0	6.7×10^{-10}
2nd charge	80.1	11.2	25.0	6.1×10^{-10}
3rd charge	79.0	8.3	32.0	6.5×10^{-10}
10th charge	83.5	7.7	140	8.04×10^{-10}

R_s: solution resistance; R_{ct}: charge-transfer resistance; C_{dl}: double-layer capacitance; and D_{Li}: diffusion coefficient of lithium.

Features of the impedance spectra of Fig. 5a may be modeled by a simple modified Randles-Ershler equivalent circuit shown in Fig. 5c. In this model, R_s is the solution resistance, and R_{ct} is the charge-transfer resistance at the electrode/electrolyte interface. A constant phase element (CPE) was used instead of a double-layer capacitance to take into account the surface roughness of the particle. C_{in} is the insertion capacitance, and Z_W is the Warburg impedance that corresponds to the solid-state diffusion of the Li-ion into the bulk anode. The Warburg element was used only for impedance data obtained at the tenth charge. The electrical components of the surface film which is likely formed on the electrode were disregarded, because no time constant related to this process could be seen in the EIS spectra. We also checked that their inclusion in the model of Fig. 5c does not improve the fit.

The solid lines in Fig. 5a, b represent the simulation results, and these show an excellent fitting obtained with the simple model of Fig. 5c over a six-decade range of frequency. The chi-square quality of fitting parameter was within 10^{-6}-10^{-5} range, and the estimated standard deviations of the individual electrical components were less than 10%. Parameters of interest obtained from the nonlinear least square fitting procedure are listed in Table I. The solution resistance was more or less constant during the first three cycles of charge, whereas it slightly increased at the tenth cycle. The charge-transfer resistance, R_{ct} decreased as the cycling increased indicating an improvement in the performance of the electrode. Moreover, it points out that the contribution of the SEI to the lithium insertion and extraction kinetics is not significant at these first ten Li insertion stages, otherwise the charge-transfer process would become difficult, and one would observe an increase in its resistance value, since the growth of a dense SEI layer would causes an electronic insulation and the lithium ions would have first to migrate through the SEI layer to reach the anode. Nonetheless, if a pinhole is present in the SEI layer, electrons will flow relatively unimpeded from the SEI layer to the anode.

The CPE exponent, n, ranged between 0.85 and unity and thus may be assimilated to the double-layer (dl) capacitance, C_{dl}. C_{dl} was found in the range of 22-32 $\mu F\ cm^{-2}$ for the first three charges but increased to about 140 $\mu F\ cm^{-2}$ at the tenth charge, which clearly indicates changes in the electrode surface condition. The insertion capacitance C_{in} remained practically unchanged from the first to the third charge as follows from the fitting results. This means that the same level of Li insertion is obtained. In contrast, C_{in} increased at the tenth charge. The element R_s should not only reflect the solution resistance but also electronic extendion from the current collector to the electrode bulk. The electronic resistance of the electrode active material may depend on cycling owing to changes in its composition; the resistance of the other passive component (current collectors) is expected to be a invariant with state of charge.

If the homogeneous diffusion ($\omega \gg 2D_{Li}/l^2$) is observed (last part of the diagram), the current is approximately 90° out of phase with the voltage. Under this condition, the real part of the impedance is independent of the frequency. The extrapolated real intercept of the straight-line region gives rise to the limiting low-frequency resistance, R_L, defined by Ho *et al.*[34]

$$Z' = R_L = \frac{V_m}{nFA}\frac{dE}{dx}\frac{l}{3D_{Li}} \quad [1]$$

V_m the molar volume of the host structure, dE/dx the slope of the coulometric titration curve *vs.* mobile ion concentration x at each x value, l the maximum length of the diffusion pathway (l can be assimilated to the electrode film thickness), and n the number of equivalent.

The imaginary part of the impedance as

$$Z'' = \frac{1}{\omega C_{in}} = \frac{V_m}{nFA}\frac{dE}{dx}\frac{1}{\omega l} \quad [2]$$

$$\frac{1}{C_{in}} = \frac{dZ''}{d\omega^{-1}} \quad [3]$$

Thus, in the range where the impedance phase angle approaches $\pi/2$, the value of the intercalation capacitance, C_{in} can be determined graphically from the slope of Eq. 3.

Therefore, D_{Li} may be deduced from Eq. 1 through Eq. 3

$$D_{Li} = \frac{l^2}{3R_L C_{in}} \quad [4]$$

Although C_{in} can be graphically determined with good precision, the determination of R_L by extrapolation is not precise and an inaccuracy is introduced in the calculation of the diffusion coefficient using Eq. 3. Consequently, R_L and C_{in} were determined by using the complex nonlinear least-squares (CNLS) fitting program. The diffusion coefficient value calculated thus at various cycle of charge are listed in Table I. There is no significant change in the D_{Li} value from the first to the third cycle of lithium insertion and sustained at an average value of $6.43 \times 10^{-10}\ cm^2\ s^{-1}$. However, at the tenth cycle, D_{Li} increased to $8.04 \times 10^{-10}\ cm^2\ s^{-1}$.

The impedance data reported here are very preliminary. A detailed investigation with EIS on the reaction mechanism of lithium insertion/extraction into/from an aged $Sn_{62}Ni_{38}$ anode (long-term cycling and potentiostatic conditions) is underway.

Structural and morphological changes of $Sn_{62}Ni_{38}$ electrode upon cycling.—*Ex situ* XRD analysis and morphological changes by SEM were performed at the $Sn_{62}Ni_{38}$ subjected to several cycles of charge and discharge. Figure 6 displays the progression of X-ray diffraction (XRD) patterns for the $Sn_{62}Ni_{38}$ at the first charge and after further cycling up to ten cycles. X-ray peaks for the as-deposited electrode are also reported for reference. Shown in Fig. 7 is the evolution of the surface morphology of the electrode at some stages of cycling. The as-deposited $Sn_{62}Ni_{38}$ had an average particle size (for 100 particles) of 30 nm (Fig. 7a).

Figure 6 shows that the Ni_3Sn_4 was the main phase confirmed from the as-deposited state. The Bragg peaks from the Ni_3Sn_4 alloy disappeared at the first charge, indicating that that a reaction between the NiSn alloy and lithium is occurring. This proves that during the first charge Ni_3Sn_4 is active. The reaction product of the first charge shows two broad X-ray peaks at $2\theta \approx 24$ and 38°, respectively. Courtney and Dahn identified these two peaks as those of LiSn alloy phases.[2] At the following cycle, peaks of Ni_3Sn_4 reappeared, whereas those of Li-Sn alloy phases disappeared. The formation of Li-rich alloy phases leads to fast mechanical degradation of the electrode due to a large volume change during cycling. This is supported by the SEM image of the electrode, which clearly shows expansion in the grains resulting in a bumpy surface with Li^+ insertion, and formation of surface cracks with Li^+ elimination (Fig.

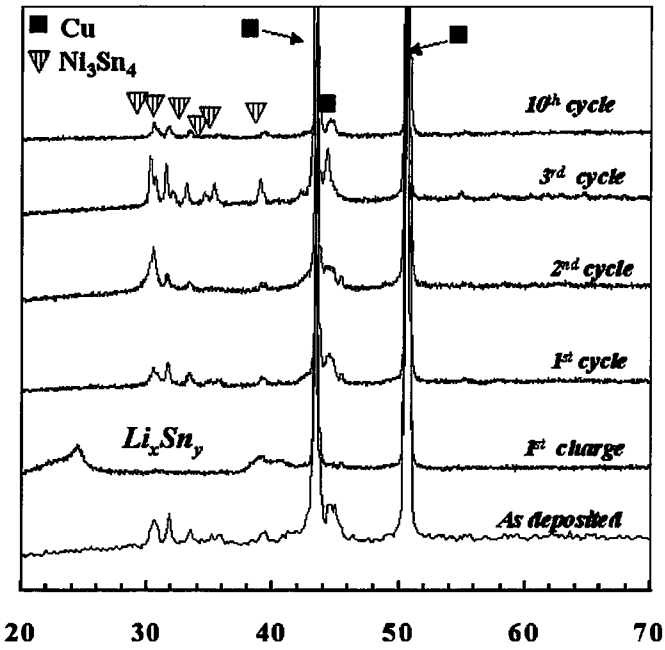

Figure 6. *Ex situ* XRD pattern taken at different stages during cycling of the 62 atom % Sn-Ni electrode in 1 M $LiClO_4$ /EC-PC solution. The XRD pattern related to the as-electrodeposited 62 atom % Sn-Ni is also reported.

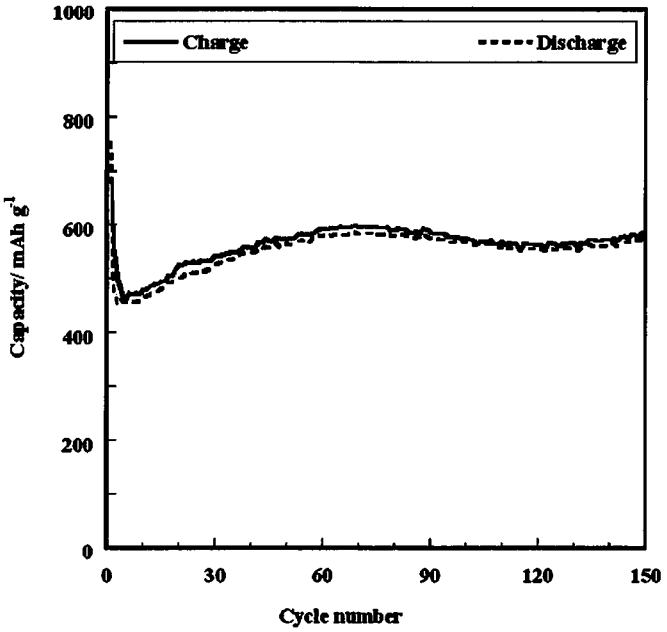

Figure 8. Cycle life performance in 1 M $LiClO_4$ /EC-PC of electrodeposited 62 atom % Sn-Ni on a Cu substrate. The electrode was charged and discharged with currents of 50 mA/g.

7c). It should be noted that the Ni_3Sn_4 phase is maintained even after extended cycling indicating the reversibility of the reaction between Ni_3Sn_4 and Li^+.

An additional study was made to evaluate the structure and morphology changes of $Sn_{62}Ni_{38}$ cycled for a longer period. Figure 8 displays the capacity *vs.* cycle number profile upon 150 cycles of charge and discharge. The profile shows an outstanding performance of the $Sn_{62}Ni_{38}$ alloy, *i.e.*, after a drop in the capacity to around 460 mAh g^{-1}, this one has markedly recovered and sustained at around an average value of 600 mAh g^{-1} over the 150 cycles tested. We have to point out with other Sn-Ni compositions tested ($Sn_{54}Ni_{46}$, $Sn_{84}Ni_{16}$, and $Sn_{92}Ni_8$), their capacities, although stable, were very much inferior and were less than 400 mAh g^{-1} upon cycling.[27] With regard to the reproducibility of the remarkable performance of the $Sn_{62}Ni_{38}$, the average charge for various experimental trials we have performed was about 625 mAh g^{-1}. The recovery in the capacity observed with this material is a very interesting phenomenon and has been observed by Mao and Dahn with the FeSn system, which showed an increase in capacity with cycle number.[18] The authors postulated that this is caused by the breakdown of the Fe-skin that impedes access to the interior of the grains of this phase by the repeated volume changes in the electrode.

Figure 9 also reports few SEM images taken at the 50th and 100th cycles. The cracks observed in the tenth cycle (Fig. 7d) have coalesced in the 50th and the 100th cycle, and higher roughness can be noticed from the surface morphology. These images are evidence that alterations in the surface condition accompanying volume changes during cycling were responsible of the $Sn_{62}Ni_{38}$ behavior.

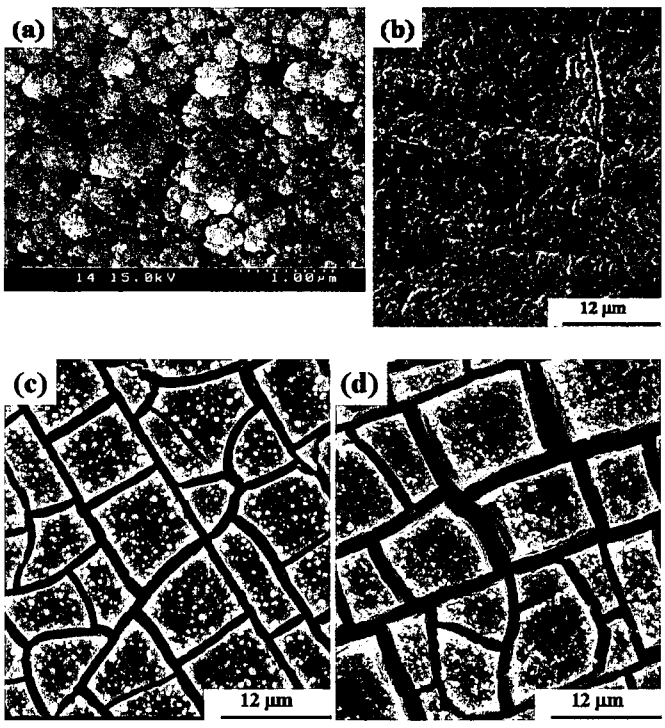

Figure 7. (a) High resolution FE-SEM image of the as-deposited 62 atom % Sn-Ni sample. (b), (c), and (d) are *ex situ* SEM images taken at 1st charge, 1st discharge, and 10th discharge, respectively.

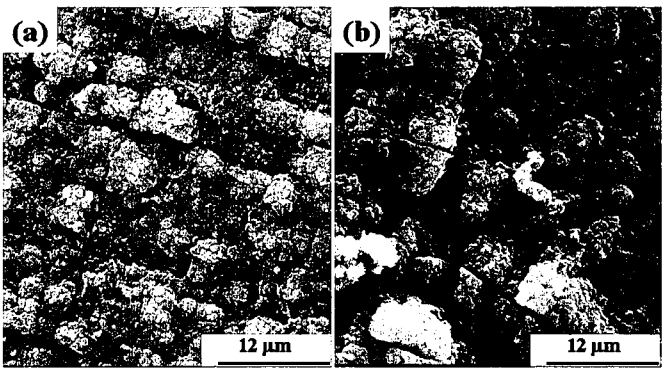

Figure 9. *Ex situ* SEM images taken at (a) 50th cycle and (b) at the 100th cycle.

It is obvious that the electrode does not return to the original volume upon lithium extraction. The major increase in volume happens in the first alloying. This volume enlargement of the host matrix causes an increase in the electrode/electrolyte interface area. The repeated formation of cracks and pores has expanded the volume of the electrode so much that it has covered up the cracks formed during the earlier cycling. The resulting expanded electrode offers a higher porosity than the original material, and provided that there is still electronic contact within the host after this activation, lithium diffusion is facilitated with lower volume expansions in the following cycles. This might be one of the reasons for the rise in the capacity seen in the cycle performance of each sample.

The other probable positive changes upon cycling are improvements in the impregnation of the porous electrode with the solution and reorganization of the surface films (better cohesion and adhesion), which improves their transport properties (Li-ion migration). SEM images for the aged (long-term cycled) electrode showed no sign of major failure mechanisms due to exfoliation, cracking, or any other bulk destruction of the SnNi particles. However, the images of the aged electrode clearly show that it is covered by granular surface films. The cracked formation exposes new surfaces to the electrolyte, which will be followed by massive precipitation of surfaces species. This explains the shift in the solution resistance observed by impedance. The observed surface films rearrange, refine, and their coherence and adherence to the anode increases which causes a decrease in the resistances for Li-ion migration through the surface layer for Li-ion transfer at the anode. The new layer will serve as a protective overlayer and enhances the long-term cycling efficiency and stability of the $Sn_{62}Ni_{38}$ anode.

Conclusions

The $Sn_{62}Ni_{38}$ exhibited a remarkable performance during lithium insertion and extraction processes. Excellent stability upon cycling was obtained with this alloy delivering capacities as high as 600 mAh g^{-1}. X-ray diffraction showed that the Ni_3Sn_4 was the main phase of the as-deposited alloy. At the first charge LiSn alloy phases are formed. This led to a volume expansion of the electrode causing the formation of cracks as demonstrated by SEM images. At the following cycles the Ni_3Sn_4 was restored and maintained over extended cycling, pointing out the reversibility of the reaction between Ni_3Sn_4 and Li^+. As to the reasons for the capacity recovery noticed with this alloy, SEM images provided evidence of modifications in the surface condition accompanying a volume change during cycling. Therefore, further analysis by *in situ* spectroscopic methods to identify the physical or chemical phenomena occurring within the film may be possible. In addition, the chemical diffusion coefficient (D_{Li}) value determined from EIS measurements during lithium insertion was within 10^{-9} to 10^{-10} cm^2 s^{-1}.

Acknowledgments

This work is supported in part by a Grant-in-Aid from the Center of Excellence (COE) Research Molecular Nano-Engineering, and the 21st Century COE Program Practical Nano-Chemistry from the Ministry of Education, Culture, Sports, Science and Technology. H. M. acknowledges a research fellowship from the Japan Society for the Promotion of Science.

Waseda University assisted in meeting the publication costs of this article.

References

1. Fuji Photo Film Co., Ltd., Euro. Pat. 0,651,450, A1 (1995).
2. I. A. Courtney and J. R. Dahn, *J. Electrochem. Soc.*, **144**, 2045 (1997).
3. I. A. Courtney and J. R. Dahn, *J. Electrochem. Soc.*, **144**, 2943 (1997).
4. J. Morales and L. Sanchez, *J. Electrochem. Soc.*, **146**, 1640 (1999).
5. J. Santos-Pena, T. Brousse, and D. M. Schleich, *Solid State Ionics*, **135**, 87 (2000).
6. X. Zhang, C. Wang, A. J. Appleby, and F. E. Little, *J. Power Sources*, **109**, 136 (2002).
7. G. M. Ehrlich, C. Durand, X. Chen, T. A. Hugener, F. Spiess, and S. L. Suib, *J. Power Sources*, **147**, 886 (2000).
8. O. Crosnier, T. Brousse, X. Devaux, P. Fragnaud, and D. M. Schleich, *J. Power Sources*, **94**, 169 (2001).
9. J. Ahn, Y. Kim, G. Wang, M. Lindsay, H. K. Liu, and S. Dou, *Mater. Trans., JIM*, **43**, 63 (2002).
10. O. Crosnier, Ph.D. Thesis, University of Nantes, France (2001).
11. H. Y. Lee, S. W. Jang, S. M. Lee, S. J. Lee, and H. K. Baik, *J. Power Sources*, **112**, 8 (2002).
12. J.-H. Ahn, G. X. Wang, J. Yao, H. K. Liu, and S. X. Dou, *J. Power Sources*, **119-121**, 45 (2003).
13. S. Yamate, J. Maruta, T. Murata, H. Yasuda, and M. Yamachi, Abstract 3B04, 44th Battery Symposium in Japan, (2002).
14. Y.-L. Kim, H.-Y Lee, S.-W. Jang, S.-J. Lee, H.-K. Baik, Y.-S. Yoon, Y.-S. Park, and S.-M. Lee, *Solid State Ionics*, **160**, 235 (2003).
15. O. Mao, R. L. Turner, I. A. Courtney, B. D. Fredericksen, M. I. Buckett, L. J. Krause, and J. R. Dahn, *Electrochem. Solid-State Lett.*, **2**, 3 (1999).
16. O. Mao, R. A. Dunlap, and J. R. Dahn, *J. Electrochem. Soc.*, **146**, 405 (1999).
17. O. Mao, R. A. Dunlap, and J. R. Dahn, *J. Electrochem. Soc.*, **146**, 414 (1999).
18. O. Mao, R. A. Dunlap, and J. R. Dahn, *J. Electrochem. Soc.*, **146**, 423 (1999).
19. D. Larcher, L. Y. Beaulieu, O. Mao, A. E. George, and J. R. Dahn, *J. Electrochem. Soc.*, **147**, 1703 (2000).
20. K. D. Kepler, J. T. Vaughey, and M. M. Thackeray, *Electrochem. Solid-State Lett.*, **2**, 307 (1999).
21. D. Larcher, L. Y. Beaulieu, D. D. MacNeil, and J. R. Dahn, *J. Electrochem. Soc.*, **147**, 1658 (2000).
22. G. X. Wang, L. Sun, D. H. Bradhurst, S. X. Dou, and H. K. Liu, *J. Alloys Compd.*, **299**, L12 (2000).
23. N. Tamura, R. Ohshita, M. Fujimoto, S. Fujitani, M. Kamino, and I. Yonezu, *J. Power Sources*, **107**, 48 (2002).
24. L. Beaulieu, D. Larcher, R. A. Dunlap, and J. R. Dahn, *J. Alloys Compd.*, **297**, 122 (2000).
25. T. Momma, N. Shiraishi, A. Yoshizawa, T. Osaka, A. Gedanken, J. Zhu, and L. Sominski, *J. Power Sources*, **97-98**, 198 (2001).
26. H. Mukaibo, A. Yoshizawa, T. Momma, and T. Osaka, *J. Power Sources*, **119-121**, 60 (2003).
27. H. Mukaibo, T. Sumi, T. Momma, and T. Osaka, *Electrochem. Solid-State Lett.*, **6**, A218 (2003).
28. T. Homma, H. Sato, H. Kobayashi, T. Arakawa, H. Kudo, T. Osaka, S. Shoji, Y. Ishisaki, T. Oshima, I. Iyomoto, R. Fujimoto, and K. Mistuda, *J. Electroanal. Chem.*, **559**, 143 (2003).
29. A. Ito and H. Enomoto, *J. Met. Finish. Soc. Jpn.*, **36**, 466 (1985).
30. M. Winter and J. O. Besenhard, *Electrochim. Acta*, **45**, 31 (1999).
31. L. Y. Beaulieu, S. D. Beattie, T. D. Hatchard, and J. R. Dahn, *J. Electrochem. Soc.*, **150**, A419 (2003).
32. J. Li, H. Li, Z. Wang, X. Huang, and L. Chen, *J. Power Sources*, **81-82**, 346 (1999).
33. M. Mohamedi, S.-J. Lee, D. Takahashi, M. Nishizawa, T. Itoh, and I. Uchida, *Electrochim. Acta*, **46**, 1161 (2001).
34. C. Ho, I. D. Raistrick, and R. A. Huggins, *J. Electrochem. Soc.*, **127**, 343 (1980).
35. M. Umeda, K. Dokko, Y. Fujita, M. Mohamedi, I. Uchida, and J. R. Selman, *Electrochim. Acta*, **47**, 885 (2001).
36. K. Dokko, Y. Fujita, M. Mohamedi, M. Umeda, I. Uchida, and J. R. Selman, *Electrochim. Acta*, **47**, 933 (2001).
37. S. D. Beattie, T. Hatchard, A. Bonakdarpour, K. C. Hewitt, and J. R. Dahn, *J. Electrochem. Soc.*, **150**, A701 (2003).

Available online at www.sciencedirect.com
SCIENCE DIRECT
ELSEVIER
Journal of Power Sources 146 (2005) 457–463
JOURNAL OF POWER SOURCES
www.elsevier.com/locate/jpowsour

Changes of electro-deposited Sn–Ni alloy thin film for lithium ion battery anodes during charge discharge cycling

H. Mukaibo [a], T. Momma [a,b], T. Osaka [a,*]

[a] *Graduate School of Science and Engineering, Waseda University, 3-4-1, Okubo, Shinjyuku-ku, Tokyo 169-8555, Japan*
[b] *CREST, Japan Science and Technology Agency, Japan*

Available online 27 April 2005

Abstract

We have reported in our past work that electrodeposited Sn–Ni alloy with different composition show considerably different performance as anode materials for Li-ion batteries, and the performance was remarkably well (ca. 650 mAh g^{-1} at 70th cycle) when the composition was controlled to $Sn_{62}Ni_{38}$. In this work, structural changes during charge discharge cycling of Sn–Ni alloy with different composition were investigated to evaluate their differences in the cycle performance. From the XRD result, Ni_3Sn_4 phase was the main phase seen in $Sn_{62}Ni_{38}$, and its reversible reactivity with Li was confirmed. We suggest that this is the key phase for its high capacity and lengthened cycle life. From $Sn_{54}Ni_{46}$, which showed low capacity, only a metastable phase close to the structure of SnNi was confirmed. The results from $Sn_{84}Ni_{16}$ indicated the presence of pure Sn and Sn rich metastable phase would lead to relatively fast electrode degradation.
© 2005 Elsevier B.V. All rights reserved.

Keywords: Sn–Ni alloy; Electrodeposition; Anode

1. Introduction

Li-ion batteries possess the highest energy density among the practical batteries, and the development of its anode material is considered as one of the breakthroughs to meet the demands for power sources with higher performance for portable electronic devices.

Presently, carbon is used as the anode material for Li-ion batteries, which is now showing a capacity close to its theoretical value of 372 mAh g^{-1}. As one of the researches for the development of Li-ion batteries, Fuji Film Company filed a patent for Sn oxide in 1994 as a novel anode material that could replaced the conventional carbonaceous material with higher capacity [1]. However, this material showed two fatal defects, high initial irreversible capacity and shorter life, compared to that of carbon. For these reasons, it could not be applied to practical use. Courtney and Dahn have reported that, in the case of Sn oxide anode, Sn is the key to the high discharge capacity and Li_2O acts as a matrix that helps to lengthen the cycle life of the electrode [2]. Without the matrix, the electrode would suffer more rapid degradation [3]. Since then, researches have focused on the selection of adequate matrix that eases the electrode stress, which appears during cycling, effectively for longer cycle life.

Elements that are inactive against Li (such as Ni) are assumed to suppress the volume change effectively without much irreversible capacity [3–20]. We have confirmed in our past work that the Sn–Ni alloy thin film prepared from electrodeposition has the potential to perform as the anode of Li-ion battery, and that the composition of $Sn_{62}Ni_{38}$ leads to a high discharge capacity of ca. 650 mAh g^{-1} at about the 70th cycle (Fig. 1) [21].

In the present study, we focused on the differences in morphology and structure of the Sn–Ni alloy thin film with different composition during charge discharge cycling. Ex situ XRD and SEM were applied to the films in different charged–discharged state to evaluate the correlation between the electrode structure, surface morphology and the cycle performance.

* Corresponding author. Tel.: +81 3 5286 3202; fax: +81 3 3205 2074.
E-mail address: osakatet@waseda.jp (T. Osaka).

0378-7753/$ – see front matter © 2005 Elsevier B.V. All rights reserved.
doi:10.1016/j.jpowsour.2005.03.043

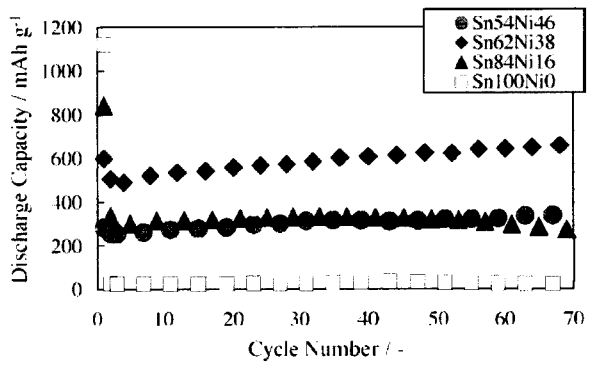

Fig. 1. Cycle performance of electrodeposited Sn_xNi_y thin films reproduced from Ref. [21].

2. Experimental

The Sn–Ni thin films with different composition were prepared by electrodeposition on Cu sheet from potassium pyrophosphate baths at 50 °C according to the procedure reported [22]. Each film was deposited for 5 min with the current density of 5 mA cm^{-2}. The compositions of the films were determined by inductively coupled plasma-atomic emission spectroscopy (Thermo Electron K.K., IRIS-AP). The anodes were cycled in conventional glass cells, with two pieces of Li foil as counter and reference electrodes and the organic electrolyte was 1 M $LiClO_4$/ethylene carbonate (EC) + propylene carbonate (PC) (1:1 vol.%). The electrochemical cells were assembled and sealed under dry Ar atmosphere (dew point was kept under −100 °C).

The galvanostatic cycling was performed using a charge–discharge equipment (Hokuto Denko, HJR-1010mSM8) in the potential range of 0.01–1.20 V versus Li/Li^+. Both charge and discharge were carried out at the current density of 250 mA g^{-1} of Sn–Ni alloy. The electrodes were rested for 10 min between charge and discharge. The cycling for structural and morphological examination was processed in a constant current–constant potential (CC–CP) mode. When in this mode during charging, the electrodes are charged in constant current until 0.01 V versus Li/Li^+ and then kept at this potential until 4 h have passed since the beginning of the charging step. Conversely, during the discharging step, the electrodes are discharged in constant current until 1.20 V versus Li/Li^+ and then kept at this potential until 4 h have passed in total. X-ray diffraction was performed on Rigaku RAD-IC using Cu Kα radiation. XRD conditions of voltage and current measurements were 40 kV and 20 mA, respectively, and the scan rate was set at 2° min^{-1}. Morphology of the film was imaged using a scanning electron microscope (HITACHI, S2500CX). Grain size, cross sectional morphology and the electron diffraction patterns of $Sn_{62}Ni_{38}$ were evaluated using transmission electron microscope (HITACHI, H-9000NAR), with samples prepared using FIB equipment (Seiko Instruments Inc., SMI-8300II). The acceleration voltage was 300 kV and the diameter of the analyzing beam for electron diffraction pattern was 2 nm.

3. Results and discussion

We have indicated that Sn–Ni alloy shows different anodic features with different compositions from our previous work, as shown in Fig. 1 [21]. Under the assumption that all Sn reacts with Li to form $Li_{4.4}Sn$, the theoretical capacity of $Sn_{54}Ni_{46}$, $Sn_{62}Ni_{38}$, and $Sn_{84}Ni_{16}$ would be 700, 763, and 909 mAh g^{-1}, respectively. Nevertheless, when they were cycled, $Sn_{54}Ni_{46}$ and $Sn_{84}Ni_{16}$ showed a relatively low discharge capacity of ca. 300 and 272 mAh g^{-1} after 70 cycles. Under the same condition, $Sn_{62}Ni_{38}$ showed the largest discharge capacity of 654 mAh g^{-1}. Another interesting feature of these samples is that they show increase in capacity with cycling after first several cycles. $Sn_{62}Ni_{38}$ showed the biggest increase in 70 cycles (166 mAh g^{-1}). $Sn_{54}Ni_{46}$ also increased about 100 mAh g^{-1} of its capacity in 70 cycles, but the capacity of $Sn_{84}Ni_{16}$ started to decrease in about 35 cycles after 30 mAh g^{-1} increase of its capacity. To evaluate these phenomena, structural and morphological changes with cycling (repeated Li^+ insertion and extraction) were investigated by XRD and SEM. Since the results of $Sn_{92}Ni_8$ reported in our previous work were similar to that of $Sn_{84}Ni_{16}$, this paper will only discuss the results of the latter case.

Fig. 2 illustrates the structure and surface morphology of $Sn_{54}Ni_{46}$, $Sn_{62}Ni_{38}$ and $Sn_{84}Ni_{16}$ before cycling. The peak assignments of the XRD are based on the results of Watanabe et al. who carried out a detailed study on the structure of electroplated Sn–Ni films [23]. Metastable phases are phases that do not appear in the equilibrium phase diagram; formed due to the electrodeposition process. The metastable phase M1 is a NiSn phase with a composition ratio of almost 50:50, and the metastable phase M2 is a phase where Ni is melted into pure Sn crystal lattice. M1 phase is the main phase confirmed from the XRD of $Sn_{54}Ni_{46}$ and not identified in $Sn_{62}Ni_{38}$ or $Sn_{84}Ni_{16}$. For $Sn_{62}Ni_{38}$, Ni_3Sn_4 phase is the only identified phase. Calculation assuming that all the Ni atom within $Sn_{62}Ni_{38}$ is forming Ni_3Sn_4 alloy with Sn, leaves at least 19 at.% Sn in excess. Nevertheless, presence of distinct pure Sn phase could not be distinguished from Fig. 2. Consulting that the peaks attributed to Ni_3Sn_4 in our results are slightly shifted from those indicated in the JCPDS data, these Sn may exist melted within the Ni_3Sn_4 lattice, or exist as a nano-crystalline or an amorphous phase in the film. The XRD peaks of $Sn_{84}Ni_{16}$ are assigned to Ni_3Sn_4, M2 and pure Sn phases. Peaks at 34.5°, 35°, 42.2° and 46.7° could not be identified. From SEM observation, the majority particles size of $Sn_{54}Ni_{46}$, $Sn_{62}Ni_{38}$ and $Sn_{84}Ni_{16}$ was 20–24, 25–29, and 40–44 nm, respectively, and films with higher Sn content lead to rougher, more granular surface.

Fig. 3 shows the results of the XRD patterns and SEM images after the first charging (Li insertion). Upon charging, the peak attributed to M1 phase of $Sn_{54}Ni_{46}$ at 30.3°

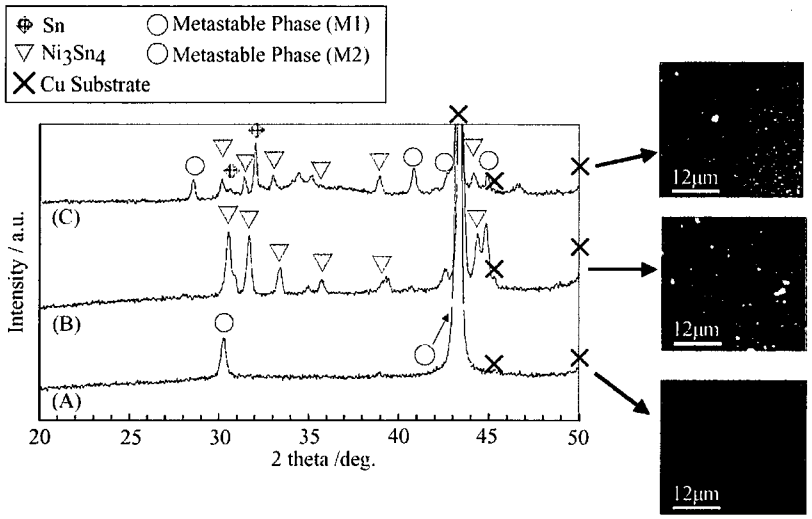

Fig. 2. XRD patterns and SEM images of (A) $Sn_{54}Ni_{46}$, (B) $Sn_{62}Ni_{38}$, and (C) $Sn_{84}Ni_{16}$ before cycling.

decreases its intensity. This suggests that part of the phase reacted with Li^+, resulting in a state of nano-crystalline or amorphous phase that could not be detected by the XRD. It should also be noted that no peaks assigned to Li–Sn alloy phase were confirmed at this charged state. This indicates that no XRD-detectable Li–Sn binary alloy phases were formed by the reaction of Sn with Li^+. On the contrary, $Sn_{62}Ni_{38}$ and $Sn_{84}Ni_{16}$ showed new peaks indicating the presence of Li–Sn alloys. As it is well known, there are several types of Li–Sn alloys with different composition [24–26]. However, the results here show them as two broad peaks, and since many peaks of various Li–Sn composition is overlapped in this range, it was not possible to attribute them to a certain Li–Sn phase. This indicates that lithiation reaction of Sn had taken place during charging in $Sn_{62}Ni_{38}$ and $Sn_{84}Ni_{16}$ thin films. Simultaneously, most of the peaks due to Ni_3Sn_4, M2 and Sn phase became unidentifiable. Peaks attributed to pure Ni were not identified. This will be discussed further with the results shown in Fig. 4. The SEM images of each sample after Li^+ insertion showed a bumpier surface compared to those images before cycling (Fig. 2).

After the first discharge process where Li^+ was extracted from the sample (Fig. 4), the XRD patterns suggest a partial recovery of the electrode structure. For $Sn_{54}Ni_{46}$, the peak intensity of the metastable phase at 30.3° grows higher again, indicating that the reaction between the M1 phase and Li^+ is reversible. The peak is also slightly broader than it was before cycling (Fig. 2) suggesting the decrease in the crystal size. In the case of $Sn_{62}Ni_{38}$, although all the peaks attributed to Ni_3Sn_4 in Fig. 2 were confirmed again, their peak intensity had become relatively weaker. From the XRD pattern of $Sn_{84}Ni_{16}$, only the peak at 45° was identified for M2 phase. Recovery of all the peaks of Ni_3Sn_4 and Sn were confirmed, but their peak intensity was different from Fig. 2 without regularity. Specifically, compared with the peak intensities of Fig. 2, the peaks at 30.3° (Ni_3Sn_4), 30.7° (Sn), 31.5° (Ni_3Sn_4)

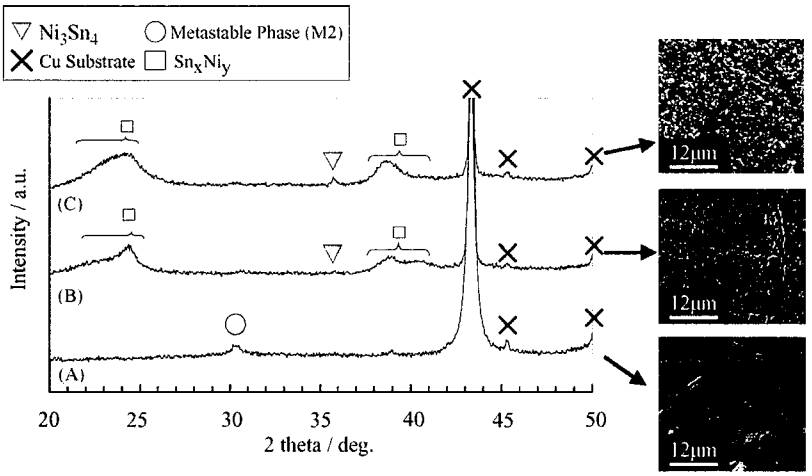

Fig. 3. XRD patterns and SEM images of (A) $Sn_{54}Ni_{46}$, (B) $Sn_{62}Ni_{38}$, and (C) $Sn_{84}Ni_{16}$ after initial charging. Charged until 0.01 V vs. Li/Li^+ at the constant current density of 250 mA g^{-1} in 1 M $LiClO_4$/EC + PC (1:1 vol.%) organic electrolyte.

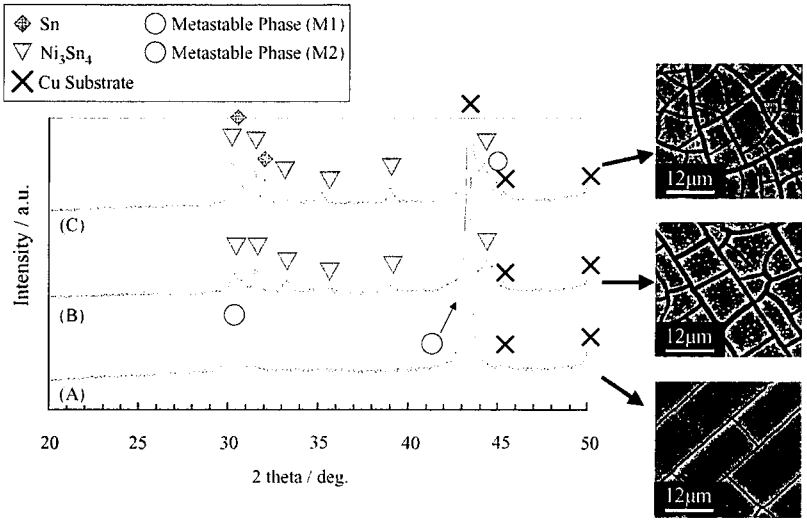

Fig. 4. XRD patterns and SEM images of (A) $Sn_{54}Ni_{46}$, (B) $Sn_{62}Ni_{38}$, and (C) $Sn_{84}Ni_{16}$ after first discharge. Cycled in the potential range of 0.01–1.20 V vs. Li/Li^+ at the constant current density of 250 mA g^{-1} in 1 M $LiClO_4$/EC + PC (1:1 vol.%) organic electrolyte.

and 44.2° (Ni_3Sn_4) showed increased intensity, while the peak at 33.1° (Ni_3Sn_4) and 45.0° (Sn) showed almost the same intensity, and peaks at 32.0° (Sn), 35.8° (Ni_3Sn_4) and 39.0° (Ni_3Sn_4) showed decreased intensity. The peaks attributed to Li–Sn alloy phases were no longer detectable for both $Sn_{62}Ni_{38}$ and $Sn_{84}Ni_{16}$. Assuming from the fact that the Ni–Sn alloy phase has recovered in both $Sn_{62}Ni_{38}$ and $Sn_{84}Ni_{16}$ with Li^+ extraction, Ni may have existed within the film in the charged state (Fig. 3) as nano-crystalline or amorphous phase; hence their phases could not be identified in XRD results. From the SEM images, formation of surface cracks with Li^+ extraction was confirmed. Relatively, the cracks after discharging are smaller for $Sn_{54}Ni_{46}$. This may be indicating that the reaction of M1 phase and Li^+ shows smaller volume change compared to the reaction between Ni_3Sn_4 and Li^+. This may be considered to be consistent with the smaller amount of Li insertion (lower discharge capacity) indicated in Fig. 1. Also, these cracks confirmed on the electrode surface can be expected to lower the diffusion resistance of Li^+ into the inner electrode. This generation of cracks may be one of the reasons for the rise in the capacity with cycling seen in the cycle performance of each electrodeposited Sn–Ni alloy anode (Fig. 1 [21]).

Fig. 5 shows the XRD results and SEM images of each sample after the 10th discharge (Li extraction). For $Sn_{54}Ni_{46}$ and $Sn_{62}Ni_{38}$, no more formation of new phases or disappearance of existing phases can be confirmed compared with the result for the sample after first discharge (Fig. 4), while both samples showed lower peak intensity. Especially for $Sn_{62}Ni_{38}$, it may be noted that the XRD result does not indicate aggregation of pure Sn phase with cycling as reported for Sn oxide materials [27]. For $Sn_{84}Ni_{16}$, all the peaks attributed

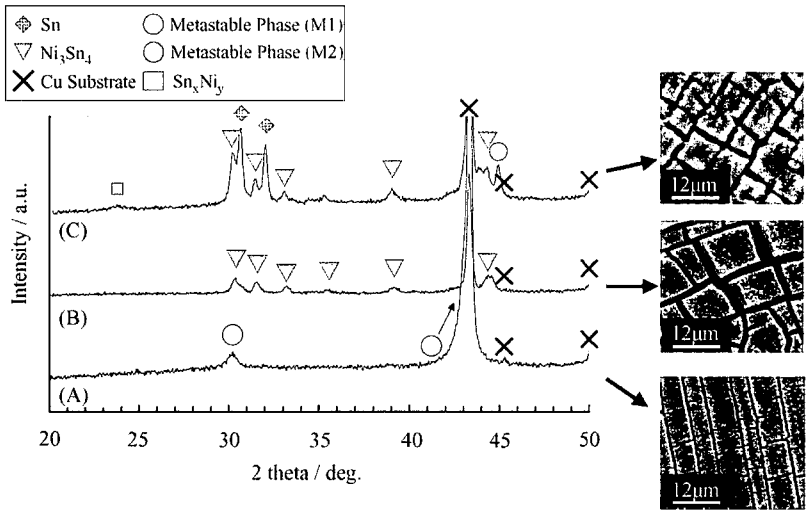

Fig. 5. XRD patterns and SEM images of (A) $Sn_{54}Ni_{46}$, (B) $Sn_{62}Ni_{38}$, and (C) $Sn_{84}Ni_{16}$ after 10th discharge. Cycled in the potential range of 0.01–1.20 V vs. Li/Li^+ at the constant current density of 250 mA g^{-1} in 1 M $LiClO_4$/EC + PC (1:1 vol.%) organic electrolyte.

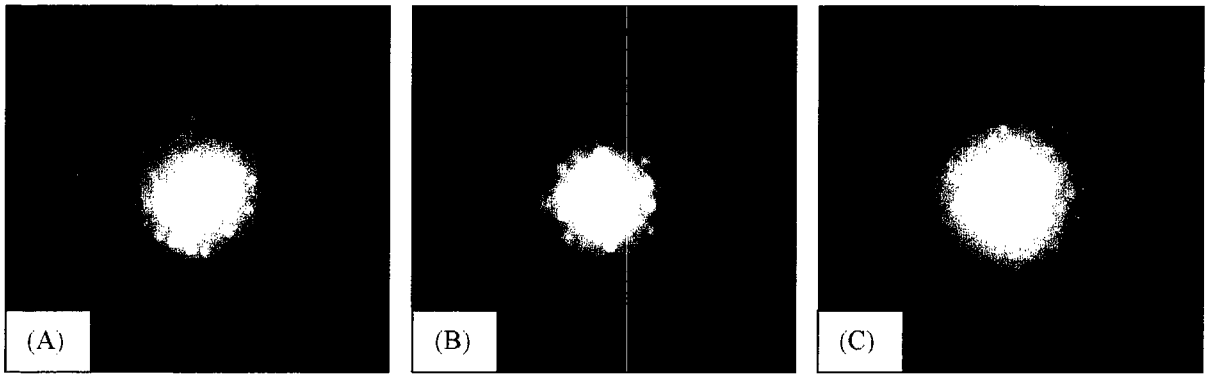

Fig. 6. μ-Electron diffraction pattern of $Sn_{62}Ni_{38}$ (A) as deposited, (B) after the first charge, and (C) after the first discharge. Cycled in the potential range of 0.01–1.20 V vs. Li/Li^+ at the constant current density of 250 mA g^{-1} in 1 M $LiClO_4$/EC + PC (1:1 vol.%) organic electrolyte.

to Sn showed increase in its intensity that may be indicating the aggregation of Sn phase with cycling. Furthermore, this sample showed small peak that was attributed to Li–Sn alloy phase at the lower degree (around 25°). This suggests that with repeated cycling, some Li gets trapped within the Li–Sn alloy, unable to dealloy during the discharge process. The SEM images show the similar cracked surface morphology as Fig. 4.

The change of the electrode crystallinitiy with cycling was also evaluated using μ-ED (Fig. 6). Clear Laue patterns can be seen from the as-deposited image and from the 1st discharge image, indicating its crystallinity. But after the first charge, broad halo can be identified, suggesting that the Li insertion has a significant effect on lowering the crystallinity of the electrode structure in the nanometer scale.

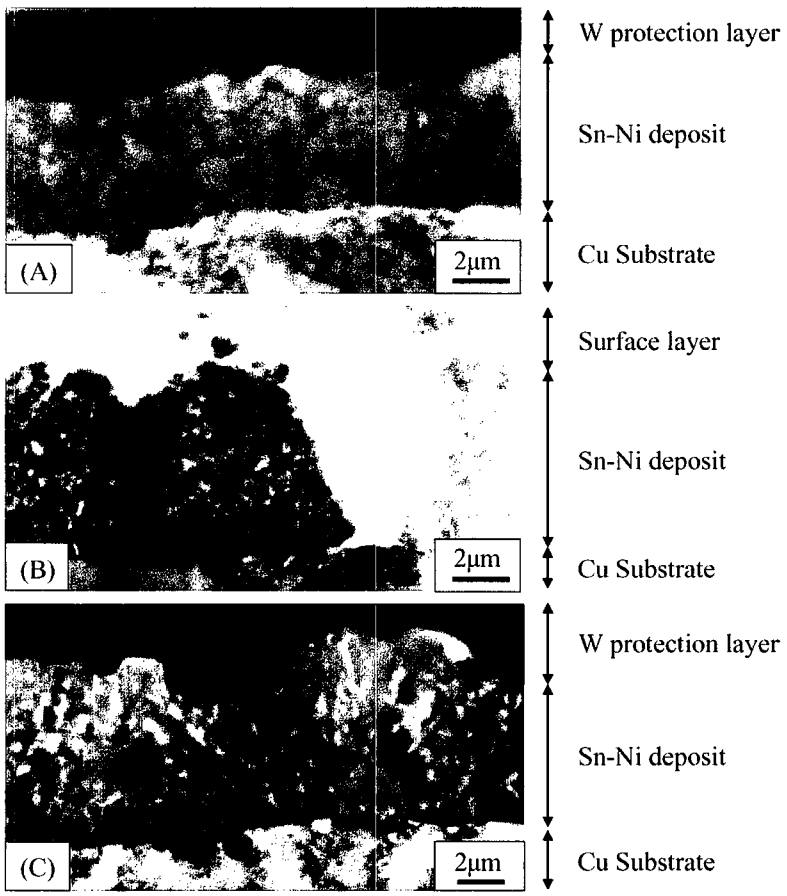

Fig. 7. TEM images of the $Sn_{62}Ni_{38}$ (A) as deposited, (B) after the first charge, and (C) after the first discharge. The $Sn_{62}Ni_{38}$ electrode was cycled in the potential range of 0.01–1.20 V vs. Li/Li^+ at the constant current density of 250 mA g^{-1} in 1 M $LiClO_4$/EC + PC (1:1 vol.%) organic electrolyte.

Table 1
Summary of the TEM results

State of sample	Film thickness (μm)	Crystal particle size (μm)	Film state	Surface film
Before cycling	0.6	0.05–0.13	Dense	Not confirmed
After first charge	1.25	0.01–0.13	Porous	Confirmed
After first discharge	0.75	0.01–0.18	Porous	Not confirmed

Overall, the obtained results suggest that a reaction mechanism of Sn–Ni alloys is different to the ones considered for the Sn oxide anodes [2]. With the Li^+ insertion during the charge process, Sn atoms segregate from the Sn–Ni alloy structure and alloys with Li to form the Li–Sn alloy phase. This reaction should be reversible. With discharge, the Li^+ is extracted from the Li–Sn alloy phase, and the dealloyed Sn atom gets absorbed into the Ni matrix again forming the Sn–Ni alloy phase.

Considering this reaction mechanism with the gained results on the cycle performance and structural changes of the electrodes, it may be suggested that the structure of $Sn_{54}Ni_{46}$ was unable to free the Sn from the metastable Sn–Ni alloy crystal to allow its full alloying with Li. This could also be supported by the fact that the initial discharge capacity was 597 mAh g^{-1} for $Sn_{62}Ni_{38}$ and 841 mAh g^{-1} for $Sn_{84}Ni_{16}$ but 334 mAh g^{-1} for $Sn_{54}Ni_{46}$. In the case of $Sn_{84}Ni_{16}$, pure Sn phases were observed which clearly did not alloy with Ni, hence leading to the large capacity drop after the second cycle. The rechargeable capacity also begins to drop from the 35th cycle indicating its relatively rapid degradation compared to $Sn_{54}Ni_{46}$ and $Sn_{62}Ni_{38}$ (Fig. 1 [21]).

It was indicated that the structure that allows Li and Sn, Sn and Ni to reversibly alloy/dealloy is the key to gain high-capacity long-life anode materials. Ni_3Sn_4 phase may have been able to realize such reversible reactions, hence resulting in the high capacity of $Sn_{62}Ni_{38}$.

To obtain further information on the changes induced by cycling, cross-sectional TEM pictures were taken on $Sn_{62}Ni_{38}$ (Fig. 7), which showed the highest performance as Li-ion battery anodes during galvanostatic cycling test [21]. The film thickness of $Sn_{62}Ni_{38}$ before cycling was ca. 0.6 μm, and the crystal particle size was 0.05–0.13 μm. The film thickness and crystal particle size varied largely upon cycling, and formation of cracks and pores were seen with cycling. The results are summarized in Table 1. With the first charging discharging process, the dense film became porous, and the thickness expanded. The surface layer seen on the film upon charging disappeared with discharging. This may indicate the growth of Li oxides during the procedure to prepare TEM samples by exposure to the air. Or it may indicate some decomposition of the organic electrolyte during charging. Decrease in the crystal size of the film was also confirmed with cycling. This may be due to the reaction where Li comes into the Ni_3Sn_4 phase to generate Ni-rich and Li–Sn alloy phases, and to the converse reaction where Li goes out from the Li–Sn alloy and Ni-rich phases and generate Ni_3Sn_4 phases. This reversible reaction could be contributing to the good anode property of $Sn_{62}Ni_{38}$.

4. Conclusion

A reaction mechanism of Sn–Ni alloys that is different to the ones considered for the Sn oxide anodes [2] was suggested from the Sn–Ni alloys with different composition ($Sn_{54}Ni_{46}$, $Sn_{62}Ni_{38}$, and $Sn_{84}Ni_{16}$) that show different anode properties. With the Li^+ insertion during the charge process, Sn atoms segregate from the Sn–Ni alloy structure and alloys with Li to form the Li–Sn alloy phase. This reaction should be reversible, and with discharge, the Li^+ is extracted from the Li–Sn alloy phase, and the dealloyed Sn atom gets absorbed into the Ni matrix again forming the Sn–Ni alloy phase.

It was suggested that the structure of $Sn_{54}Ni_{46}$ was unable to free the Sn from the metastable Sn–Ni alloy crystal to allow its full alloying with Li. For $Sn_{84}Ni_{16}$, pure Sn phases were observed which clearly did not alloy with Ni, hence leading to the large capacity drop after the second cycle. It was indicated that the structure that allows Li and Sn, Sn and Ni to reversibly alloy/dealloy is the key to gain high-capacity long-life anode materials. Ni_3Sn_4 phase may realize such reversible reactions, and $Sn_{62}Ni_{38}$, which was mainly composed of this Ni_3Sn_4 structure, results in high capacity.

It was also indicated that the lithiation procedure has the effect of lowering the crystallinity of the electrode. Formation of surface cracks with cycling was also confirmed with cycling. This generation of cracks may be one of the reasons for the rise in the capacity with cycling seen in the cycle performance of each electrodeposited Sn–Ni alloy anodes.

Acknowledgements

This work is supported in part by a Grant-in-Aid for Scientific Research (A), 15205024, and Center of Excellence (COE) Research "Molecular Nano-Engineering from the Ministry of Education, Culture, Sports, Science and Technology", and conducted at the 21st Century COE Program "The center for Practical Nano-Chemistry". Hitomi Mukaibo acknowledges a research fellowship from the Japan Society for the Promotion of Science.

References

[1] Fuji Photo Film Co. Ltd., European Patent 0,651,450, A1 (1995).

[2] I.A. Courtney, J.R. Dahn, J. Electrochem. Soc. 144 (1997) 2045.
[3] N. Tamura, R. Ohshita, M. Fujimoto, S. Fujitani, M. Kamino, I. Yonezu, J. Power Sources 107 (2002) 48.
[4] O. Mao, R.L. Turner, I.A. Courtney, B.D. Fredericksen, M.I. Buckett, L.J. Krause, J.R. Dahn, Electrochem. Solid-State Lett. 2 (1999) 3.
[5] O. Mao, R.A. Dunlap, J.R. Dahn, J. Electrochem. Soc. 146 (1999) 405.
[6] O. Mao, R.A. Dunlap, J.R. Dahn, J. Electrochem. Soc. 146 (1999) 414.
[7] O. Mao, R.A. Dunlap, J.R. Dahn, J. Electrochem. Soc. 146 (1999) 423.
[8] D. Larcher, L.Y. Beaulieu, O. Mao, A.E. George, J.R. Dahn, J. Electrochem. Soc. 147 (2000) 1703.
[9] K.D. Kepler, J.T. Vaughey, M.M. Thackeray, Electrochem. Solid-State Lett. 2 (1999) 307.
[10] D. Larcher, L.Y. Beaulieu, D.D. MacNeil, J.R. Dahn, J. Electrochem. Soc. 147 (2000) 1658.
[11] G.X. Wang, L. Sun, D.H. Bradhurst, S.X. Dou, H.K. Liu, J. Alloys Compd. 299 (2000) L12.
[12] L. Beaulieu, D. Larcher, R.A. Dunlap, J.R. Dahn, J. Alloys Compd. 297 (2000) 122.
[13] G.M. Ehrlich, C. Durand, X. Chen, T.A. Hugener, F. Spiess, S.L. Suib, J. Electrochem. Soc. 147 (2000) 886.
[14] O. Crosnier, T. Brousse, X. Devaux, P. Fragnaud, D.M. Schleich, J. Power Sources 94 (2001) 169.
[15] J. Ahn, Y. Kim, G. Wang, M. Lindsay, H.K. Liu, S. Dou, Mater. Trans. 43 (2002) 63.
[16] O. Crosnier, Doctorate Thesis, University of Nantes, 2001.
[17] H.Y. Lee, S.W. Jang, S.M. Lee, S.J. Lee, H.K. Baik, J. Power Sources 112 (2002) 8.
[18] J.-H. Ahn, G.X. Wang, J. Yao, H.K. Liu, S.X. Dou, J. Power Sources 119–121 (2003) 45.
[19] S. Yamate, J. Maruta, T. Murata, H. Yasuda, M. Yamachi, Proceedings of the 44th Battery Symposium in Japan, 2002 (abstract no. 3B04).
[20] Y.-L. Kim, H.-Y. Lee, S.-W. Jang, S.-J. Lee, H.-K. Baik, Y.-S. Yoon, Y.-S. Park, S.-M. Lee, Solid State Ionics 160 (2003) 235.
[21] H. Mukaibo, T. Sumi, T. Yokoshima, T. Momma, T. Osaka, Electrochem. Solid-State Lett. 6 (2003) A218.
[22] A. Ito, H. Enomoto, J. Met. Fin. Soc. Jpn. 36 (1985) 466.
[23] T. Watanabe, T. Hirose, K. Arai, M. Chikazawa, J. Jpn. Inst. Met. 63 (1999) 496.
[24] C.J. Wen, R.A. Huggins, J. Electrochem. Soc. 128 (1981) 1181.
[25] J. Chouvin, J. Olivier-Fourcade, J.C. Jumas, B. Simon, O. Godiveau, Chem. Phys. Lett. 308 (1999) 413.
[26] M. Winter, J.O. Besenhard, Electrochim. Acta 45 (1999) 31.
[27] I.A. Courtney, W.R. McKinnon, J.R. Dahn, J. Electrochem. Soc. 146 (1999) 59.

第46回電池討論会講演要旨集, pp. 484-485 (2005).

高分子ゲル電解質被覆による $Sn_{62}Ni_{38}$ 合金負極の負極特性向上の検討

(早大院理工[1]，早大理工[2]，学術振興会特別研究員[3]，CREST, JST[4]，日立電線[5])
○*向坊仁美*[1,3]，福原佳樹[2]，*門間聰之*[1,4]，逢坂哲彌[1,2]，小平宗男[5]

Study on the Effect of Coating $Sn_{62}Ni_{38}$ Alloy Anode with Polymer Gel Electrolyte

Hitomi Mukaibo[1], Yoshiki Fukuhara[2], *Momma Toshiyuki*[1,2], Tetsuya Osaka[1], and Muneo Kodaira[3]
[1]Waseda University,
3-4-1 Okubo Shinjuku, Tokyo 169-8555, Japan
[2]CREST, JST, [3]Hitachi Cable, Ltd.

Electroplated Sn alloys are reported to crack with cycling due to its large volume changes during the reaction with Li^+. We have taken advantage of this phenomenon and fabricated $Sn_{62}Ni_{38}$ alloy electrode with high surface area by simple 1 cycle of charge-discharge. Polymer gel mixed with conductive additives was coated on this electrode to suppress the electrode degradation with further cycling and for better electric conductivity. Insights on the effect of this treatment on electrochemical properties and anode performance will be reported.

1. 緒言

Li^+と可逆的に反応し，高い理論容量値を有するSn系合金材料はリチウムイオン二次電池の新規負極材料として注目を浴びている．しかし，充放電時に過度な体積変化を繰り返す結果，電極の微粉化やひび割れが進行し，物理的に崩壊するため寿命が短いという問題を抱えている．過去に我々が報告した $Sn_{62}Ni_{38}$ 合金薄膜についても充放電により電極に亀裂が入り，形態が粗化することを確認している[1),2)]．

本検討では上記の現象を利用し，粗化後の電極に崩壊を抑制するマトリクスとしてリチウムイオン伝導性の高分子ゲル電解質を被覆し，負極特性の改善を図った．また，高分子ゲル電解質の低電子導電性を補助するために導電材を付与した際の影響についても検討した．本報告では被覆処理を施した電極と従来の被覆処理を施していない電極とを比較し，本処理が電極の電気化学的特性および負極特性に及ぼす影響について報告する．

2. 実験方法

Sn-Ni合金薄膜はピロリン酸浴[3)]を用い 5 mA/cm^2, 5 min で Cu 基板上に電析して作製した．補助電極(Li)，基準電極(Li)および電解液を 1M - $LiClO_4$ / EC+PC (1:1 vol.)とした三極式セルを用い，得られた電極を 0.3C(=250mA/g)の電流密度で一度充放電し，電極の形態粗化を行った．電解液と PVdF-HFP を THF 中に溶解し，PC で洗浄した粗化電極上にキャストし，-210 mmHg で 30 分間減圧保持後乾燥させ，電解液を真空含浸させ被覆処理電極とした．導電材付与の被覆処理電極はケッチェンブラック(KB)を THF 中に加え，同様にして作製した．一度充放電後 PC で洗浄した電極を未処理電極とした．以上の電極を用いて断面観察，交流インピーダンス測定および定電流充放電測定を行った．

断面はエポキシ樹脂で固めた導電材付与の被覆処理電極を SEM により観察した．電気化学特性の評価のために交流インピーダンス測定（周波数：10 k ~ 10 mHz，開回路電位）を行った．また充放電試験によるサイクル特性は上記の作用極と対極(Li)を Ar 雰囲気中でコインセルに組み，電位範囲：0.01～1V vs. Li/Li^+，電流密度：250mA/g で評価した．

3. 結果と考察

Fig. 1 に導電材付与の被覆処理電極の断面 SEM 像を示す．一度充放電させたことにより生じた電極の亀裂が保持されたまま，高分子ゲル電解質が内部まで均一に被覆されている状態が確認された．

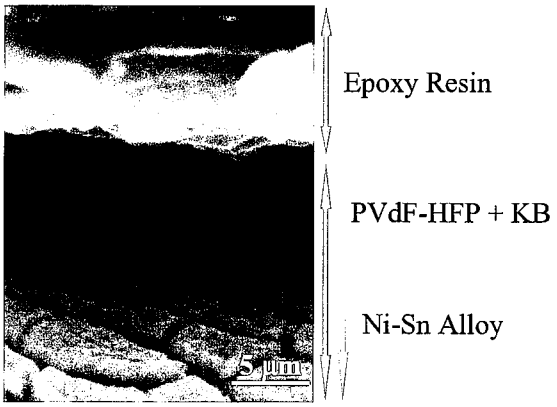

Fig.1 Cross sectional view of gel coated $Sn_{62}Ni_{38}$ alloy thin film after 1 galvanostatic cycling.

Fig. 2 には未処理，および被服処理、導電材付与の被覆処理を施した各電極の交流インピーダンス測定の結果を示す．低周波数側の挙動に大差は確認されなかったが，高周波数側では被覆処理を施すことにより未処理には確認されなかった半円が確認された．また導電材を付与することにより半円の半径が低減することが確認された．これは導電材付与により電極の抵抗が減少し，高電流密度に対する耐性が向上したことを示唆していると考えられる．

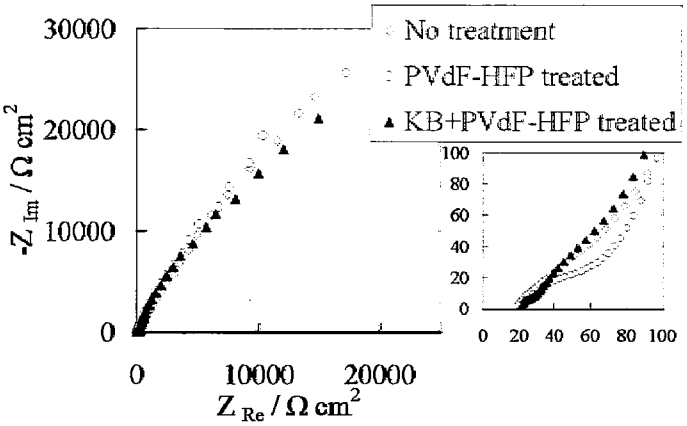

Fig.2 Cole-Cole plot of $Sn_{62}Ni_{38}$ alloy thin film at open circuit potential.

定電流充放電測定の結果，10 サイクル目までは被覆処理電極と未処理電極の間に殆ど差異はなく，どちらも 300～350 mAh/g の容量値を示した．本報告ではさらにサイクルを重ねた結果に加え，導電材を付与した影響，本被覆処理が電気化学的特性に与える効果などについてより詳細に報告する．

本研究は一部，文部科学省科学研究費(基盤研究(A)，No. 15205024)および文部科学省特別推進研究(COE)「分子ナノ工学」の助成を受け，21 世紀 COE プログラム「実践的ナノ化学教育研究拠点」にて行われた．

参考文献

1) H. Mukaibo, T. Sumi, T. Yokoshima, T. Momma, and T. Osaka, *Electrochem. Solid-State Lett.*, **6,** A218 (2003).
2) H. Mukaibo, T. Momma, M. Mohamedi, and T. Osaka, *J. Electrochem. Soc.*, **152**, A560, (2005).
3) 伊崎　昌伸, 榎本　英彦, *金属表面技術*, **36,** 466 (1985).